

A Review of Generative Adversarial Networks in Cancer Imaging: New Applications, New Solutions

Richard Osuala^{a,*}, Kaisar Kushibar^a, Lidia Garrucho^a, Akis Linardos^a, Zuzanna Szafranowska^a, Stefan Klein^b, Ben Glocker^c, Oliver Diaz^{a,**}, Karim Lekadir^{a,**}

^aArtificial Intelligence in Medicine Lab (BCN-AIM), Faculty of Mathematics and Computer Science, University of Barcelona, Spain

^bBiomedical Imaging Group Rotterdam, Department of Radiology & Nuclear Medicine, Erasmus MC, Rotterdam, The Netherlands

^cBiomedical Image Analysis Group, Department of Computing, Imperial College London, UK

Abstract

Despite technological and medical advances, the detection, interpretation, and treatment of cancer based on imaging data continue to pose significant challenges. These include high inter-observer variability, difficulty of small-sized lesion detection, nodule interpretation and malignancy determination, inter- and intra-tumour heterogeneity, class imbalance, segmentation inaccuracies, and treatment effect uncertainty. The recent advancements in Generative Adversarial Networks (GANs) in computer vision as well as in medical imaging may provide a basis for enhanced capabilities in cancer detection and analysis. In this review, we assess the potential of GANs to address a number of key challenges of cancer imaging, including data scarcity and imbalance, domain and dataset shifts, data access and privacy, data annotation and quantification, as well as cancer detection, tumour profiling and treatment planning. We provide a critical appraisal of the existing literature of GANs applied to cancer imagery, together with suggestions on future research directions to address these challenges. We analyse and discuss 163 papers that apply adversarial training techniques in the context of cancer imaging and elaborate their methodologies, advantages and limitations. With this work, we strive to bridge the gap between the needs of the clinical cancer imaging community and the current and prospective research on GANs in the artificial intelligence community.

Keywords: Cancer Imaging, Generative Adversarial Network, GAN, Synthetic Data, Survey

1. Introduction

The evident improvement in global cancer survival in the last decades is arguably attributable not only to health care reforms, but also to advances in clinical research (e.g., targeted therapy based on molecular markers) and diagnostic imaging technology (e.g. whole-body magnetic resonance imaging (MRI) [1], and positron emission tomography–computed tomography (PET-CT) [2]. Nonetheless, cancers still figure among the leading causes

of morbidity and mortality worldwide [3], with an approximated 9.6 million cancer related deaths in 2018 [4]. The most frequent cases of cancer death worldwide in 2018 are lung (1.76 million), colorectal (0.86 million), stomach (0.78 million), liver (0.78 million), and breast (0.63 million) [4]. These figures are prone to continue to increase in consequence of the ageing and growth of the world population [5].

A large proportion of the global burden of cancer could be prevented due to treatment and early detection [5]. For example, an early detection can provide the possibility to treat a tumour before it acquires critical combinations of genetic alterations (e.g., metastasis with evasion of apoptosis [6]). Solid tumours become detectable by medical

*Corresponding author

** Authors contributed equally

Email address: richard.osuala@ub.edu (Richard Osuala)

imaging modalities only at an approximate size of 10^9 cells ($\approx 1\text{ cm}^3$) after evolving from a single neoplastic cell typically following a Gompertzian [7] growth pattern [8]¹. To detect and diagnose tumours, radiologists inspect, normally by visual assessment, medical imaging modalities such as magnetic resonance imaging (MRI), computed tomography (CT), ultrasound (US), x-ray mammography (MMG), PET [8, 10, 11].

Medical imaging data evaluation is time demanding and therefore costly in nature. In addition, volumes of new technologies (e.g., digital breast tomosynthesis [12]) become available and studies generally show an extensive increase in analysable imaging volumes [13]. Also, the diagnostic quality in radiology varies and is very much dependent on the personal experience, skills and invested time of the data examiner [10, 14, 15]. Hence, to decrease cost and increase quality, automated or semi-automated diagnostic tools can be used to assist radiologists in the decision-making process. Such diagnostic tools comprise traditional machine learning, but also recent deep learning methods, which promise an immense potential for detection performance improvement in radiology.

The rapid increase in graphics processing unit (GPU) processing power has allowed training deep learning algorithms such as convolutional neural networks (CNNs) [16, 17] on large image datasets achieving impressive results in Computer Vision [18, 19], and Cancer Imaging [20]. In particular, the success of AlexNet in the 2012 ImageNet challenge [19] triggered an increased adoption of deep neural networks to a multitude of problems in numerous fields and domains including medical imaging, as reviewed in [21, 22, 23]. Despite the increased use of medical imaging in clinical practice, the public availability of medical imaging data remains limited [13]. This represents a key impediment for the training, research, and use of deep learning algorithms in radiology and oncology. Clinical centres refrain from sharing such data for ethical, legal, technical, and financial (e.g., costly annotation) reasons [24].

¹In vitro studies reported a *theoretical* detection limit around 10^5 to 10^6 for human cancer cell lines using PET. In clinical settings, the *theoretical* detection limit is larger and depends, among others, on background radiation, cancer cell line, and cancer type [9].

Such cancer imaging data not only is necessary to train deep learning models, but also to provide them with sufficient learning possibility to acquire robustness and generalisation capabilities. We define robustness as the property of a predictive model to remain accurate despite of variations in the input data (e.g., noise levels, resolution, contrast, etc). We refer to a model’s generalisation capability as its property of preserving predictive accuracy on new data from unseen sites, hospitals, scanners, etc. Both of these properties are in particular desirable in cancer imaging considering the frequent presence of biased or unbalanced data with sparse or noisy labels². Both robustness and generalisation are essential to demonstrate the trustworthiness of a deep learning model for usage in a clinical setting, where every edge-case needs to be detected and a false negative can cost the life of a patient.

We hypothesise that the variety of data needed to train robust and well-generalising deep learning models for cancer images can be largely synthetically generated using Generative Adversarial Networks (GANs) [25]. The unsupervised adversarial learning scheme in GANs is based on a generator that generates synthetic (alias ‘fake’) samples of a target distribution trying to fool a discriminator, which classifies these samples as either real or fake. Various papers have provided reviews of GANs in the medical imaging domain [26, 27, 28, 29, 30, 31], but they focused on general presentation of the main methods and possible applications. In cancer imaging, however, there are specificities and challenges that call for specific implementations and solutions based on GANs, including:

- (i) the small size and complexity of cancerous lesions
- (ii) the high heterogeneity between tumours within as well as between patients and cancer types
- (iii) the difficulty to annotate, delineate and label cancer imaging studies at large scale
- (iv) the high data imbalance in particular between healthy and pathological subjects or between benign and malignant cases

²Alongside tumour manifestation heterogeneity, and multi-centre, multi-organ, multi-modality, multi-scanner, and multi-vendor data.

- (v) the difficulty to gather large consented datasets from highly vulnerable patients undergoing demanding care plans

Hence, the present paper contributes a unique perspective and comprehensive analysis of GANs attempting to address the specific challenges in the cancer imaging domain. To the authors’ best knowledge, this is the first survey that exclusively focuses on GANs in cancer imaging. In this context, we define cancer imaging as the entirety of approaches for research, diagnosis, and treatment of cancer based on medical images. Our survey comprehensively analyses cancer imaging GAN applications focusing on radiology modalities. As presented in Figure 1, we recognise that non-radiology modalities are also widely used in cancer imaging. For this reason, we do not restrict the scope of our survey to radiology, but rather also analyse relevant GAN publications in these other modalities including histopathology and cytopathology (e.g., in section 4.5), and dermatology (e.g., in section 4.3.2 and 4.4).

Lastly, our survey uncovers and highlights promising GAN research directions that can facilitate the sustainable adoption of AI in clinical oncology and radiology.

In this paper, we start by introducing the GAN methodology, before highlighting extensions of the GAN framework that are relevant for cancer imaging. Next, we structure the paper around the challenges of cancer imaging, where each section corresponds to a challenge category. For each category, we provide descriptions and examples for various corresponding cancer imaging challenges and sub-challenges. After introducing each challenge, we analyse the literature to learn how GANs have addressed it in the past and highlight prospective avenues of future research to point out unexploited potential of GANs in cancer imaging. Figure 3 depicts an overview of the structure of our paper containing the mapping of cancer imaging challenges to solutions based on adversarial training techniques.

2. Review Methodology

Our review comprises two comprehensive literature screening processes. The first screening process surveyed the current challenges in the field of cancer imaging with

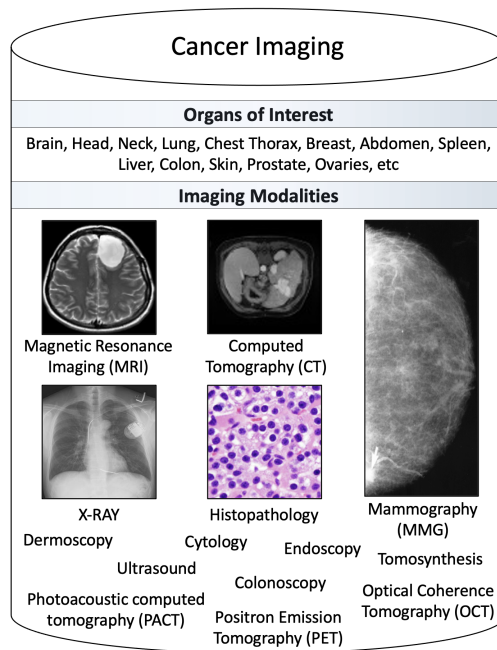


Figure 1: Overview of the most common organs and modalities targeted by the surveyed cancer imaging publications. A respective histogram that shows the number of papers per modality and per organ can be found in Figure 2.

a focus on radiology imaging modalities. After screening and gaining a deepened understanding of AI-specific and general cancer imaging challenges, we grouped these challenges for further analysis into the following five categories.

- *Data scarcity and usability challenges* (section 4.1); discussing dataset shifts, class imbalance, fairness, generalisation, domain adaptation and the evaluation of synthetic data.
- *Data access and privacy challenges* (section 4.2); comprising patient data sharing under privacy constraints, security risks, and adversarial attacks.
- *Data annotation and segmentation challenges* (section 4.3.2); discussing costly human annotation, high inter and intra-observer variability, and the consistency of extracted quantitative features.

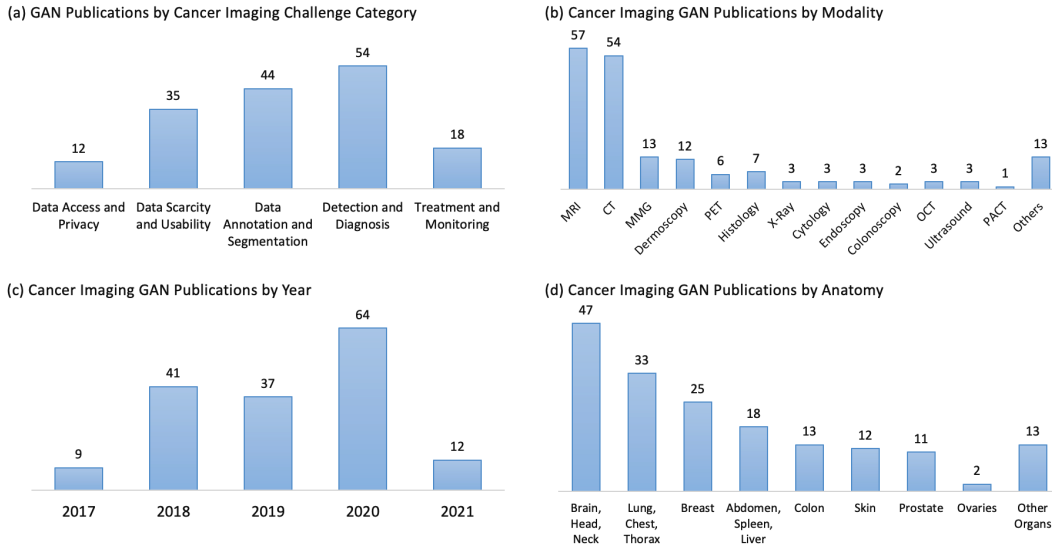


Figure 2: Histograms showing the distribution of the 163 analysed GAN publications in this paper by (a) cancer imaging challenge category, (b) imaging modality, (c) year of publication, and (d) anatomy/organ. These numbers are retrieved exclusively from the information in tables 2 - 6 of the respective sections 4.1 - 4.5. Note that (b) and (d) contain more publications in total than (a) and (c), which is caused by GAN publications that evaluate on (and are assigned to) more than one modality (b) and/or anatomy (d) due to multiple experiments or cross-domain translation. In (c), the final count for 2021 is still pending, as the GAN papers herein analysed have been published on or before 7th March 2021.

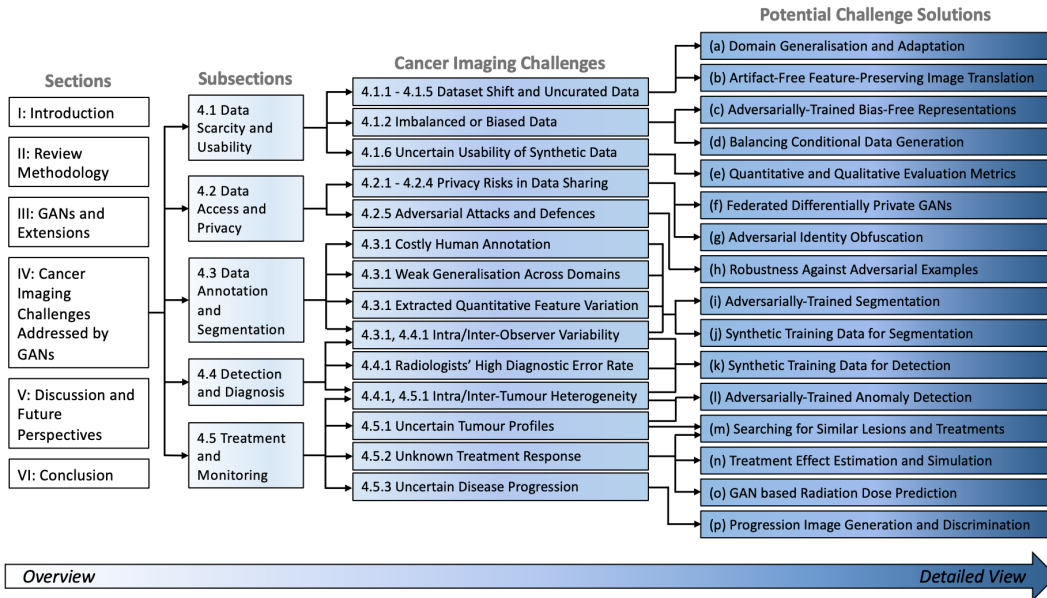


Figure 3: Illustration of the structure of the present paper starting with paper sections on the left and going into detail towards the right culminating in a selection of cancer imaging challenges and solutions. These solutions (a)-(p) are part of the solutions found in the surveyed GAN literature or are proposed extensions thereof, as is further discussed in section 4.

- *Detection and diagnosis challenges* (section 4.4); analysing the challenges of high diagnostic error rates among radiologists, early detection, and detection model robustness.
- *Treatment and monitoring challenges* (section 4.5); examining challenges of high inter and intra-tumour heterogeneity, phenotype to genotype mapping, treatment effect estimation and disease progression.

The second screening process comprised first of a generic and second a specific literature search to find all papers that apply adversarial learning (i.e. GANs) to cancer imaging. In the generic literature search, generic search queries such as ‘Cancer Imaging GAN’, ‘Tumour GANs’ or ‘Nodule Generative Adversarial Networks’ were used to recall a high number of papers. The specific search focused on answering key questions of interest to the aforesaid challenges such as ‘Carcinoma Domain Adaptation Adversarial’, ‘Skin Melanoma Detection GAN’, ‘Brain Glioma Segmentation GAN’, or ‘Cancer Treatment Planning GAN’.

In section 4, we map the papers that propose GAN applications applied to cancer imaging (second screening) to the surveyed cancer imaging challenges (first screening). The mapping of GAN-related papers to challenges categories facilitates analysing the extent to which existing GAN solutions solve the current cancer imaging challenges and helps to identify gaps and further potential for GANs in this field. The mapping is based on the evaluation criteria used in the GAN-related papers and on the relevance of the reported results to the corresponding section. For example, if a GAN generates synthetic data that is used to train and improve a tumour detection model, then this paper is assigned to the detection and diagnosis challenge section 4.4. If a paper describes a GAN that improves a segmentation model, then this paper is assigned to the segmentation and annotation challenge section 4.3.2, and so forth.

To gather the literature (e.g., first papers describing cancer imaging challenges, second papers proposing GAN solutions), we have searched in medical imaging, computer science and clinical conference proceedings and journals, but also freely on the web using the search engines Google, Google Scholar, and PubMed. After retrieving all papers with a title related to the subject, their abstract was

read to filter out non-relevant papers. A full-text analysis was done for the remaining papers to determine whether they were to be included into our manuscript. We analysed the reference sections of the included papers to find additional relevant literature, which also underwent filtering and full-text screening. Applying this screening process, we reviewed and included a total of 163 GAN cancer imaging publications comprising both peer-reviewed articles and conference papers, but also relevant preprints from arXiv and bioRxiv.

Details about these 163 GAN cancer imaging publications can be found in tables 2-6. The distribution of these publications across challenge category, year, modality, and anatomy is outlined in Figure 2.

3. GANs and Extensions

3.1. Introducing the Theoretical Underpinnings of GANs

Generative Adversarial Networks (GANs) [25] are a type of generative model with a differentiable generator network [32]. GANs are formalised as a minimax two-player game, where the generator network (G) competes against an adversary network called discriminator (D). As visualised in Figure 4, given a random noise distribution z , G generates samples $x = G(z; \theta(g))$ that D classifies as either real (drawn from training data, i.e. $x \sim p_{data}$) or fake (drawn from G, i.e. $x \sim p_g$). x is either sampled from p_{data} or from p_g with a probability of 50%. D outputs a value $p = D(x; \theta(d))$ indicating the probability that x is a real training example rather than one of G’s fake samples [32]. As defined by Goodfellow et al [25], the task of the discriminator can be characterised as binary classification (CLF) of samples x . Hence, the discriminator can be trained using binary-cross entropy resulting in the following loss function L_D :

$$L_D = -\mathbb{E}_{x \sim p_{data}} [\log D(x)] + \mathbb{E}_{z \sim p_z} [\log(1 - D(G(z)))] \quad (1)$$

D’s training objective is to minimise L_D (or maximise $-L_D$) while the goal of the generator is the opposite (i.e. minimise $-L_D$) resulting in the value function $V(G, D)$ of a two-player zero-sum game between D and G:

$$\min_G \max_D V(D, G) = \min_G \max_D [\mathbb{E}_{x \sim p_{data}} [\log D(x)] + \mathbb{E}_{z \sim p_z} [\log(1 - D(G(z)))]] \quad (2)$$

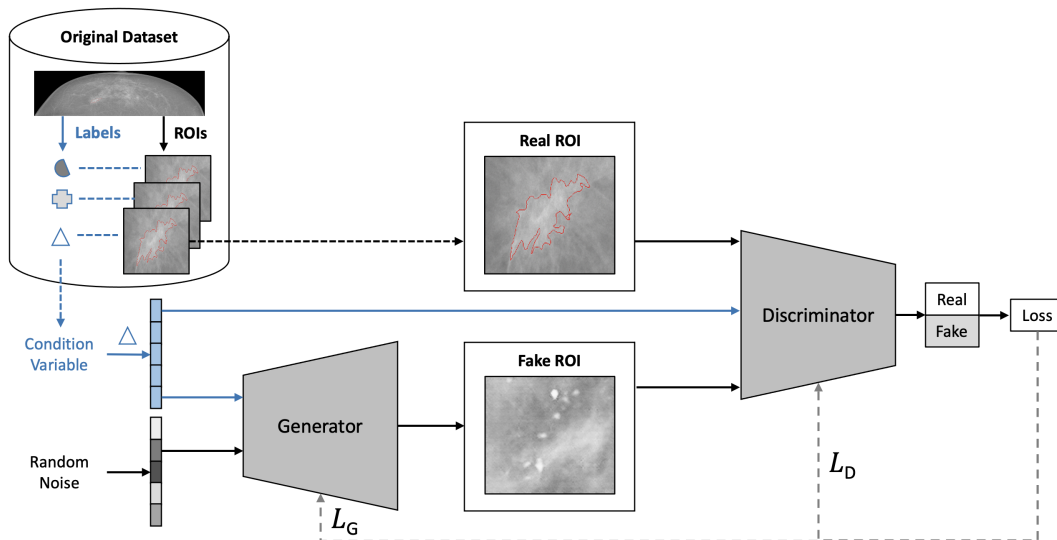


Figure 4: An example of a generic GAN architecture applied to generation of synthetic mammography region of interest (ROI) images based on the INbreast dataset [33]. Note that including the ‘Condition’ depicted in blue colour extends the vanilla GAN architecture [25] to the cGAN architecture [34].

In theory, in convergence, the generator’s samples become indistinguishable from the real training data ($x \sim p_{data} = p_g$) and the discriminator outputs $p = 1/2$ for any given sample x [32]. As this is a state where both D and G cannot improve further on their objective by changing only their own strategy, it represents a Nash equilibrium [35, 36]. In practice, achieving convergence for this or related adversarial training schemes is an open research problem [37, 38, 35].

3.2. Extensions of the Vanilla GAN Methodology

Numerous extensions of GANs have shown to generate synthetic images with high realism [39, 40, 41, 42] and under flexible conditions [34, 43, 44]. GANs have been successfully applied to generate high-dimensional data such as images and, more recently, have also been proposed to generate discrete data [45]. Apart from image generation, GANs have also widely been proposed and applied for paired and unpaired image-to-image translation, domain-adaptation, data augmentation, image inpainting, image perturbation, super-resolution, and image registration and reconstruction [26, 27, 46].

Table 1 introduces a selection of common GAN extensions found to be frequently applied to cancer imaging. The key characteristics of each of these GAN extensions are described in the following paragraphs.

3.2.1. Noise-to-Image GAN Extensions

As depicted in blue in Figure 4, cGAN adds a discrete label as conditional information to the original GAN architecture that is provided as input to both generator and discriminator to generate class conditional samples [34].

AC-GAN feeds the class label only to the generator while the discriminator is tasked with correctly classifying both the class label and whether the supplied image is real or fake [43].

LSGAN strives to overcome the vanishing gradient problem in GANs by replacing the binary sigmoid cross entropy loss function with a least squares loss function [47].

WGAN is motivated by mathematical rationale and based on the Wasserstein-1 distance (alias ‘earth mover distance’ or ‘Kantorovich distance’) between two distributions. WGAN extends on the theoretic formalisation and optimisation objective of the vanilla GAN to better

approximate the distribution of the real data. By applying an alternative loss function (i.e. Wasserstein loss), the discriminator (alias ‘critic’ or ‘ f_w ’) maximises - and the generator minimises - the difference between the critic’s scores for generated and real samples. A important benefit of WGAN is the empirically observed correlation of the loss with sample quality, which helps to interpret WGAN training progress and convergence [48].

In WGAN, the weights of the critic are clipped, which means they have to lie within a compact space $[-c, c]$. This is needed to fulfil that the critic is constraint to be in the space of 1-Lipschitz functions. With clipped weights, however, the critic is biased towards learning simpler functions and prone to have exploding or vanishing gradients if the clipping threshold c is not tuned with care. [49, 48].

In WGAN-GP, the weight clipping constraint is replaced with a gradient penalty. Gradient penalty of the critic is a tractable and soft version of the following notion: By constraining that the norm of the gradients of a differentiable function is at most 1 everywhere, the function (i.e. the critic) would fulfil the 1-Lipschitz criterion without the need of weight clipping. Compared, among others, to WGAN, WGAN-GP was shown to have improved training stability (i.e. across many different GAN architectures), training speed, and sample quality [49].

DCGAN generates realistic samples using a convolutional network architecture with batch normalization [50] for both generator and discriminator and progressively increases the spatial dimension in the layers of the generator using transposed convolution (alias ‘fractionally-strided convolution’) [51].

PGGAN is tested with loss and configurations introduced in WGAN GP. It starts by generating low pixel resolution images, but progressively adds new layers to the generator and discriminator during training resulting in increased pixel resolution and finer image details. It is suggested that after early convergence of initial low-resolution layers, the introduced additional layers enforce the network to only refine the learned representations by increasingly smaller-scale effects and features [39].

In SRGAN, the generator transforms a low-resolution (LR) to a high-resolution (HR, alias ‘super-resolution’) image, while the discriminator learns to distinguish between real high-resolution images and fake super-resolution images. Apart from an adversarial loss, a per-

ceptual loss called ‘content loss’ measures how well the generator represents higher level image features. This content loss is computed as the euclidean distance between feature representations of the reconstructed image and the reference image based on feature maps of a pre-trained 19 layer VGG [52] network [53].

3.2.2. Image-to-Image GAN Extensions

In image-to-image translation, a mapping is learned from one image distribution to another. For example, images from one domain can be transformed to resemble images from another domain via a mapping function implemented by a GAN generator.

CycleGAN achieves realistic unpaired image-to-image translation using two generators (G , F) with one traditional adversarial loss each and an additional cycle-consistency loss. Unpaired image-to-image translation transforms images from domain X to another domain Y in the absence of paired training data i.e. corresponding image pairs for both domains. In CycleGAN, the input image x from domain X is translated by generator $G(x)$ to resemble a sample from domain Y . Next, the sample is translated back from domain Y to domain X by generator $F(G(x))$. The cycle consistency loss enforces that $F(G(x)) \approx x$ (forward cycle consistency) and that $G(F(y)) \approx y$ (backward cycle consistency) [54].

Both pix2pix and SPADE are used in paired image-to-image translation where corresponding image pairs for both domains X and Y are available. pix2pix (alias ‘condGAN’) is a conditional adversarial network that adapts the U-Net architecture³ [58] for the generator to facilitate encoding an conditional input image into a latent representation before decoding it back into an output image. pix2pix uses L1 loss to enforce low level (alias ‘low frequency’) image reconstruction and a patch-based discriminator (‘PatchGAN’) to enforce high level (alias ‘high frequency’) image reconstruction that the authors suggest to interpret as texture/style loss. Note that the input into the PatchGAN discriminator is a concatenation⁴

³To reduce information loss in latent space compression, U-Net uses skip connections between corresponding layers (e.g., first to last) in the encoder and decoder.

⁴Note the concatenation of real_A and fake_B before computing the loss in the discriminator backward pass (L93) in the authors’ [pix2pix implementation](#).

Table 1: A selection of the GAN architectures that we found to be the ones most frequently applied in cancer imaging.

Publication	Input G	Input D	Losses	Task
Noise to Image				
GAN (2014) [25]	Noise	Image	Binary cross-entropy based adversarial loss (L_{ADV})	Image synthesis
conditional GAN (cGAN, 2014) [34]	Noise & label	Image & label	L_{ADV}	Conditional image synthesis
Auxiliary Classifier GAN (AC-GAN, 2017) [43]	Noise & label	Image	L_{ADV} & cross-entropy loss (label classification)	Conditional image synthesis, classification
Deep Convolutional GAN (DCGAN, 2015) [51]	Noise	Image	L_{ADV}	Image synthesis
Wasserstein GAN (WGAN, 2017) [48]	Noise	Image	Wasserstein loss (L_{WGAN})	Image synthesis
WGAN Gradient Penalty (WGAN GP, 2017) [49]	Noise	Image	L_{WGAN} with GP	Image synthesis
Least Squares GAN (LSGAN, 2017) [47]	Noise	Image	Least squares loss	Image synthesis
Progressively Growing GAN (PGGAN, 2017) [39]	Noise	Image	L_{WGAN} with GP [49]	Image synthesis
Image to Image				
Super-Resolution GAN (SRGAN, 2017) [53]	Image (LR)	Image (HR)	L_{ADV} & content loss (based on VGG [52] features)	Super-resolution
CycleGAN (2017) [54]	Source image	Target image	L_{ADV} & cycle consistency loss & identity loss	Unpaired image-to-image translation
pix2pix (2017) [55]	Source image	Concatenated source and target images	L_{ADV} & reconstruction loss (i.e. L1)	Paired image-to-image translation
SPatially-Adaptive (DE)normalization (SPADE, 2019) [56]	Noise or encoded source image & segmentation map	Concatenated target image and segmentation map	Hinge & perceptual & feature matching losses [57]	Paired image-to-image translation

of the original image (i.e. the generator’s input image; e.g. this can be a segmentation map) and the real/generated image (i.e. the generator’s output image) [55].

In SPADE, the generator architecture does not rely on an encoder for downsampling, but uses a conditional normalisation method during upsampling instead: A segmentation mask as conditional input into the SPADE generator is provided to each of its upsampling layers via spatially-adaptive residual blocks. These blocks embed the masks and apply two two-layer convolutions to the embedded mask to get two tensors with spatial dimensions. These two tensors are multiplied/added to each upsampling layer prior to its activation function. The authors demonstrate that this type of normalisation achieves better fidelity and preservation of semantic information in comparison to other normalisation methods that are commonly applied in neural networks (e.g., Batch Normalization). The multi-scale discriminators and the loss functions from pix2pixHD [57] are adapted in SPADE, which contains a hinge loss (i.e. as substitute of the adversarial loss), a perceptual loss, and a feature matching loss [56].

3.2.3. GAN Network Architectures and Adversarial Loss

For further methodological detail on the aforementioned GAN methods, loss functions, and architectures, we point the interested reader to the GAN methods review by Wang et al [46]. Due to the image processing capabilities of CNNs [17], the above-mentioned GAN architectures generally rely on CNN layers internally. Recently, TransGAN [59] was proposed, which diverges from the

CNN design pattern to using Transformer Neural Networks [60] as the backbone of both generator and discriminator. Due to TransGAN’s promising performance on computer vision tasks, we encourage future studies to investigate the potential of transformer-based GANs for applications in medical and cancer imaging.

Multiple deep learning architectures apply the adversarial loss proposed in [25] together with other loss functions (e.g., segmentation loss functions) for other tasks than image generation (e.g., image segmentation). This adversarial loss is useful for learning features or representations that are invariant to some part of the training data. For instance, adversarial learning can be useful to discriminate a domain to learn domain-invariant representations [61], as has been successfully demonstrated for medical images [62]. In the scope of our GAN survey, we include and consider all relevant cancer imaging papers that apply or build upon the adversarial learning scheme defined in [25].

4. Cancer Imaging Challenges Addressed by GANs

In this section we follow the structure presented in Figure 3, where we categorise cancer imaging challenges into five categories consisting of *data scarcity and usability* (4.1), *data access and privacy* (4.2), *data annotation and segmentation* (4.3.2), *detection and diagnosis* (4.4), and *treatment and monitoring* (4.5). In each subsection, we group and analyse respective cancer imaging challenges

and discuss the potential and the limitations of corresponding GAN solutions. In this regard, we also identify and highlight key needs to be addressed by researchers in the field of cancer imaging GANs towards solving the surveyed cancer imaging challenges. We provide respective tables 2-6 for each subsection 4.1-4.5 containing relevant information (publication, method, dataset, modality, task, highlights) for all of the reviewed cancer imaging GAN solutions.

4.1. Data Scarcity and Usability Challenges

4.1.1. Challenging Dataset Sizes and Shifts

Although data repositories such as The Cancer Imaging Archive (TCIA) [63] have made a wealth of cancer imaging data available for research, the demand is still far from satisfied. As a result, data augmentation techniques are widely used to artificially enlarge the existing datasets, traditionally including simple spatial (e.g., flipping, rotation) or intensity transformations (e.g., noise insertion) of the true data. GANs have shown promise as a more advanced augmentation technique and have already seen use in medical and cancer imaging [64, 26].

Aside from the issue of lacking sizeable data, data scarcity often forces studies to be constrained on small-scale single-centre datasets. The resulting findings and models are likely to not generalise well due to diverging distributions between the (synthetic) datasets seen in training and those seen in testing or after deployment, a phenomenon known as dataset shift [65]⁵. An example of this in clinical practice are cases where training data is preselected from specific patient sub-populations (e.g., only high-risk patients) resulting in bias and limited generalisability to the broad patient population [67, 24].

From a causality perspective, dataset shift can be split into several distinct scenarios [68]:

- *Population shift*, caused by differences in age, sex, ethnicities etc.
- *Acquisition shift*, caused by differences in scanners, resolution, contrast etc.

⁵More concretely, this describes a case of covariate shift [65, 66] defined by a change of distribution within the independent variables between two datasets

- *Annotation shift*, caused by differences in annotation policy, annotator experience, segmentation protocols etc.
- *Prevalence shift*, caused by differences in the disease prevalence in the population, often resulting from artificial sampling of data
- *Manifestation shift*, caused by differences in how the disease is manifested

GANs may inadvertently introduce such types of dataset shifts (i.e. due to mode collapse [25]), but it has been shown that this shift can be studied, measured and avoided [69, 70]. GANs can be a sophisticated tool for data augmentation or curation [71] and by calibrating the type of shift introduced, they have the potential to turn it into an advantage, generating diverse training data that can help models generalise better to unseen target domains. The research line studying this problem is called *domain generalisation*, and it has presented promising results for harnessing adversarial models towards learning of domain-invariant features [72]. GANs have been used in various ways in this context, using multi-source data to generalise to unseen targets [73, 74] or in an unsupervised manner using adaptive data augmentation to append adversarial examples iteratively [75]. As indicated in Figure 3(a), the domain generalisation research line has recently been further extended to cancer imaging [76, 77].

In the following, further cancer imaging challenges in the realm of data scarcity and usability are described and related GAN solutions are referenced. Given these challenges and solutions, we derive a workflow for clinical adoption of (synthetic) cancer imaging data, which is illustrated in Figure 5.

4.1.2. Imbalanced Data and Fairness

Apart from the rise of data-hungry deep learning solutions and the need to cover the different organs and data acquisition modalities, a major problem that arises from data scarcity is that of imbalance—i.e. the overrepresentation of a certain type of data over others [24]. In its more common form, imbalance of diagnostic labels can hurt a model’s specificity or sensitivity, as a prior bias from the data distribution may be learned. The Lung Screening Study (LSS) Feasibility Phase exemplifies the common class imbalance in cancer imaging data: 325 (20.5%)

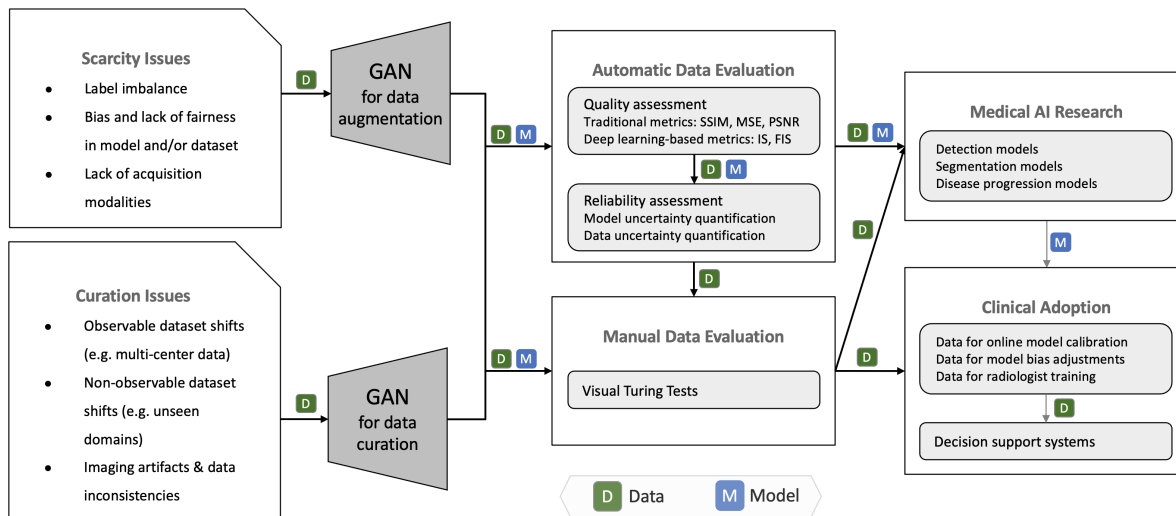


Figure 5: Illustration of a workflow that applies GANs to the challenges of data scarcity and data curation. After the GAN generates synthetic data specific to the issue at hand, the data is automatically and manually evaluated before further used in medical AI research. Ultimately, both synthetic data and medical AI models are integrated as decision support tools into clinical practice.

suspicious lung nodules were detected in the 1586 first low-dose CT screening, of which only 30 (1.89%) were lung cancers [78, 79, 80]. This problem directly translates to multi-task classification (CLF), with imbalance between different types of cancer leading to worse sensitivity on the underrepresented categories [81]. It is important to note that by solving the imbalance with augmentation techniques, bias is introduced as the prior distribution is manipulated, causing prevalence shift. As such, the test set should preserve the population statistics. Aside from imbalance of labels, more insidious forms of imbalance such as that of race [82] or gender [83] of patients are easily omitted in studies. This leads to fairness problems in real world applications as underrepresenting such categories in the training set will hurt performance on these categories in the real world (population shift) [84]. Because of their potential to generate synthetic data, GANs are a promising solution to the aforementioned problems and have already been thoroughly explored in Computer Vision [85, 86]. Concretely, the discriminator and generator can be conditioned on underrepresented labels, forc-

ing the generator to create images for a specific class⁶, as indicated in Figure 3(d). Many lesions classifiable by complex scoring systems such as RADS reporting are rare and, hence, effective conditional data augmentation is needed to improve the recognition of such lesions by ML detection models [88]. GANs have already been used to adjust label distributions in imbalanced cancer imaging datasets, e.g. by generating underrepresented grades in a risk assessment scoring system [89] for prostate cancer. A further promising applicable method is to enrich the data using a related domain as proxy input [90]. Towards the goal of a more diverse distribution of data with respect to gender and race, similar principles can be applied. For instance, Li et al [84] proposed an adversarial training scheme to improve fairness in classification of skin lesions for underrepresented groups (age, sex, skin tone) by learning a neutral representation using an adversarial bias discrimination loss. Fairness imposing GANs can also generate synthetic data with a preference for underrepresented groups, so that models may ingest a more bal-

⁶The class can be something as simple as ‘malignant’ or ‘benign’, or a more complex score for risk assessment of a tumour such as the BiRADS scoring system for breast tumours [87]

anced dataset, improving demographic parity without excluding data from the training pipeline. Such models have been trained in computer vision tasks [91, 92, 93, 94, 95], but corresponding research on medical and cancer imaging denoted by Figure 3(c) has been limited [84, 96].

4.1.3. Cross-modal Data Generation

In cancer, multiple acquisition modalities are enlisted in clinical practice [97, 98, 99, 100, 101]; thus automated diagnostic models should ideally learn to interpret various modalities as well or learn a shared representation of these modalities. Conditional GANs offer the possibility to generate one modality from another, alleviating the need to actually perform the potentially more harmful screenings—i.e. high-dose CT, PET—that expose patients to radiation, or require invasive contrast agents such as intravenous iodine-based contrast media (ICM) in CT [102], gadolinium-based contrast agents in MRI [103](in Table 5) or radioactive tracers in PET [104, 105]. Furthermore, extending the acquisition modalities used in a given task would also enhance the performance and generalisability of AI models, allowing them to learn shared representations among these imaging modalities [24, 106]. Towards this goal, multiple GAN domain-adaptation solutions have been proposed to generate CT using MRI [107, 108, 109, 110, 111, 112, 113], PET from MRI [104], PET from CT [114], [115] (in Table 5), and CT from PET as in Armanious et al [116], where also PET denoising and MR motion correction are demonstrated. If not indicated otherwise, these image-to-image translation studies are outlined in Table 2. Because of its complexity, clinical cancer diagnosis is based not only on imaging but also non-imaging data (genomic, molecular, clinical, radiological, demographic, etc). In cases where this data is readily available, it can serve as conditional input to GANs towards the generation of images with the corresponding phenotype-genotype mapping, as is also elaborated in regard to tumour profiling for treatment in section 4.5.1. A multimodal cGAN was recently developed, conditioned on both images and gene expression code [117]; however, research along this line is otherwise limited.

4.1.4. Feature Hallucinations in Synthetic Data

As displayed in Figure 6 and denoted in Figure 3(b), conditional GANs can unintentionally⁷ hallucinate non-existent artifacts into a patient image. This is particularly likely to occur in cross-modal Data augmentation, especially but not exclusively if the underlying dataset is imbalanced. For instance, Cohen et al [118] describe GAN image feature hallucinations embodied by added and removed brain tumours in cranial MRI. The authors tested the relationship between the ratio of tumour images in the GAN target distribution and the ratio of images diagnosed with tumours by a classifier. The classifier was trained on the GAN generated target dataset, but tested on a balanced holdout testset. It was thereby shown that the generator of CycleGAN effectively learned to hide source domain image features in target domain images, which arguably helped it to fool its discriminator. Paired image-to-image translation with pix2pix [55] was more stable, but still some hallucinations were shown to likely have occurred. A cause for this can be a biased discriminator that has learned to discriminating specific image features (e.g., tumours) that are more present in one domain. Cohen et al [118, 119] and Wolterink et al [120] warn that models that map source to target images, have an incentive to add/remove features during translation if the feature distribution in the target domain is distinct from the feature distribution in the source domain⁸.

Domain-adaptation with unpaired image-to-image translation GANs such as CyleGAN has become increasingly popular in cancer imaging [107, 109, 121, 122, 105, 123, 124, 108, 125, 126, 127]. As described, these unsupervised methods are hallucination-prone and, thus, can put patients at risk when used in clinical settings. More research is needed on how to robustly avoid or detect and eliminate hallucinations in generated data. To this end, we highlight the potential of investigating feature preserving image translation techniques and methods for evaluating features have been accurately translated. For instance, in the presence of feature masks or annotations, an additional local reconstruction loss function can be introduced in GANs that enforces feature translation in specific im-

⁷Intentional feature injection or removal is discussed in 4.2.5

⁸For example, if one domain contains mainly healthy images, while the other domain contains mainly pathological images.

age areas.

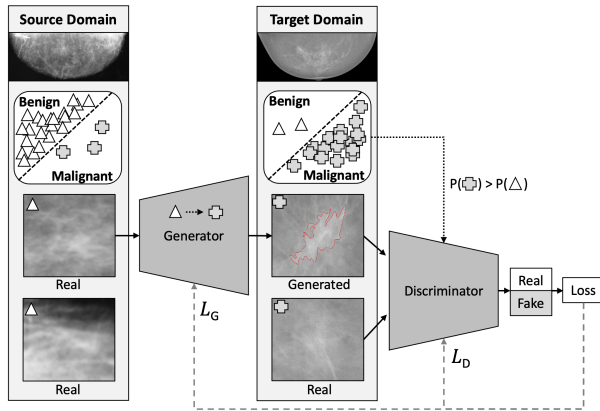


Figure 6: Example of a GAN that translates Film Scanned MMG (source) to Full-Field Digital MMG (target). The generator transforms ‘benign’ source images (triangles) into ‘malignant’ target images (plus symbols). As opposed to source, the target domain contains more malignant MMGs than benign ones. If the discriminator thus learns to associate malignancy with realness, this incentivises the generator to inject malignant features (depicted by dotted arrows). For simplicity additional losses (e.g., reconstruction losses) are omitted.

4.1.5. Data Curation and Harmonisation

Aside from the limited availability of cancer imaging datasets, a major problem is that the ones available are often not readily usable and require further curation [106]. Curation includes dataset formatting, normalising, structuring, de-identification, quality assessment and other methods to facilitate subsequent data processing steps, one of which is the ingestion of the data into AI models [71]. In the past, GANs have been proposed for curation of data labelling, segmentation and annotation of images (details in section 4.3.2) and de-identification of facial features, EHRs, etc (details in section 4.2). Particular to cancer imaging datasets and of significant importance is the correction of artifacts (patient motion, metallic objects, chemical shifts and others caused by the image processing pipeline [128, 129]) which run the risk of confusing models with spurious information. Towards the principled removal of artifacts, several GAN solutions have been proposed [130, 131]. As for the task of reconstruction of compressed data (e.g., compressed sensing MRI [132]), markedly, Yang et al [133] proposed

DAGAN, which is based on U-net [58], reduces aliasing artifacts, and faithfully preserves texture, boundaries and edges (of brain tumours) in the reconstructed images. Kim et al [134] feed down-sampled high-resolution brain tumour MRI into a GAN framework similar to pix2pix to reconstruct high-resolution images with different contrast. The authors highlight the possible acceleration of MR imagery collection while retaining high-resolution images in multiple contrasts, necessary for further clinical decision-making. As relevant to the context of data quality curation, GANs have also been proposed for image super-resolution in cancer imaging (e.g., for lung nodule detection [135], abdominal CT [136], and breast histopathology [137]).

Beyond the lack of curation, a problem particular to multi-centre studies is that of inconsistent curation between data derived in different centres. These discontinuities arise from different scanners, segmentation protocols, demographics, etc, and can cause significant problems to subsequent ML algorithms that may overfit or bias towards one configuration over another (i.e. acquisition and annotation shifts). GANs have the potential to contribute in this domain as well by bringing the distributions of images across different centres closer together. In this context a recent work by Li et al [138] and Wei et al [139] used GAN-based volumetric normalisation to reduce the variability of heterogeneous 3D chest CT scans of different slice thickness and dose levels. The authors showed that features in subsequent radiomics analysis exhibit increased alignment. Other works in this domain include a framework that could standardise heterogeneous datasets with a single reference image and obtained promising results on an MRI dataset [123], and GANs that learn bidirectional mappings between different vendors to normalise dynamic contrast enhanced (DCE) breast MRI [121]. An interesting research direction to be explored in the future is synthetic multi-centre data generation using GANs, simulating the distribution of various scanners/centres.

4.1.6. Synthetic Data Assessment

As indicated in Figure 3(e), a condition of paramount importance is proper evaluation of GAN-generated or GAN-curated data. This evaluation is to verify that synthetic data is usable for a desired downstream task (e.g., segmentation, classification) and/or indistinguish-

able from real data while ensuring that no private information is leaked. GANs are commonly evaluated based on *fidelity* (realism of generated samples) and *diversity* (variation of generated samples compared to real samples) [140]. Different quantitative measures exist to assess GANs based on the fidelity and diversity of its generated synthetic medical images [26, 140].

Visual Turing tests (otherwise referred to as Visual Assessment, Mean Opinion Score (MOS) Test, and sometimes used interchangeably with In-Silico Clinical Trials) are arguably the most reliable approach, where clinical experts are presented with samples from real and generated data and are tasked to identify which one is generated. Korkinof et al [141] showed that their PGGAN [39]-generated 1280x1024 mammograms were inseparable by the majority of participants, including trained breast radiologists. A similar visual Turing test was successfully done in the case of skin disease [96], super-resolution of CT [136], brain MRI [88, 64], lung cancer CT scans [142], and histopathology images [143]. For instance, Chuquicusma et al [142] trained a DC-GAN [51] on the LIDC-IDRI dataset [144] to generate 2D (56x56 pixel) pulmonary lung nodule scans that were realistic enough to deceive 2 radiologists with 11 and 4 years of experience. In contrast to computer vision techniques where synthetic data can often be easily evaluated by any non-expert, the requirement of clinical experts makes Visual Turing Tests in this domain much more costly. Furthermore, a lack of scalability and consistency in medical judgement needs to be taken into account as well [145] and visual Turing tests should in the ideal case engage a range of experts to address inter-observer variation in the assessments. Also, iterating over the same observer addresses intra-observer variation—i.e. repeating the process within a certain amount of intervals that could be days or weeks. These problems are further magnified by the shortage of radiology experts [146, 147] which brings up the necessity for supplementary metrics that can automate the evaluation of generative models. Such metrics allow for preliminary evaluation and can enable research to progress without the logistical hurdle of enlisting experts.

Furthermore, in cases where the sole purpose of the generated data is to improve a downstream task—i.e. classification or segmentation—then the prediction success of the downstream task would be the metric of interest.

The latter can reasonably be prioritised over other metrics given that the underlying reasons why the synthetic data alters downstream task performance are examined and clarified⁹.

Image Quality Assessment Metrics. Wang et al [148] have thoroughly investigated image quality assessment metrics. The most commonly applied metrics include structural similarity index measure (SSIM)¹⁰ between generated image and reference image [148], mean squared error (MSE)¹¹ and peak signal-to-noise ratio (PSNR)¹². In a recent example that followed this framework of evaluation, synthetic brain MRI with tumours generated by edge-aware EA-GAN [149] was assessed using three such metrics: PSNR, SSIM, and normalised mean squared error (NMSE). The authors integrated an end-to-end sobel edge detector to create edge maps from real/synthetic images that are input into the discriminator in the dEa-GAN variant to enforce improved textural structure and object boundaries. Interestingly, aside from evaluating on the whole image, the authors demonstrated evaluation results focused on the tumour regions, which were overall significantly lower than the whole image. Other works that have evaluated their synthetic images in an automatic manner have focused primarily on the SSIM and PSNR metrics and include generation of CT [108, 124] and PET scans [105]. While indicative of image quality, these similarity-based metrics might not generalise well to human judgement of image similarity, the latter depending on high-order image structure and context [150]. Finding evaluation metrics that are strong correlates of human judgement of perceptual image similarity is a promising line of research. In the context of cancer and medical imaging, we highlight the need for evaluation metrics for synthetic images that correlate with the

⁹For example, synthetic data may balance imbalanced datasets, reduce overfitting on limited training data, or improve model robustness to better capture domain shifts in the test dataset.

¹⁰SSIM predicts perceived quality and considers image statistics to assess structural information based on luminance, contrast, and structure.

¹¹MSE is computed by averaging the squared intensity differences between corresponding pixels of the generated image and the reference image.

¹²PSNR is an adjustment to the MSE score, commonly used to measure reconstruction quality in lossy compression.

perceptual image similarity judged by medical experts. Apart from perceptual image similarity, further evaluation metrics in cancer and medical imaging are to be investigated that are able to estimate the diagnostic value of (synthetic) images and, in the presence of reference images, the diagnostic value proportion between target and reference image.

GAN-specific Assessment Metrics. In recent years, the Inception score (IS) [151] and Fréchet Inception distance (FID) [152] have emerged, offering a more sophisticated alternative for the assessment of synthetic data. The IS uses a classifier to generate a probability distribution of labels given a synthetic image. If the probability distribution is highly skewed, it is indicative that a specific object is present in the image (resulting in a higher IS), while in the case where it is uniform, the image contains a jumble of objects and that is more likely to be non-sense (resulting in a lower IS).¹³ The FID metric compares the distance between the synthetic image distribution to that of the real image distribution by comparing extracted high-level features from one of the layers of a classifier (e.g., Inception v3 as in IS). Both metrics have shown great promise in the evaluation of GAN-generated data; however, they come with several bias issues that need to be taken into account during evaluation [153, 154, 155]. As these metrics have not been used in cancer imaging yet, their applicability on GAN-synthesised cancer images remains to be investigated. In contrast to computer vision datasets containing diverse objects, medical imaging datasets commonly only contain images of one specific organ. We promote further research as to how object diversity based methods such as IS can be applied to medical and cancer imaging, which requires, among others, meaningful adjustments of the dataset-specific pretrained classifications models (i.e. Inception v3) that IS and FID rely upon.

Uncertainty Quantification as GAN Evaluation Metric? A general problem facing the adoption of deep learning methods in clinical tasks is their inherent unreliability ex-

emplified by high prediction variation caused by minimal input variation (e.g., one pixel attack [156]). This is further exacerbated by the nontransparent decision making process inside deep neural networks thus often described as ‘black box models’ [24]; Also, the performance of deep learning methods in out-of-domain datasets has been assessed as unreliable [157]. To eventually achieve beneficial clinical adoption and trust, examining and reporting the inherent uncertainty of these models on each prediction becomes a necessity. Besides classification, segmentation [158, 159], etc, uncertainty estimation is applicable to models in the context of data generation as well [157, 160, 158]. Edupuganti et al [161] studied a GAN architecture based on variational autoencoders (VAE) [162] on the task of MRI reconstruction, with emphasis on uncertainty studies. Due to their probabilistic nature, VAEs allowed for a Monte Carlo sampling approach which enables quantification of pixel-variance and the generation of uncertainty maps. Furthermore, they used Stein’s Unbiased Risk Estimator (SURE) [163] as a measure of uncertainty that serves as surrogate of MSE even in the absence of ground truth. Their results indicated that adversarial losses introduce more uncertainty. Parallel to image reconstruction, uncertainty has also been studied in the context of brain tumours (glioma) in MRI enhancement [164]. In this study, a probabilistic deep learning framework for model uncertainty quantification was proposed, decomposing the problem into two uncertainty types: *intrinsic uncertainty* (particular to image enhancement and pertaining to the one-to-many nature of the super-resolution mapping) and *parameter uncertainty* (a general challenge, it pertains to the choice of the optimal model parameters). The overall model uncertainty in this case is a combination of the two and was evaluated for image super-resolution. Through a series of systematic studies the utility of this approach was highlighted, as it resulted in improved overall prediction performance of the evaluated models even for out-of-distribution data. It was further shown that predictive uncertainty highly correlated with reconstruction error, which not only enabled spotting unrealistic synthetic images, but also highlights the potential in further exploring uncertainty as an evaluation metric for GAN-generated data. A further use-case of interest for GAN evaluation via uncertainty estimation is the ‘adherence’ to provided conditional inputs. As elaborated in 4.1.4 for image-to-image translation, conditional

¹³Not only a low label entropy within an image is desired, but also a high label entropy across images: IS also assesses the variety of peaks in the probability distributions generated from the synthetic images, so that a higher variety is indicative of more diverse objects being generated by the GAN (resulting in a higher IS).

GANs are likely to introduce features that do not correspond to the conditional class label or source image. After training a classification model on image features of interest (say, tumour vs non-tumour features), we can examine the classifier’s prediction and estimated uncertainty¹⁴ for the generated images. Given the expected features in the generated images are known beforehand, the classifier’s uncertainty of the presence of these features can be used to estimate not only image fidelity (e.g., image features are not generated realistic enough), but also ‘condition adherence’ (e.g., expected image features are altered during generation).

Outlook on Clinical Adoption. Alongside GAN-specific and standard image assessment metrics, uncertainty-based evaluation schemes can further automate the analysis of generative models. To this end, the challenge of clinical validation for predictive uncertainty as a reliability metric for synthetic data assessment remains [164]. In practice, building clinical trust in AI models is a non-trivial endeavour and will require rigorous performance monitoring and calibration especially in the early stages [167, 168]. This is particularly the case when CAde and CADx models are trained on entirely (or partially) synthetic data given that the data itself was not first assessed by clinicians. Until a certain level of trust is built in these pipelines, automatic metrics will be a preliminary evaluation step that is inevitably followed by diligent clinical evaluation for deployment. A research direction of interest in this context would be ‘gatekeeper’ GANs—i.e. GANs that simulate common data (and/or difficult edge cases) of the target hospital, on which deployment-ready candidate models (e.g., segmentation, classification, etc) are then tested to ensure they are sufficiently generalisable. If the candidate model performance on such test data satisfies a predefined threshold, it has passed this quality gate for clinical deployment.

4.2. Data Access and Privacy Challenges

Access to sufficiently large and labelled data resources is the main constraint for the development of deep learning models for medical imaging tasks [187]. In cancer

imaging, the practice of sharing validated data to aid the development of AI algorithms is restricted due to technical, ethical, and legal concerns [24]. The latter is exemplified by regulations such as the Health Insurance Portability and Accountability Act (HIPAA) [188] in the United States of America (USA) or the European Union’s General Data Protection Regulation (GDPR) [189] with which respective clinical centres must comply with. Alongside the need and numerous benefits of patient privacy preservation, it can also limit data sharing initiatives and restrict the availability, size and usability of public cancer imaging datasets. Bi et al [24] assess the absence of such datasets as a noteworthy challenge for AI in cancer imaging.

The published GANs that are suggested for or applied to cancer imaging challenges within this section 4.2 are summarised below in Table 3.

4.2.1. Decentralised Data Generation

As AI systems are often developed and trained outside of medical institutions, prior approval to transfer data out of their respective data silos is required, adding significant hurdles to the logistics of setting up a training pipeline or rendering it entirely impossible. In addition, medical institutions can often not guarantee a secured connection to systems deployed outside their centres [106], which further limits their options to share valuable training data.

One privacy preserving approach solving this problem is federated learning [190], where copies of an AI model are trained in a distributed fashion inside each clinical centre in parallel and are aggregated to a global model in a central server. This eliminates the need for sensitive patient data to leave any of the clinical centres [191, 192]. However, it is to be noted that federated learning cannot guarantee full patient privacy. Hitaj et al [193] demonstrated that any malicious user can train a GAN to violate the privacy of the other users in a federated learning system. While difficult to avoid, the risk of such GAN-based attacks can be minimised, e.g., by using a combination of selective parameter updates [194] (sharing only a small selected part of the model parameters across centres) and the sparse vector technique¹⁵ as shown by Li et al [197].

¹⁴The uncertainty can be estimated using methods such as Monte-Carlo Dropout [165] or Deep Ensembles [166].

¹⁵Sparse Vector Technique (SVT) [195] is a Differential Privacy (DP) [196] method that introduces noise into a deep learning model’s

Table 2: Overview of adversarially-trained models applied to cancer imaging data scarcity and usability challenges. Publications are clustered by section and ordered by year in ascending order.

Publication	Method	Dataset	Modality	Task	Highlights
Imbalanced Data & Fairness					
Hu et al (2018) [89]	ProstateGAN	Private	Prostate MRI	Conditional Synthesis	Gleason score (cancer grade) class conditions.
Ghorbani et al (2020) [96]	DermGAN	Private	Dermoscopy	Image synthesis	Adapted pix2pix, evaluated via Turing Tests and <i>rare</i> skin condition CLF.
Li et al (2021) [84]	Encoder	ISIC 2018 [169]	Dermoscopy	Representation learning	Fair Encoder with bias discriminator and skin lesion CLF.
Cross-Modal Data Generation					
Wolterink et al (2017) [107]	CycleGAN	Private	Cranial MRI/CT	Unpaired translation	First CNN for unpaired MR-to-CT translation. Evaluated via PSNR and MAE.
Ben-Cohen et al (2017) [114]	pix2pix	Private	Liver PET/CT	Paired translation	Paired CT-to-PET translation with focus on hepatic malignant tumours.
Nie et al (2017) [111]	context-aware GAN	ADNI [170, 171]	Cranial/pelvic MRI/CT	Paired translation	Supervised 3D GAN for MR-to-CT translation with 'Auto-Context Model' (ACM).
Wang et al (2018) [104]	Locality Adaptive GAN (LA-GAN)	BrainWeb [172]	Cranial MRI, PET phantom	Paired translation	3D auto-context, synthesising PET from low-dose PET and multimodal MRI.
Tanner et al (2018) [109]	CycleGAN	VISCERAL [173]	Lung/abdominal MRI/CT	Image registration	Unsupervised MR-CT CycleGAN for registration.
Kaiser et al (2019) [110]	pix2pix, context-aware GAN [111]	RIRE [174]	Cranial MRI/CT	Paired translation	Detailed preprocessing description, MR-to-CT translation, comparison with U-Net.
Prokopenko et al (2019) [113]	DualGAN, SRGAN	CPTAC3 [63, 175], Head-Neck-PET-CT [176, 63]	Cranial MRI/CT	Unpaired translation	DualGAN for unpaired MR-to-CT, visual Turing tests.
Zhao et al (2020) [105]	S-CycleGAN	Private	Cranial low/full dose PET	Paired translation	Low (LDPET) to full dose (FDPET) translation with supervised loss for paired images.
Kearney et al (2020) [108]	VAE-enhanced A-CycleGAN	Private	Cranial MRI/CT	Unpaired translation	MR-to-CT evaluated via PSNR, SSIM, MAE. Superior to paired alternatives.
Kazemifar et al (2020) [112]	context-aware GAN	Private	Cranial MRI/CT	Paired translation	Feasibility of generated CT from MRI for dose calculation for radiation treatment.
Armanious et al (2020) [116]	MedGAN	Private	Liver PET/CT	Paired translation	CasNet architecture, PET-to-CT, MRI motion artifact correction, PET denoising.
Xu et al (2020) [117]	multi-conditional GAN	NSCLC [177]	Lung CT, gene expression	Conditional synthesis	Image-gene data fusion/correlation, nodule generator input: background image, gene code.
Haubold et al (2021) [102]	Pix2PixHD [57]	Private	Arterial phase CT	Paired translation	Low-to-full ICM CT (thorax, liver, abdomen), 50% reduction in intravenous ICM dose.
Feature Hallucinations					
Cohen et al (2018) [118, 119]	CycleGAN, pix2pix	BRATS2013 [178]	Cranial MRI	Paired/unpaired translation	Removed/added tumours during image translation can lead to misdiagnosis.
Data Curation					
Yang et al (2018) [133]	DAGAN	MICCAI 2013 grand challenge dataset	Cranial MRI	Image reconstruction	Fast GAN compressed sensing MRI reconstruction outperformed conventional methods.
Kim et al (2018) [134]	pix2pix-based	BRATS [178]	Cranial MRI	Reconstruction/ super-resolution	Information transfer between different contrast MRI, effective pretraining/fine-tuning.
Hognon et al (2019) [123]	CycleGAN, pix2pix	BRATS [178], BrainWeb [172]	Cranial MRI	Paired/unpaired translation, normalisation	CycleGAN translation to BrainWeb reference image, pix2pix back-translation to source.
Modanwal et al (2019) [121]	CycleGAN	Private	Breast MRI	Unpaired translation	Standardising DCE-MRI across scanners, anatomy preserving mutual information loss.
You et al (2019) [136]	CycleGAN-based	Mayo Low Dose CT [179]	Abdominal CT	Super-resolution	Joint constraints to Wasserstein loss for structural preservation. Evaluated by 3 radiologists.
Gu et al (2020) [135]	MedSRGAN	LUNA16 [180]	MRI/thoracic CT	Super-resolution	Residual Whole Map Attention Network (RW-MAN) in G. Evaluated by 5 radiologists.
Vu et al (2020) [130]	WGAN-GP-based	k-Wave toolbox [181]	Photoacoustic CT (PACT)	Paired translation	U-NET and WGAN-GP based generator for artifact removal. Evaluated via SSIM, PSNR.
Koike et al (2020) [131]	CycleGAN	Private	Head/neck CT	Unpaired translation	Metal artifact reduction via CT-to-CT translation, evaluated via radiotherapy dose accuracy.
Wei et al (2020) [139]	WGAN-GP-inspired	Private	Chest CT	Paired translation	CT normalisation of dose/slice thickness. Evaluated via Radiomics Feature Variability.
Shahidi et al (2021) [137]	WA-SRGAN	BreakHis [182], Camelyon [183]	Breast/lymph node histopathology	Super-resolution	Wide residual blocks, self-attention SRGAN for improved robustness & resolution
Li et al (2021) [138]	SingleGAN-based [184]	Private	Spleen/colorectal CT	Unpaired translation	Multi-centre (4) CT normalisation. Evaluated via cross-centre radiomics features variation. Short/long-term survivor CLF improvement.
Synthetic Data Assessment					
Kazuhiro et al (2018) [88]	DCGAN	Private	Cranial MRI	Image synthesis	Feasibility study for brain MRI synthesis evaluated by 7 radiologists.
Han et al (2018) [64]	DCGAN, WGAN	BRATS 2016 [178]	Cranial MRI	Image synthesis	128x128 brain MRI synthesis evaluated by one expert physician.
Chuquicusma et al (2018) [142]	DCGAN	LIDC-IDRI[144]	Thoracic CT	Image synthesis	Malignant/benign lung nodule ROI generation evaluated by two radiologists.
Yu et al (2019) [149]	Ea-GAN	BRATS 2015 [178], IXI [185]	Cranial MRI	Paired translation	Loss based on edge maps of synthetic images. Evaluated via PSNR, NMSE, SSIM.
Korkinof et al (2020) [141]	PGGAN	Private	Full-field digital MMG	Image synthesis	1280x1024 MMG synthesis from > 10 ⁶ image dataset. Evaluated by 55 radiologists.
Levine et al (2020) [143]	PGGAN, VAE, ESRGAN	TCGA[186], OVCARE archive	Ovarian Histopathology	Image synthesis	1024x1024 whole slide synthesis. Evaluated via FID and by 15 pathologists (9 certified)

To solve the challenge of privacy assurance of clinical medical imaging data, a distributed GAN [198, 199, 200, 201, 202] can be trained on sensitive patient data to generate synthetic training data. The technical, legal, and ethical constraints for sharing such de-identified synthetic data are typically less restrictive than for real patient data. Such generated data can be used instead of the real patient data to train models on disease detection, segmentation, or prognosis.

For instance, Chang et al [100, 101] proposed the Distributed Asynchronized Discriminator GAN (AsynDGAN), which consists of multiple discriminators deployed inside various medical centres and one central generator deployed outside the medical centres. The generator never needs to see the private patient data, as it learns by receiving the gradient updates of each of the discriminators. The discriminators are trained to differentiate images of their medical centre from synthetic images received from the central generator. After training AsynDGAN, its generator is used and evaluated based on its ability to provide a rich training set of images to successfully train a segmentation model. AsynDGAN is evaluated on MRI brain tumour segmentation and cell nuclei segmentation. The segmentation models trained only on AsynDGAN-generated data achieves a competitive performance when compared to segmentation models trained on the entire dataset of real data. Notably, models trained on AsynDGAN-generated data outperform models trained on local data from only one of the medical centres. To our best knowledge, AsynDGAN is the only distributed GAN applied to cancer imaging to date. Therefore, we promote further research in this line to fully exploit the potential of privacy-preservation using distributed GANs. As demonstrated in Figure 7 and suggested in Figure 3(f), for maximal privacy preservation we recommend exploring methods that combine privacy during training (e.g., federated GANs) with privacy after training (i.e. differentially-private GANs), the latter being described in the following section.

4.2.2. Differentially-Private Data Generation

Shin et al [203] train a GAN to generate brain tumour images and highlight the usefulness of their method for

gradients.

anonymisation, as their synthetic data cannot be attributed to a single patient but rather only to an instantiation of the training population. However, it is to be scrutinised whether such synthetic samples are indeed fully private, as, given a careful analysis of the GAN model and/or its generated samples, a risk of possible reconstruction of part of the GAN training data exists [204]. For example, Chen et al [205] propose a GAN for model inversion (MI) attacks, which aim at reconstructing the training data from a target model’s parameters. A potential solution to avoid training data reconstruction is highlighted by Xie et al [206], who propose the Differentially Private Generative Adversarial Network (DPGAN). In Differential Privacy (DP) [196] the parameters (ϵ, δ) denote the privacy budget [207], where ϵ measures the privacy loss and δ represents the probability that a range of outputs with a privacy loss $> \epsilon$ exists¹⁶. Hence, the smaller the parameters (ϵ, δ) for a given model, the less effect a single sample in the training data has on model output. The less effect of such a single sample, the stronger is the confidence in the privacy of the model to not reveal samples of the training data.

Examples of GANs with Differential Privacy Guarantees.

In DPGAN noise is added to the model’s gradients during training to ensure training data privacy. Extending on the concept of DPGAN, Jordon et al [208] train a GAN coined PATE-GAN based on the Private Aggregation of Teacher Ensembles (PATE) framework [204, 209]. In the PATE framework, a student model learns from various unpublished teacher models each trained on data subsets. The student model cannot access an individual teacher model nor its training data. PATE-GAN consists of k discriminator teachers, T_1, \dots, T_k , and a student discriminator S that backpropagates its loss back into the generator. This limits the effect of any individual sample in PATE-GAN’s training. In a $(\epsilon = 1, \delta = 10^{-5})$ -DP setting, classification models trained on PATE-GAN’s synthetic data achieves competitive performances e.g. on a *non-imaging*

¹⁶For example, if an identical model M is trained two times, once with training data D resulting in M_D and once with marginally different training data D' resulting in $M_{D'}$, it is (ϵ) -DP if the following holds true: For any possible output x , the output probability for x of model M_D differs no more than $\exp(\epsilon)$ from the output probability for x of $M_{D'}$.

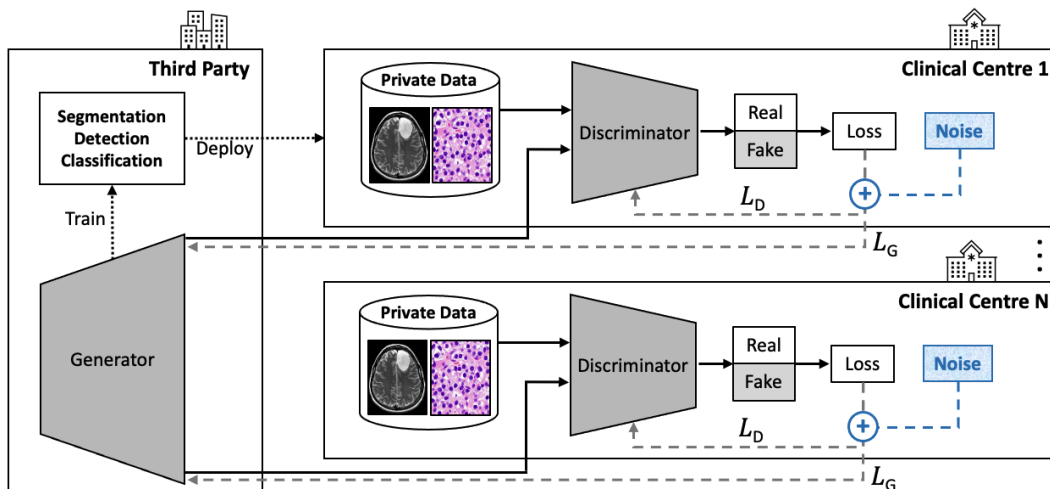


Figure 7: Visual example of a GAN in a federated learning setup with a central generator trying to generate realistic samples that fool all of the discriminators, which are distributed across clinical centres as in Chang et al [100, 101]. Once trained, the generator can produce training data for a downstream task model (e.g., segmentation, detection, classification). As depicted in blue colour, we suggest to extend the federated learning setup by adding ‘Noise’ to the gradients providing a differential privacy guarantee. This reduces the possibility of reconstruction of specific records of the training data (i.e. images of a specific patient) by someone with access to the trained GAN model (i.e. to the generator) or by someone intercepting the synthetic images while they are transferred from the central generator to the centres during training.

cervical cancer dataset [210] compared to an upper bound vanilla GAN baseline without DP.

On the same dataset, Torfi et al [207] achieve competitive results using a Rényi Differential Privacy and Convolutional Generative Adversarial Networks (RDP-CGAN) under an equally strong ($\epsilon = 1, \delta = 10^{-5}$)-DP setting.

For the generation of biomedical participant data in clinical trials, Beaulieu-Jones et al [211] apply an AC-GAN under a ($\epsilon = 3.5, \delta = 10^{-5}$)-DP setting based on Gaussian noise added to AC-GAN’s gradients during training.

Bae et al [212] propose AnomiGAN to anonymise private medical data via some degree of output randomness during inference. This randomness of the generator is achieved by randomly adding, for each layer, one of its separately stored training variances. AnomiGAN achieves competitive results on a *non-imaging* breast cancer dataset and a *non-imaging* prostate cancer for any of the reported privacy parameter values $\epsilon \in [0.0, 0.5]$ compared to DP, where Laplacian noise is added to samples.

Outlook on Synthetic Cancer Image Privacy. Despite the above efforts, DP in GANs has only been applied to non-

imaging cancer data which indicates research potential for extending these methods reliably to cancer imaging data. According to Stadler et al [213], using synthetic data generated under DP can protect outliers in the original data from linkage attacks, but likely also reduces the statistical signal of these original data points, which can result in lower utility of the synthetic data. Apart from this privacy-utility tradeoff, it may not be readily controllable/predictable which original data features are preserved and which omitted in the synthetic datasets [213]. In fields such as cancer imaging where patient privacy is critical, desirable privacy-utility tradeoffs need to be defined and thoroughly evaluated to enable trust, shareability, and usefulness of synthetic data. Consensus is yet to be found as to how privacy preservation in GAN-generated data can be evaluated and verified in the research community and in clinical practice. Promising approaches include methods that define a privacy gain/loss for synthetic samples [213, 214]. Yoon et al [214], for instance, define and backpropagate an identifiability loss to the generator to synthesis anonymised electronic health records (EHRs). The identifiability loss is based on the notion that the minimum weighted euclidean distance be-

tween two patient records from two different patients can serve as a desirable anonymisation target for synthetic data. Designing or extending reliable methods and metrics for standardised quantitative evaluation of patient privacy preservation in synthetic medical images is a line of research that we call attention to.

4.2.3. *Obfuscation of Identifying Patient Features in Images*

If the removal of all sensitive patient information within a cancer imaging dataset allows for sharing such datasets, then GANs can be used to obfuscate such sensitive data. As indicated by Figure 3(g), GANs can learn to remove the features from the imaging data that could reveal a patient’s identity, e.g. by learning to apply image inpainting to pixel or voxel data of burned in image annotations or of identifying body parts. Such identifying body parts could be the facial features of a patient, as was shown by Schwarz et al [215] on the example of cranial MRI. Numerous studies exist where GANs accomplish facial feature de-identification on non-medical imaging modalities [216, 217, 218, 219]. For medical imaging modalities, GANs have yet to prove themselves as tool of choice for anatomical and facial feature de-identification against common standards [220, 221, 222, 223] with solid baselines. These standards, however, have shown to be susceptible to reconstruction achieved by unpaired image-to-image GANs on MRI volumes with high reversibility for blurred faces and partial reversibility for removed facial features [224]. Van der Goten et al [225] provide a first proof-of-concept for GAN-based facial feature de-identification in 3D (128^3 voxel) cranial MRI. The generator of their conditional de-identification GAN (C-DeID-GAN) receives brain mask, brain intensities and a convex hull of the brain MRI as input and generates de-identified MRI slices. C-DeID-GAN generates the entire de-identified brain MRI scan and, hence, may not be able to guarantee that the generation process does not alter any of the original brain features. A solution to this can be to only generate and replace the 2D MRI slices or parts thereof that do contain non-pathological facial features while retaining all other original 2D MRI slices. Presuming preservation of medically relevant features and robustness of de-identification, GAN-based approaches can allow for subsequent medical analysis, privacy preserving data sharing and provision of de-identified training

data. Hence, we highlight the research potential of GANs for robust medical image de-identification e.g. via image inpainting GANs that have already been successful applied to other tasks in cancer imaging such as synthetic lesion inpainting into mammograms [226, 227] and lung CT scans [228]. Also, GAN methods that are adjustable and trainable to remain quantifiably robust against adversarial image reconstruction are a research line of interest.

4.2.4. *Identifying Patient Features in Latent Representations*

In line with Figure 3(g), a further example for privacy preserving methods are autoencoders¹⁷ that learn patient identity-specific features and obfuscate such features when encoding input images into latent space representation. Such an identity-obfuscated representation can be used as input into further models (classification, segmentation, etc) or decoded back into a de-identified image. Adversarial training has been shown to be effective for learning a privacy-preserving encoding function, where a discriminator tries to succeed at classifying the private attribute from the encoded data [232, 233, 234, 235]. Apart from being trained via the backpropagated adversarial loss, the encoder needs at least one further utility training objective to learn to generate useful representations, such as denoising [236] or classification of a second attribute (e.g., facial expressions [237, 238]). Siamese Neural Networks [239] such as the Siamese Generative Adversarial Privatizer (SGAP) have been used effectively for adversarial training of an identity-obfuscated representation encoder. In SGAP, two weight-sharing Siamese Discriminators are trained using a distance based loss function to learn to classify whether a pair of images belongs to the same person [238]. As visualised in Figure 8, Kim et al [229] follow a similar approach with the goal of de-identifying and segmenting brain MRI data. Two feature maps are encoded from a pair of MRI scans and fed into a Siamese Discriminator that evaluates via binary classification whether the two feature maps are from the same patient. The generated feature maps are also fed into a segmentation model that backpropagates a Dice loss [240] to

¹⁷For example adversarial autoencoders [230, 231], which adversarially learn latent space representations that match a chosen prior distribution.

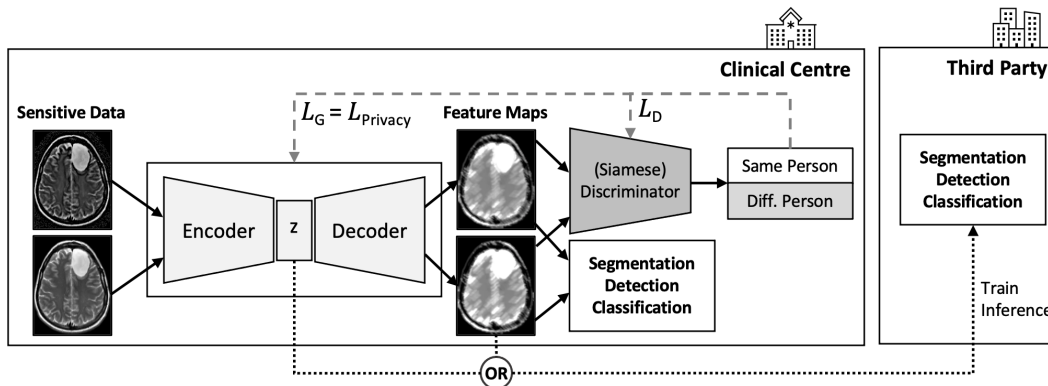


Figure 8: Example of an autoencoder architecture trained via adversarial loss to learn privacy-preserving feature maps as in Kim et al [229] and/or a privacy-preserving latent representation z . Once trained and after thorough periodic manual verification of its ability to preserve privacy, the representation z and/or the feature maps can be sent to third parties outside the clinical centre for model training or inference requests.

train the encoder. Figure 8 illustrates the scenario where the encoder is deployed in a trusted setting after training, e.g. in a clinical centre, and the segmentation model is deployed in an untrusted setting, e.g. outside the clinical centre at a third party. The encoder shares the identity-obfuscated feature maps with the external segmentation model without the need of transferring the sensitive patient data outside the clinical centre. This motivates further research into adversarial identity-obfuscated encoding methods e.g., to allow sharing and usage of cancer imaging data representations and models across clinical centres.

4.2.5. Adversarial Attacks Putting Patients at Risk

Apart from preserving privacy, GANs can also be a threat to sensitive patient data when used to launch adversarial attacks. Such adversarial attacks can fool machines (i.e. deep learning models) as well as humans (i.e. radiologists). Consider an intrusive generator that maliciously alters MRI images that are subsequently ingested into Computer-Aided Detection (CADe) or Diagnosis (CADx) systems. Apart from generating malicious images, adversarial models can also remove or add data perturbations such as artifacts, evidence, or adversarial noise into existing images [241, 242, 243]. Tampering with medical images, e.g. by introducing anatomical or appearance variations [244], puts the patient at risk of being wrongfully provisioned with an incorrect diagnosis or treatment. The susceptibility of medical imaging deep learn-

ing systems to white box and black box adversarial attacks is reviewed [245, 243] and investigated [246, 228, 247] in recent studies. Cancer imaging models show a high level of susceptibility [248, 156, 249]. Besides imaging data, image quantification features such as radiomics features [250] are also commonly used in cancer imaging as input into CADe and CADx systems. Adversarial perturbations of radiomics features threaten patient safety and highlight the need for defence strategies against adversarial radiomics examples [251].

Examples of GAN-based Tampering with Cancer Imaging Data. For instance, Mirsky et al [228] added and removed evidence of cancer in lung CT scans. Of two identical deep 3D convolutional cGANs (based on pix2pix), one was used to inject (diameter $\geq 10mm$) and the other to remove (diameter $< 3mm$) multiple solitary pulmonary nodules indicating lung cancer. The GANs were trained on 888 CT scans from the Lung Image Database Consortium image collection (LIDC-IDRI) dataset [144] and inpainted on an extracted region of interest of 32^3 voxel cuboid shape. The trained GANs can be autonomously executed by malware and are capable of ingesting nodules into standard CT scans that are realistic enough to deceive both radiologists and AI disease detection systems. Three radiologists with 2, 5 and 7 years of experience analysed 70 tampered and 30 authentic CT scans. Spending on average 10 minutes on each scan, the radiologists diagnosed 99% of the scans with added nodules as

malignant and 94% of the scans with removed nodules as healthy. After disclosing the presence of the attack to the radiologists, the percentages dropped to 60% and 87%, respectively [228].

Becker et al [227] trained a CycleGAN [54] on 680 down-scaled mammograms from the Breast Cancer Digital Repository (BCDR) [252] and the INbreast [33] datasets to generate suspicious features and was able to remove or inject them into existing mammograms. They showed that their approach can fool radiologists at lower pixel dimensions (i.e. 256×256) demonstrating that alterations in patient images by a malicious attacker can remain undetected by clinicians, influence the diagnosis, and potentially harm the patient [227].

Defending Adversarial Attacks. In regard to fooling diagnostic models, one measure to circumvent adversarial attacks is to increase model robustness against adversarial examples [253], as suggested by Figure 3(h). Augmenting the robustness has been shown to be effective for medical imaging segmentation models [254, 255], lung nodule detection models [256, 257], skin cancer recognition [258, 259], and classification of histopathology images of lymph node sections with metastatic tissue [260]. Liu et al [256] provide model robustness by adding adversarial chest CT examples to the training data. These adversarial examples are composed of synthetic nodules that are generated by a 3D convolutional variational encoder trained in conjunction with a WGAN-GP [49] discriminator. To further enhance robustness, Projected Gradient Descent (PGD) [253] is applied to find and protect against noise patterns for which the detector network is prone to produce over-confident false predictions [256].

Apart from being the adversary, GANs can also detect adversarial attacks and thus are applicable as security counter-measure enabling attack anticipation, early warning, monitoring and mitigation. Defense-GAN, for example, learns the distribution of non-tampered images and can generate a close output to an inference input image that does not contain adversarial modifications [261].

We highlight the research potential in adversarial attacks and examples, alongside prospective GAN detection and defence mechanisms that can, as elaborated, highly impact the field of cancer imaging. Apart from the image injection of entire tumours and the generation of adversarial radiomics examples, a further attack vector to consider

in future studies is the perturbation of the specific imaging features within an image that are used to compute radiomics features.

4.3. Data Annotation and Segmentation Challenges

4.3.1. Annotation-Specific Issues in Cancer Imaging

Missing Annotations in Datasets. In cancer imaging, not only the availability of large datasets is rare, but also the availability of labels, annotations, and segmentation masks within such datasets. The generation and evaluation of such labels, annotations, and segmentation masks is a task for which trained health professionals (radiologists, pathologists) are needed to ensure validity and credibility [106, 24]. Nonetheless, radiologist annotations of large datasets can take years to generate [24]. The tasks of labelling and annotating (e.g., bounding boxes, segmentation masks, textual comments) cancer imaging data is, hence, expensive both in time and cost, especially considering the large amount of data needed to train deep learning models.

Intra/Inter-Observer Annotation Variability. This cancer imaging challenge is further exacerbated by the high intra- and inter-observer variability between both pathologists [269, 270, 271, 272] and radiologists [14, 273, 274, 275, 276, 15, 277] in interpreting cancer images across imaging modalities, affected organs, and cancer types. Automated annotation processes based on deep learning models allow to produce reproducible and standardised results in each image analysis. In one of most common case where the annotations consist of a segmentation mask, reliably segmenting both tumour and non-tumour tissues is crucial for disease analysis, biopsy, and subsequent intervention and treatment [106, 278] the latter being further discussed in section 4.5. For example, automatic tumour segmentation models are useful in the context of radiotherapy treatment planning [279].

Human Biases in Cancer Image Annotation. During routine tasks, such as medical image analysis, humans are prone to account for only a few of many relevant qualitative image features. On the contrary, the strength of GANs and deep learning models is the evaluation of large numbers of multi-dimensional image features alongside

Table 3: Overview of adversarially-trained models applied/applicable to data access and privacy cancer imaging challenges. Publications are clustered by section and ordered by year in ascending order.

Publication	Method	Dataset	Modality	Task	Highlights
Decentralised GANs					
Chang et al (2020) [100, 101]	AsynDGAN, PatchGAN [55]	BRATS 2018 [178, 262], Multi-Organ [263]	Cranial MRI, nuclei images	Paired translation	Mask-to-image, central G gets distributed Ds' gradients, synthetic only-trained segmentation.
Differential-Privacy GANs					
Xie et al (2018) [206]	DPGAN	MNIST [264], MIMIC-III [265]	MNIST images, EHRs	Image synthesis	Noisy gradients during training ensure DP guarantee.
Jordon et al (2018) [208]	PATE-GAN	Cervical cancer [210]	[non-imaging] Medical records	Data synthesis	DP via PATE framework. G gradient from student D that learns from teacher Ds.
Beaulieu-Jones et al (2019) [211]	AC-GAN	MIMIC-III [265]	[non-imaging] EHRs, clinical trial data	Conditional synthesis	DP via Gaussian noise added to AC-GAN gradient. Treatment arm as conditional input.
Bae et al (2020) [212]	AnomiGAN	UCI Breast [266] & Prostate [266]	[non-imaging] Cell nuclei tabular data	Conditional synthesis, classification	DP via training variances added to G's layers in inference. Real data row as G's condition.
Torfi et al (2020) [207]	RDP-CGAN	Cervical cancer [210], MIMIC-III [265]	[non-imaging] Medical records, EHRs	Data synthesis	DP GAN based on Rényi divergence. Allows to track a DP loss.
Patient De-Identification					
Abramian et al (2019) [224]	CycleGAN	IXI [185]	Cranial MRI	Unpaired translation	Reconstruction of blurring/removed faces in MRI shows privacy vulnerability.
Kim et al (2019) [229]	PrivacyNet	PPMI [267]	Cranial MRI	Representation learning, segmentation	Segmenting de-identified representations learned via same-person CLF by Siamese Ds.
Van der Goten et al (2021) [225]	C-DeID-GAN	ADNI [170, 171], OASIS-3 [268]	Cranial MRI	Paired translation	Face de-id. Concatenated convex hull, brain mask & brain volumes as G & D inputs.
Adversarial Data Tampering					
Mirsky et al (2019) [228]	pix2pix-based CT-GAN	LIDC-IDRI [144]	Lung CT	Image inpainting	Injected/removed lung nodules in CT fool radiologists and AI models.
Becker et al (2019) [227]	CycleGAN	BCDR [252], IN-breast [33]	Digital/Film MMG	Unpaired translation	Suspicious features can be learned and injected/removed from MMG.
Liu et al (2020) [256]	Variational Encoder, WGAN-GP	LUNA [180], NLST [80]	Lung CT	Conditional synthesis	Robustness via adversarial data augmentation, reduce false positives in nodule detection

their (non-linear) inter-relationships and combined importance [106]. Deep learning models are likely to react to unexpected and subtle patterns in the imaging data (e.g., anomalies, hidden comorbidities, etc.) that medical practitioners are prone to overlook for instance due to any of multiple existing cognitive biases (e.g., anchoring bias, framing bias, availability bias) [277] or inattentional blindness [280]. Inattentional blindness occurs when radiologists (or pathologist) have a substantial amount of their attention drawn to a specific task, such as finding an expected pattern (e.g., a lung nodule) in the imaging data, that they become blind to other patterns in that data.

Implications of Low Segmentation Model Robustness. As for the common annotation task of segmentation mask delineation, automated segmentation models can minimise the risk of the aforesaid human biases. However, to date, segmentation models have difficulties when confronted with intricate segmentation problems including domain shifts, rare diseases with limited sample size, or small lesion and metastasis segmentation. In this sense, the performance of many automated and semi-automated clinical segmentation models has been sub-optimal [281]. This emphasises the need for expensive manual verification of

segmentation model results by human experts [106]. The challenge of training automated models for difficult segmentation problems can be approached by applying unsupervised learning methods that learn discriminative features without explicit labels. Such methods include GANs and variational autoencoders [162] capable of automating robust segmentation [106].

In addition, segmented regions of interest (ROI) are commonly used to extract quantitative imaging features with diagnostic value such as radiomics features. The latter are used to detect and monitor tumours (e.g., lymphoma [282]), biomarkers, and tumour-specific phenotypic attributes [250, 283]. The accuracy and success of such commonly applied diagnostic image feature quantification methods, hence, depends on accurate and robust ROI segmentations. Segmentation models need to be able to provide reproducibility of extracted quantitative features and biomarkers [24] with reliably-low variation, among others, across different scanners, CT slice thicknesses, and reconstruction kernels [284, 285]. To this end, we promote lines of research that use adversarial training schemes to target the robustification of segmentation models. Progress in this open research challenge can ben-

officially unlock trust, usability, and clinical adoption of biomarker quantification methods in clinical practice.

4.3.2. GAN Cancer Image Segmentation Examples

Table 4 summarises the collection of segmentation publications that utilise such adversarial training approaches and GAN-based data synthesis for cancer imaging. In the following sections, we provide a summary of the commonly used techniques and trends in the GAN literature that address the challenges in cancer image segmentation.

Robust quantitative imaging feature extraction. For example, Xiao et al [286] addressed the challenge of robustification of segmentation models and reliable biomarker quantification. The authors in [286] provide radiomics features as conditional input to the discriminator of their adversarially trained liver tumour segmentation model. Their learning procedure strives to inform the generator to create segmentations that are specifically suitable for subsequent radiomics feature computation. Apart from adversarially training segmentation models, we also highlight the research potential of adversarially training quantitative imaging feature extraction models (e.g., deep learning radiomics) for reliable application in multi-centre and multi-domain settings.

Synthetic Segmentation Model Training Data. By augmenting and varying the training data of segmentation models, it is possible to substantially decrease the amount of manually annotated images during training while maintaining the performance [287]. A general pipeline of such usage of GAN based generative models is demonstrated in Figure 9(a) and mentioned in Figure 3(j).

Over the past few years, CycleGAN [54] based approaches have been widely used for synthetic data generation due to the possibility of using unpaired image sets in training, as compared to paired image translation methods like pix2pix [55] or SPADE [56]. CycleGAN based data augmentation has been shown to be useful for segmentation model training, in particular, for generating images with different acquisition characteristics such as contrast enhanced MRI from non-contrast MRI [288], cross-modality image translation between different modalities such as CT and MRI images [289], and domain adaptation tasks [126]. The popularity of the CycleGAN based methods lies not only in image synthesis or domain adaptation,

but also in the inclusion of simultaneous image segmentation in its pipeline [290].

Although pix2pix methods require paired samples, it is also a widely used type of GAN in data augmentation for medical image segmentation (see Table 4). Several works on segmentation have demonstrated its effectiveness in generating synthetic medical images. By manipulating its input, the variability of the training dataset for image segmentation could be remarkably increased in a controlled manner [291, 292]. Similarly, the conditional GAN methods have also been used for controllable data augmentation for improving lesion segmentation [293]. Providing a condition as an input to generate a mask is particularly useful to specify the location, size, shape, and heterogeneity of the synthetic lesions. One of the recent examples, proposed in [294], demonstrates this in brain MRI tumour synthesis by conditioning an input with simplified controllable concentric circles to specify lesion location and characteristics. A further method for data augmentation is the inpainting of generated lesions into healthy real images or into other synthetic images, as depicted by Figure 9(f). Overall, the described data augmentation techniques have shown to improve generalisability and performance of segmentation models by increasing both the number and the variability of training samples [295, 287, 290].

Segmentation Models with Integrated Adversarial Loss. As stated in Figure 3(i), GANs can also be used as the algorithm that generates robust segmentation masks, where the generator is used as a segmentor and the discriminator scrutinises the segmentation masks given an input image. One intuition behind this approach is the detection and correction of higher-order inconsistencies between the ground truth segmentation maps and the ones created by the segmentor via adversarial learning [296, 158, 297]. This approach is demonstrated in Figure 9(b). With the additional adversarial loss when training a segmentation model, this approach has been shown to improve semantic segmentation accuracy [298, 299]. Using adversarial training, similarity of a generated mask to manual segmentation given an input image is taken under consideration by the discriminator allowing a global assessment of the segmentation quality. A unique way of incorporating the adversarial loss from the discriminator has been recently proposed in [300]. In their work, the authors utilise

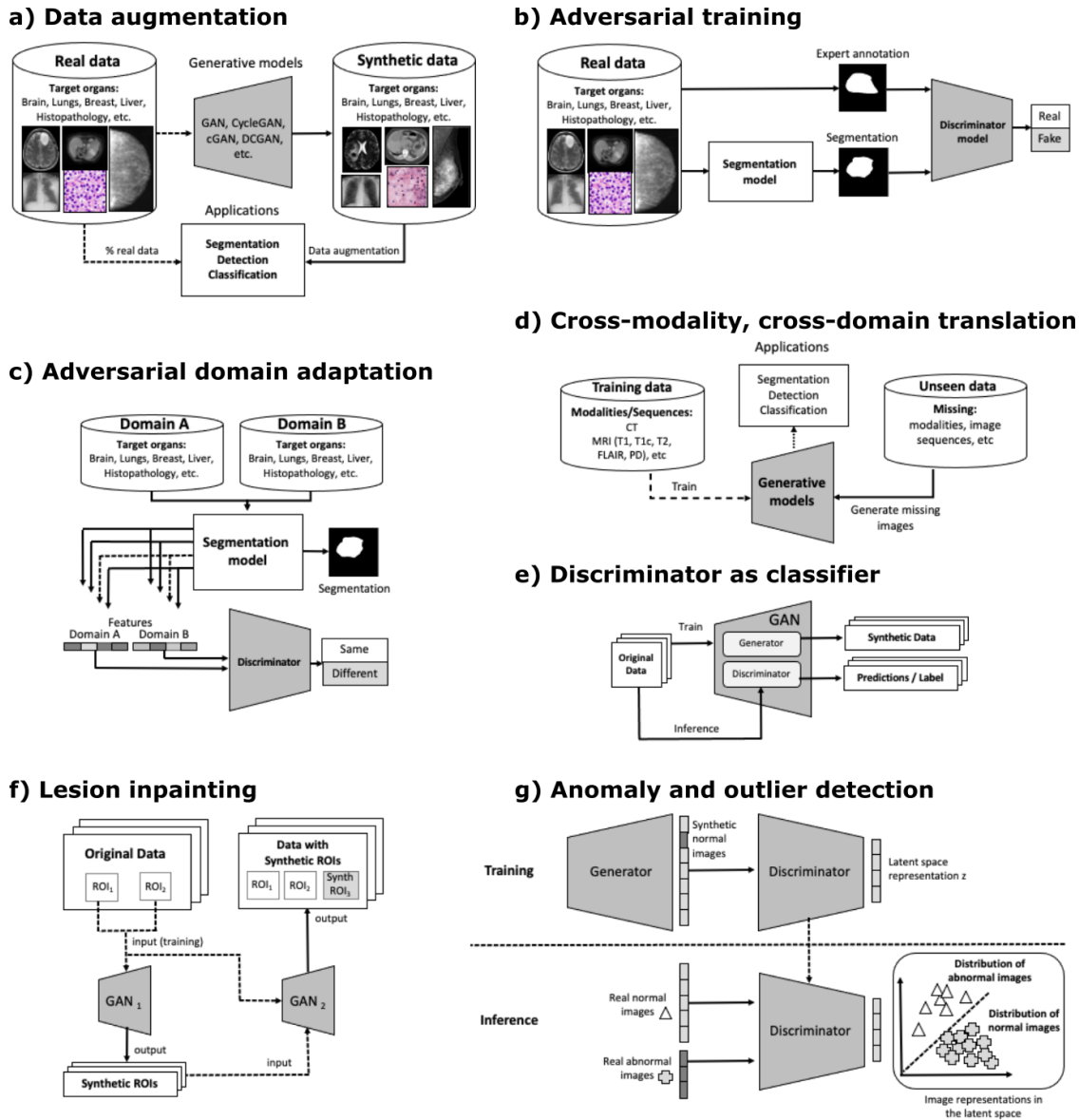


Figure 9: Overview of cancer imaging GAN applications for detection and segmentation. (a) describes training data augmentation of downstream task models (e.g., segmentation, detection, classification, etc). In (b) a discriminator scrutinises the segmentations created by a segmentation model, while in (c) the discriminator enforces the model to create domain-agnostic latent representations. (d) illustrates domain-adaptation, where the translated target domain images are used for downstream model training. In (e), the AC-GAN [43] discriminator classifies original data. In (f), one GAN generates ROIs while another inpaints them into full-sized images. (g) uses the discriminator’s latent space to find abnormal/outlier representations.

a fully-convolutional network as a discriminator, unlike its counterparts that use binary, single neuron output networks. In doing so, a dense confidence map is produced by the discriminator, which is further used to train the segmentor with an attention mechanism.

Overall, using an adversarial loss as an additional global segmentation assessment is likely to be a helpful further signal for segmentation models, in particular, for heterogeneously structured datasets of limited size [301], as is common for cancer imaging datasets. We highlight potential further research in GAN-based segmentation models to learn to segment increasingly fine radiologic distinctions. These models can help to solve further cancer imaging challenges, for example, accurate differentiation between neoplasms and tissue response to injury in the regions surrounding a tumour after treatment [24].

Segmentation Models with Integrated Adversarial Domain Discrimination. Moreover, a similar adversarial loss can also be performed intrinsically on the segmentation model features as illustrated in Figure 9(c). Such an approach can benefit domain adaptation and domain generalisation by enforcing the segmentation model to learn to base its prediction on domain invariant feature representations [62].

4.3.3. Limitations and Future Prospects for Cancer Imaging Segmentation

As shown in Table 4, the applications of GANs in cancer image segmentation cover a variety of clinical requirements. Remarkable steps have been taken to advance this field of research over the past few years. However, the following limitations and future prospects can be considered for further investigation:

- Although the data augmentation using GANs could increase the number of training samples for segmentation, the variability of the synthetic data is limited to the training data. Hence, it may limit the potential of improving the performance in terms of segmentation accuracy. Moreover, training a GAN that produce high sample variability requires a large dataset also with a high variability, and, in most of the cases, with corresponding annotations. Considering the data scarcity challenge in the cancer imaging domain, this can be difficult to achieve.

- In some cases, using GANs could be excessive, considering the difficulties related to convergence of competing generator and discriminator parts of the GAN architectures. For example, the recently proposed SynthSeg model [302] is based on Gaussian Mixture Models to generate images and train a contrast agnostic segmentation model. Such approaches can be considered as an alternative to avoid common pitfalls of the GAN training process (e.g., mode collapse). However, this approach needs to be further investigated for cancer imaging tasks where the heterogeneity of tumours is challenging.
- A great potential for using synthetic cancer images is to generate common shareable datasets as benchmarks for automated segmentation methods [24]. Although this benchmark dataset needs its own validation, it can be beneficial in testing the limits of automated methods with systematically controlled test cases. Such benchmark datasets can be generated by controlling the shape, location, size, intensities of tumours, and can simulating diverse images of different domains that reflect the distributions from real institutions. To avoid learning patterns that are only available in synthetic datasets (e.g., checkerboard artifacts), it is a prospect to investigate further metrics that measure the distance of such synthetic datasets to real-world datasets and the generalisation and extrapolation capabilities of models trained on synthetic benchmarks to real-world data.

4.4. Detection and Diagnosis Challenges

4.4.1. Common Issues in Diagnosing Malignancies

Clinicians' High Diagnostic Error Rates. Studies of radiological error report high ranges of diagnostic error rates (e.g., discordant interpretations in 31–37% in Oncologic CT, 13% major discrepancies in Neuro CT and MRI). [277]. After McCreadie et al [11] critically reviewed the radiology cases of the last 30 months in their clinical centre, they found that from 256 detected errors (62% CT, 12% Ultrasound, 11% MRI, 9% Radiography, 5% Fluoroscopy) in 222 patients, 225 errors (88%) were attributable to poor image interpretation (14 false positive, 155 false negative, 56 misclassifications). A recent literature review on diagnostic errors by Newman et al [348]

Table 4: Overview of adversarial training and GAN-based approaches applied to segmentation in cancer imaging tasks. Publications are clustered by organ type and ordered by year in ascending order.

Publication	Method	Dataset	Modality	Task	Metric (Baseline) w/o GAN	Metric with GAN (Baseline+ Δ)	Highlights
Head/Brain/Neck							
Rezaei et al (2017) [303]	pix2pix, MarkovianGAN [304]	BRATS 2017 [178, 262, 305]	MRI	Adversarial training	Dice: 0.80	n.a.	G generates masks that D tries to detect for high/low grade glioma (HGG/LGG) segmentation.
Mok et al (2018) [306]	CB-GAN	BRATS [178]	MRI	Data augmentation	Dice: 0.79	0.84	Coarse-to-fine G captures training set manifold, generates generic samples in HGG & LGG segmentation.
Yu et al (2018) [307]	pix2pix-based	BRATS [178]	MRI	Data augmentation	Dice: 0.82	0.68	Cross-modal paired FLAIR to T1 translation, training tumour segmentation with T1+real/synthetic FLAIR.
Shin et al (2018) [203]	pix2pix	BRATS [178]	MRI	Data augmentation	Dice: 0.81	0.81	Training on synthetic, before fine-tuning on 10% of the real data.
Kim et al (2020) [294]	GAN	BRATS [262, 178]	MRI	Image inpainting, data augmentation	Dice: 0.57	0.59	Simplifying tumour features into concentric circle & grade mask to inpaint.
Hu et al (2020) [158]	UNet-based GAN segmenter	Private	CT, PET	Adversarial training	Dice: 0.69	0.71	Spatial context information & hierarchical features. Nasal-type lymphoma segmentation with uncertainty estimation.
Qasim et al (2020) [295]	SPADE-based [56]	BRATS [262], ISIC [308]	MRI, dermoscopy	Cross-domain translation	Dice: n.a.	B:0.66 S:0.62	Brain and skin segmentation. Frozen segmenter as 3rd player in GAN to condition on local apart from global information.
Foroozandeh et al (2020) [287]	PGGAN, SPADE	BRATS [178]	MRI	Data augmentation	Av. dice error(%): 16.80	16.18	Sequential noise-to-mask and paired mask-to-image translation to synthesise labelled tumour images.
Lee et al (2020) [290]	CycleGAN-based	Private	MRI	Adversarial training	n.a.	n.a.	Unpaired image-to-mask translation and vice versa. Comparison of UNet and ResNet CycleGAN backbones.
Cirillo et al (2020) [297]	vox2vox: 3D pix2pix	BRATS [178]	MRI	Adversarial training	Dice: 0.87	0.93	3D adversarial training to enforce segmentation results to look realistic.
Han et al (2021) [309]	Symmetric adaptation network	BRATS [178]	MRI	Cross-domain translation	Dice: 0.77	0.67	Simultaneous source/target cross-domain translation and segmentation. T2 to other sequences translation.
Xue et al (2018) [310]	SegAN	BRATS [178]	MRI	Adversarial training	Dice: n.a.	0.85	Paired image-to-mask. New multi-scale loss: L1 distance of D representations between GT- & prediction-masked input MRI.
Giacomello et al (2020) [311]	SegAN-CAT	BRATS [178]	MRI	Adversarial training	Dice: n.a.	0.859	Paired image-to-mask. Combined dice loss & multi-scale loss using concatenation on channel axis instead of masking.
Alshehhi et al (2021) [159]	U-Net based GAN segmenter	BRATS [178]	MRI	Adversarial training	Dice: n.a.	0.89	Paired image-to-mask translation. Uncertainty estimation using Bayesian active learning in brain tumour segmentation.
Breast							
Singh et al (2018) [312]	pix2pix	DDSM [313]	Film MMG	Adversarial training	Dice: 0.86	0.94	Adversarial loss to make automated segmentation close to manual masks for breast mass segmentation.
Caballo et al (2020) [314]	DCGAN [51]	Private	CT	Data augmentation	Dice: 0.70	0.93	GAN based data augmentation; Validated by matching extracted radiomics features.
Negi et al (2020) [315]	GAN, WGAN-RDA-UNET	Private	Ultrasound	Adversarial training	Dice: 0.85	0.88	Outperforms state-of-the-art using Residual-Dilated-Attention-Gate-UNet and WGAN for lesion segmentation.
Abdominal							
Huo et al (2018) [289]	Conditional PatchGAN	Private	MRI	Adversarial training	Dice: n.a.	0.94	Adversarial loss as segmentation post-processing for spleen segmentation.
Chen et al (2019) [316]	DC-FCN-based GAN segmenter	LiTS [317]	CT	Adversarial training	Dice: n.a.	0.684	Cascaded framework with densely connected adversarial training.
Sandfort et al (2019) [127]	CycleGAN	NIH [318], Decathlon [319], DeepLesion [320]	CT	Cross-domain translation	Dice (od): 0.916, 0.101	0.932, 0.747	Contrast enhanced to non-enhanced translation. Image synthesis to improve out-of-distribution (od) segmentation.
Xiao et al (2019) [286]	Radiomics-guided GAN	Private	MRI	Adversarial training	Dice: n.a.	0.92	Radiomics-guided adversarial mechanism to map relationship between contrast and non-contrast images.
Oliveira (2020) [292]	pix2pix, SPADE	LiTS [317]	CT	Image inpainting	Dice: 0.58	0.61	Realistic lesion inpainting in CT slices to provide controllable set of training samples.
Chest and lungs							
Jiang et al (2018) [126]	CycleGAN-based	NSCLC [318]	CT, MRI	Cross-domain translation	Dice: n.a.	0.70	Tumour-aware loss for unsupervised cross-domain adaptation.
Jin et al (2018) [321]	cGAN	LIDC [144]	CT	Image inpainting	Dice: 0.96	0.99	Generated lung nodules to improve segmentation robustness; A novel multi-mask reconstruction loss.
Dong et al (2019) [322]	UNet-based GAN segmenter	AAPM Challenge [323]	CT	Adversarial training	Dice: 0.97 (l), 0.83 (sc), 0.71 (o), 0.85 (h)	0.97, 0.90, 0.75, 0.87	Adversarial training to discriminate manual and automated segmentation of lungs, spinal cord, oesophagus, heart.
Tang et al (2019) [324]	MUNIT [325]	JSRT [326], Montgomery [327]	Chest X-Ray	Lung segmentation	Dice: 0.97	0.98	Unpaired normal-to-abnormal (pathological) translation. Synthetic data augmentation for lung segmentation.
Shi et al (2020) [299]	AUGAN	LIDC-IDRI [144]	CT	Adversarial training	Dice: 0.82	0.85	A deep layer aggregation based on U-net++.
Munawar et al (2020) [328]	Unet-based GAN segmenter	JSRT [326], Montgomery [327], Shenzhen [327]	Chest X-Ray	Adversarial training	Dice: 0.96	0.97	Adversarial training to discriminate manual and automated segmentation.
Prostate							
Kohl et al (2017) [301]	UNet-based GAN segmenter	Private	MRI	Adversarial training	Dice: 0.35	0.41	Adversarial loss to discriminate manual and automated segmentation.
Grall et al (2019) [329]	pix2pix	Private	MRI	Adversarial training	Dice: 0.67 (ADC), 0.74 (DWI), 0.67 (T2)	0.73, 0.79, 0.74	Paired prostate image-to-mask translation. Investigated the robustness of the pix2pix against noise.
Nie et al (2020) [300]	GAN	Private, PROMISE12 [330]	MRI	Adversarial confidence learning	Dice: 88.25 (b), 90.11 (m), 86.67 (a)	89.52, 90.97, 88.20	Difficulty-aware mechanism to alleviate the effect of easy samples during training, b = base, m = middle, a = apex.
Zhang et al (2020) [331]	PGGAN	Private	CT	Data augmentation	Dice: 0.85	0.90	Semi-supervised training using both annotated and un-annotated data. Synthetic data augmentation using PGGAN.
Cem Birbiri et al (2020) [332]	pix2pix, CycleGAN	Private, PROMISE12 [330]	MRI	Data augmentation	Dice: 0.72	0.76	Compared the performance of pix2pix, U-Net, and CycleGAN.
Colorectal							
Liu et al (2019) [333]	GAN, LAGAN	Private	CT	Adversarial training	Dice: 0.87	0.92	Automatic post-processing to refine the segmentation of deep networks.
Poorneshwaran et al (2019) [334]	pix2pix	CVC-clinic [335]	Endoscopy	Adversarial training	Dice: n.a.	0.88	Adversarial learning to make automatic segmentation close to manual.
Xie et al (2020) [336]	MF-GAN, CycleGAN	CVC-clinic [335], ETIS-Larib [337]	Endoscopy	Cross-domain translation	Dice: 0.66	0.73	Content features and domain information decoupling and maximising the mutual information.
Pathology							
Quiros et al (2019) [338]	PathologyGAN	Private	Histopathology	Data augmentation	n.a.	n.a.	Images generated from structured latent space, combining BigGAN [339], StyleGAN [40], and RAD [340]
Pandey et al (2020) [341]	GAN & cGAN	Kaggle [342]	Histopathology	Data augmentation	Dice: 0.79	0.83	Two-stage GAN to generate masks and conditioned synthetic images.
Other							
Chi et al (2018) [343]	pix2pix	ISBI ISIC [169]	Dermoscopy	Data augmentation	Dice: 0.85	0.84	Similar performance replacing half of real with synthetic data. Colour labels as lesion specific characteristics.
Abhishek et al (2019) [291]	pix2pix	ISBI ISIC [169]	Dermoscopy	Data augmentation	Dice: 0.77	0.81	Generate new lesion images given any arbitrary mask.
Sarker et al (2019) [344]	MobileGAN	ISBI ISIC [169]	Dermoscopy	Adversarial training	Dice: n.a.	0.91	Lightweight and efficient GAN model with position and channel attention.
Zaman et al (2020) [345]	pix2pix	Private	Ultrasound	Data augmentation	Dice: n.a.	A+0.25	Recommendations on standard data augmentation approaches.
Chaitanya et al (2021) [346]	cGAN, DCGAN-based D	ACDC [347], Decathlon [319]	MRI, CT	Data augmentation	Dice: 0.40	0.53	GAN data augmentation for intensity and shape variations.

estimated a false negative rate¹⁸ of 22.5% for lung cancer, 8.9% for breast cancer, 9.6% for colorectal cancer, 2.4% for prostate and 13.6% for melanoma. These findings exemplify the uncomfortably high diagnostic and image interpretation error rates that persist in the field of radiology despite decades of interventions and research [10].

The Challenge of Reducing Clinicians' High Workload. In some settings, radiologists must interpret one CT or MRI image every 3–4 seconds in an average 8-hour workday [13]. Automated CADe and CADx systems can provide a more balanced quality-focused workload for radiologists, where radiologists focus on scrutinising the automated detected lesions (false positive reduction) and areas/patches with high predictive uncertainty (false negative reduction). A benefit of CADe/CADx deep learning models are their real-time inference and strong pattern recognition capabilities that are not readily susceptible to cognitive bias (discussed in 4.3.1), environmental factors [10], or inter-observer variability (discussed in 4.3.1).

Detection Model Performance on Critical Edge Cases. Challenging cancer imaging problems are the high intra- and inter-tumour heterogeneity [24], the detection of small lesions and metastasis across the body (e.g., lymph node involvement and distant metastasis [106]) and the accurate distinction between malignant and benign tumours (e.g., for detected lung nodules that seem similar on CT scans [106]). Methods are needed to extend on and further increase the current performance of deep learning detection models [24].

4.4.2. GAN Cancer Detection and Diagnosis Examples

As we detail in the following, the capability of the unsupervised adversarial learning to improve malignancy detection has been demonstrated for multiple tumour types and imaging modalities. To this end, Table 5 summarises the collection of recent publications that utilise GANs and adversarial training for cancer detection, classification, and diagnosis.

¹⁸In [348], the false negative rates includes both missed (patient encounters at which the diagnosis might have been made but was not) and delayed diagnosis (diagnostic delay relative to urgency of illness detection).

Adversarial Anomaly and Outlier Detection Examples. Schlegl et al [349] captured imaging markers relevant for disease prediction using a deep convolutional GAN named AnoGAN. AnoGAN learnt a manifold of normal anatomical variability, accompanying a novel anomaly scoring scheme based on the mapping from image space to a latent space. While Schlegl et al validated their model on retina optical coherence tomography images, their unsupervised anomaly detection approach is applicable to other domains including cancer detection, as indicated in Figure 3(l). Chen et al [350] used a Variational Autoencoder GAN for unsupervised outlier detection using T1 and T2 weighted brain MRI images. The scans from healthy subjects were used to train the autoencoder model to learn the distribution of healthy images and detect pathological images as outliers. Creswell et al [231] proposed a semi-supervised Denoising Adversarial Autoencoder (ssDAAE) to learn a representation based on unlabelled skin lesion images. The semi-supervised part of their CNN-based architecture corresponds to malignancy classification of labelled skin lesions based on the encoded representations of the pretrained DAAE. As the amount of labelled data is smaller than the unlabelled data, the labelled data is used to fine-tune classifier and encoder. In ssDAAE, not only the adversarial autoencoder's chosen prior distribution [230], but also the class label distribution is discriminated by a discriminator, the latter distinguishing between predicted continuous labels and real binary (malignant/benign) labels. Kuang et al [351] applied unsupervised learning to distinguish between benign and malignant lung nodules. In their multi-discriminator GAN (MDGAN) various discriminators scrutinise the realness of generated lung nodule images. After GAN pretraining, an encoder is added in front of the generator to the end-to-end architecture to learn the feature distribution of benign pulmonary nodule images and to map these features into latent space. The benign and malignant lung nodules were scored similarly as in the f-AnoGAN framework [352], computing and combining an image reconstruction loss and a feature matching loss, the latter comparing the discriminators' feature representations between real and encoded-generated images from intermediate discriminator layers. As exemplified in Figure 9(g), the model yielded high anomaly scores on malignant images and low anomaly scores on benign images despite limited dataset size. Benson et al [353]

used GANs trained from multi-modal MRI images as a 3-channel input (T1-T2 weighted, FLAIR, ADC MRI) in brain anomaly detection. The training of the generative network was performed using only healthy images together with pseudo-random irregular masks. Despite the training dataset consisting of only 20 subjects, the resulting model increased the anomaly detection rate.

Synthetic Detection Model Training Data. Among the GAN publications trying to improve classification and detection performance, data augmentation is the most recurrent approach to balance, vary, and increase the detection model’s training set size, as suggested in Figure 3(k). For instance in breast imaging, Wu et al [226] trained a class-conditional GAN to perform contextual in-filling to synthesise lesions in healthy scanned mammograms. Guan et al [354] trained a GAN on the same dataset [313] to generate synthetic patches with benign and malignant tumours. The synthetic generated patches had clear artifacts and did not match the original dataset distribution. Jendele et al [355] used a CycleGAN [54] and both film scanned and digital mammograms to improve binary (malignant/benign) lesion detection using data augmentation. Detecting mammographically-occult breast cancers is another challenging topic addressed by GANs. For instance, Lee et al [356] exploit asymmetries between mammograms of the left and right breasts as signals for finding mammography-occult cancer. They trained a conditional GAN (pix2pix) to generate a healthy synthetic mammogram image of the contralateral breast (e.g., left breast) given the corresponding single-sided mammogram (e.g., right breast) as input. The authors showed that there is a higher similarity (MSE, 2D-correlation) between simulated-real (SR) mammogram pairs than real-real (RR) mammogram pairs in the presence of mammography-occult cancer. Consequently, distinguishing between healthy and mammography-occult mammograms, their classifier yielded a higher performance when trained with both RR and SR similarity as input (AUC = 0.67) than when trained only with RR pair similarity as input (AUC = 0.57). 3-dimensional image synthesis with GANs has been shown, for instance, by Han et al [357], who proposed a 3D Multi-Conditional GAN (3DMCGAN) to generate realistic and diverse nodules placed naturally on lung CT images to boost sensitivity in 3D object detection. Bu et al [358] built a 3D

conditional GAN based on pix2pix, where the input is a 3D volume of interest (VOI) that is cropped from a lung CT scan and contains a missing region in its centre. Both generator and discriminator contain squeeze-and-excitation [359] residual[360] neural network (SE-ResNet) modules to improve the quality of the synthesised lung nodules. Another example based on lung CT images is the method by Nihio et al [361], where the proposed GAN model used masked 3D CT images and nodule size information to generate images.

As to multi-modal training data synthesis, van Tulder et al [362] replaced missing sequences of a multi-sequence MRI with synthetic data. The authors illustrated that if the synthetic data generation model is more flexible than the classification model, the synthetic data can provide features that the classifier has not extracted from the original data, which can improve the performance. During colonoscopy, depth maps can enable navigation alongside aiding detection and size measurements of polyps. For this reason, Rau et al [363] demonstrated the synthesis of depth maps using a conditional GAN (pix2pix) with monocular endoscopic images as input, reporting promising results on synthetic, phantom and real datasets. In breast cancer detection, Muramatsu et al [364] translated lesions from lung CT to breast MMG using cycleGAN yielding a performance improvement in breast mass classification when training a classifier with the domain-translated generated samples.

4.4.3. Future Prospects for Cancer Detection and Diagnosis

Granular Class Distinctions for Synthetic Tumour Images. Further research opportunity exists in exploring a more fine-grained classification of tumours that characterises different subtypes and disease grades instead of binary malignant-benign classification. Being able to robustly distinguish between different disease subtypes with similar imaging phenotypes (e.g., glioblastoma versus primary central nervous system lymphoma [282]) addresses the challenge of reducing diagnostic ambiguity [24]. GANs can be explored to augment training data with samples of specific tumour subtypes to improve the distinction capabilities of disease detection models. This can be achieved by training a detection model on training data generated by various GANs, where each GAN is trained on a different tumour subtype distribution. An-

other option we estimate worth exploring is to use the tumour subtype or the disease grade (e.g., the Gleason Score for prostate cancer [89]) as a conditional input into the GAN to generate additional labelled synthetic training data.

Cancer Image Interpretation and Risk Estimation. Besides the detection of prospectively cancerous characteristics in medical scans, ensuring a high accuracy in the subsequent interpretation of these findings are a further challenge in cancer imaging. Improving the interpretation accuracy can reduce the number of unnecessary biopsies and harmful treatments (e.g., mastectomy, radiation therapy, chemotherapy) of indolent tumours [24]. For instance, the rate of overdiagnosis of non-clinically significant prostate cancer ranges widely between 1.7% up to a noteworthy 67% [365]. To address this, detection models can be extended to provide risk and clinical significance estimations. For example, given both an input image, and an array of risk factors (e.g., BRCA1/BRCA2 status for breast cancer [366], comorbidity risks), a deep learning model can weight and evaluate a patient’s risk based on learned associations between risk factors and input image features. The GAN framework is an example of this, where clinical, non-clinical and imaging data can be combined, either as conditional input for image generation or as prediction targets. For instance, given an input image, an AC-GAN [43, 367] can classify the risk as continuous label (see Figure 9(e)) or, alternatively, a discriminator can be used to assess whether a risk estimate provided by a generator is realistic. Also, a generator can learn a function for transforming and normalising an input image given one or several conditional input target risk factors or tumour characteristics (e.g., a specific mutation status, a present comorbidity, etc) to generate labelled synthetic training data.

4.5. Treatment and Monitoring Challenges

After a tumour is detected and properly described, new challenges arise related to planning and execution of medical intervention. In this section we examine these challenges, in particular: tumour profiling and prognosis; challenges related to choice, response and discovery of treatments; as well as further disease monitoring. Table 6 provides an overview of the cancer imaging GANs that

are applied to treatment and monitoring challenges, which are discussed in the following.

4.5.1. Disease Prognosis and Tumour Profiling

Challenges for Disease Prognosis. An accurate prognosis is crucial to plan suitable treatments for cancer patients. However, in specific cases, it could be more beneficial to actively monitor the tumours instead of treating them [24]. Challenges in cancer prognosis include the differentiation between long-term and short term survivors [24], patient risk estimation considering the complex intra-tumour heterogeneity of the tumour microenvironment (TME) [421], or the estimation of the probability of disease stages and tumour growth patterns, which can strongly affect outcome probabilities [24]. In this sense, GANs [138, 422] and AI models in general [279, 270] have shown potential in prognosis and survival prediction for oncology patients.

GAN Disease Prognosis Examples. Li et al [138] (in Table 2) show that their GAN-based CT normalisation framework for overcoming the domain shift between images from different centres significantly improves accuracy of classification between short-term and long-term survivors. Ahmed et al [423] trained omicsGAN to translate between microRNA and mRNA expression data pairs, but could be readily enhanced to also translate between cancer imaging features and genetic information. The authors evaluate omicsGAN on breast and ovarian cancer datasets and report improved prediction signals for synthetic data tested via cancer outcome classification. Another non-imaging approach is provided by Kim et al [422], who apply a GAN for patient cancer prognosis prediction based on identification of prognostic biomarker genes. They train their GAN on reconstructed human biology pathways data, which allows for highlighting genes relevant to cancer development, resulting in improvement of the prognosis prediction accuracy. In regard to these works on non-imaging approaches, we promote future extensions combining prognostic biomarker genes and -omics data with the phenotypic information present in cancer images into multi-modal prognosis models.

GAN Tumour Profiling Examples. Related to Figure 3(I), Vu et al [424] propose that conditional GANs (Benign-GAN) can learn latent characteristics of tissues of tu-

Table 5: Overview of adversarially-trained models applied to detection and diagnosis tasks in cancer imaging. Publications are clustered by organ type and ordered by year in ascending order.

Publication	Method	Dataset	Modality	Task	Metric w/o GAN (Baseline)	Metric with GAN (Baseline+ Δ)	Highlights
Brain							
Chen et al (2018) [350]	VAE GAN	Cam-CAN [368], BRATS [178], ATLAS [369]	MRI	Anomaly detection	AUC(%): 80.0	70.0	Comparison of unsupervised outlier detection methods.
Han et al (2018) [370]	PGGAN	BRATS [178]	MRI	Data augmentation	Accuracy(%): 90.06	91.08	PGGAN-based augmentation method of whole brain MRI.
Han et al (2018) [371]	PGGAN, SimGAN	BRATS [178]	MRI	Data augmentation	Sensitivity(%): 93.67	97.48	Two-step GAN for noise-to-image and image-to-image data augmentation.
Benson et al (2018) [353]	GAN	TCLIA [372]	MRI	Anomaly detection	Accuracy(%): 73.48	74.96	Multi-modal MRI images as input to the GAN.
Han et al (2019) [373]	GAN	Private	MRI	Data augmentation	Sensitivity(%): 67.0	77.0	Synthesis and detection of brain metastases in MRI with bounding boxes.
Sun et al (2020) [374]	Fixed-Point GAN	BRATS [178]	MRI	Anomaly detection	Sensitivity(%): n.a.	84.5	Fixed-point translation concept.
Siddiquee et al (2020) [375]	ANT-GAN	BRATS 2013 [178]	MRI	Data augmentation	F1-Score(%): 89.6	91.7	Abnormal to normal image translation in cranial MRI, lesion detection.
Breast							
Wu et al (2018) [226]	ciGAN	DDSM [313]	Film MMG	Data augmentation	ROC AUC(%): 88.7	89.6	Synthetic lesion in-filling in healthy mammograms.
Mammo-ciGAN							
Guan et al (2019) [354]	GAN	DDSM [313]	Film MMG	Data augmentation	Accuracy(%): 73.48	74.96	Generate patches containing benign and malignant tumours.
Jendele et al (2019) [355]	CycleGAN	BCDR [252], INbreast [33], CBIS-DDSM [376]	Digital/Film MMG	Data augmentation	ROC AUC(%): 83.50, F1(%): 62.53	Δ -1.46, Δ +1.28	Scanned & digital mammograms evaluated together for lesion detection.
BreastGAN							
Lee et al (2020) [356]	CGAN	Private	Digital MMG	Data augmentation	ROC AUC: 0.57	0.67	Synthesising contralateral mammograms.
Wu et al (2020) [377]	U-Net based GAN	OPTIMAM [378]	Digital MMG	Data augmentation	ROC AUC(%): 82.9	84.6	Removing/adding lesion into MMG for malignant/benign classification.
Alyafi et al (2020) [379]	DCGAN	OPTIMAM [378]	Digital MMG	Data augmentation	F1-Score(%): n.a.	Δ +0.09(%)	Synthesise breast mass patches with high diversity.
Desai et al (2020) [380]	DCGAN	DDSM [313]	Film MMG	Data augmentation	Accuracy(%): 78.23	87.0	Synthesise full view MMGs and used them in visual Turing test.
Muramatsu et al (2020) [364]	CycleGAN	DDSM [313]	CT, Film MMG	Data augmentation	Accuracy(%): 79.2	81.4	CT lung nodule to MMG mass translation and vice versa.
Swiderski et al (2020) [381]	AGAN	DDSM [313]	Film MMG	Data augmentation	ROC AUC(%): 92.50	94.10	AutoencoderGAN (AGAN) augments data in normal abnormal classification.
Kansal et al (2020) [382]	DCGAN	Private	OCT	Data augmentation	Accuracy(%): 92.0	93.7	Synthetic Optical Coherence Tomography (OCT) images.
Shen et al (2021) [383]	ciGAN	DDSM [313]	Film MMG	Data augmentation	Detection rate(%): n.a.	Δ +5.03	Generate labelled breast mass images for precise detection.
Pang et al (2021) [384]	TripleGAN-based	Private	Ultrasound	Data augmentation	Sensitivity(%): 86.60	87.94	Semi-supervised GAN-based Radiomics model for mass CLF.
Liver							
Frid-Adar et al (2018) [385]	DCGAN, ACGAN	Private	CT	Data augmentation	Sensitivity(%): 78.6	85.7	Synthesis of high quality focal liver lesions from CT for lesion CLF.
Zhao et al (2020) [103]	Tripartite GAN	Private	MRI	Data augmentation	Accuracy(%): 79.2	89.4	Synthetic contrast-enhanced MRI \rightarrow tumour detection without contrast agents.
Doman et al (2020) [386]	DCGAN	JAMIT 3Dircadb [388]	CT	Data augmentation	Detection rate: 0.65	0.95	Generate metastatic liver lesions in abdominal CT for improved cancer detection.
Stomach/Colon/Prostate							
Kanayama et al (2019) [389]	DCGAN	Private	Endoscopy	Data augmentation	AP(%): 59.6	63.2	Synthesise lesion images for gastric cancer detection.
Shin et al (2018) [390]	cGAN	CVC-CLINIC [391], CVC-ClinicVideoDB [392]	Colonoscopy	Data augmentation	Precision(%): 81.9	85.3	Synthesise polyp images from normal colonoscopy images for polyp detection.
Rau et al (2019) [363]	pix2pix-based	Private	Colonoscopy	Data augmentation	Mean RMSE: 2.207	1.655	Transform monocular endoscopic images from two domains to depth maps.
ColonoscopyDepth							
Yu et al (2020) [393]	CapGAN	BrainWeb phantom [172], Prostate MRI [394]	MRI	Data augmentation	ROC AUC(%): 85.1	88.5	Synthesise prostate MRI using Capsule Network-Based DCGAN instead of CNN.
Krause et al (2020) [395]	CGAN	TCCG, NLCS [396]	Histopathology	Data augmentation	ROC AUC(%): 75.7	77.7	GANs to enhance genetic alteration detection in colorectal cancer histology.
Skin							
Bissoto et al (2018) [397] gan-skin-lesion	PGAN, DCGAN, pix2pix	Dermofit [398], ISIC 2017 [169], IAD [399]	ISIC	Dermscopy	ROC AUC(%): 83.4	84.7	Comparative study of GANs for skin lesions generation
Creswell et al (2018) [231]	ssDAAE	ISIC 2017 [169]	Dermscopy	Representation learning, classification	ROC AUC(%): 89.0	89.0	Adversarial autoencoder fine-tuned on few labelled lesion classification samples.
Baur et al (2018) [400]	DCGAN, LAPGAN	ISIC 2017 [169]	Dermscopy	Data augmentation	Accuracy(%): n.a.	74.0	Comparative study, 256x256px skin lesions synthesis. LAPGAN acc=74.0%
Rashid et al (2019) [401]	GAN	ISIC 2017 [169]	Dermscopy	Data augmentation	Accuracy(%): 81.5	86.1	Boost CLF performance with GAN-based skin lesions augmentation.
Fossen-Romsaas et al (2020) [122]	AC-GAN, CycleGAN	HAM10000 & BCN20000 [402, 403], ISIC 2017 [169]	Dermscopy	Data augmentation	Recall(%): 72.1	76.3	Realistic-looking, class-specific synthetic skin lesions.
Qin et al (2020) [404]	Style-based GAN	ISIC 2017 [169]	Dermscopy	Data augmentation	Precision(%): 71.8	76.9	Style control & noise input tuning in G to synthesise high quality lesions for CLF.
Lung							
Bi et al (2017) [115]	M-GAN	Private	PET	Data augmentation	F1-Score(%): 66.38	63.84	Synthesise PET data via multi-channel GAN for tumour detection.
Salehinejad et al (2018) [405]	DCGAN	Private	Chest X-Rays	Data augmentation	Accuracy(%): 70.87	92.10	Chest pathology CLF using synthetic data.
Zhao et al (2018) [406]	F&JBGAN	LIDC-IDRI [144]	CT	Data augmentation	Accuracy(%): 92.86	95.24	Forward GAN generates diverse images. Backward GAN improves their quality.
Onishi et al (2019) [407]	WGAN	Private	CT	Data augmentation	Accuracy(%): 63 (Benign), 82 (Malign)	67, 94	Synthesise pulmonary nodules on CT images for nodule CLF.
Gao et al (2019) [408]	WGAN-GP	LIDC-IDRI [144]	CT	Data augmentation	Sensitivity(%): 84.8	95.0	Synthesise lung nodule 3D data for nodule detection.
3DGANLungNodules							
Han et al (2019) [357]	3DMCGAN	LIDC-IDRI [144]	CT	Data augmentation	CPM(%): 51.8	55.0	3D multi-conditional GAN (2 Ds) for misdiagnosis prevention in nodule detection.
Yang et al (2019) [409]	GAN	LIDC-IDRI [144]	CT	Data augmentation	ROC AUC(%): 87.56	88.12	Class-aware 3D lung nodule synthesis for nodule CLF.
Wang et al (2020) [410] CA-MW-AS	CGAN	LIDC-IDRI [144]	CT	Data augmentation	F1-Score(%): 85.88	89.03	Nodule synthesis conditioned on semantic features.
Kuang et al (2020) [351]	Multi-D GAN	LIDC-IDRI [144]	CT	Anomaly detection	Accuracy(%): 91.6	95.32	High anomaly scores on malignant images, low scores on benign.
Ghosal et al (2020) [411]	WGAN-GP	LIDC-IDRI [144]	CT	Data augmentation	ROC AUC(%): 95.0	97.0	Unsupervised AE & clustering augmented learning method for nodule CLF.
Sun et al (2020) [412]	DCGAN	LIDC-IDRI [144]	CT	Data augmentation	Accuracy(%): 93.8	94.5	Nodule CLF: Pre-training AlexNet [9] on synthetic, fine-tuning on real.
Wang et al (2020) [413]	pix2pix, PGWGAN, WGAN-GP	Private	CT	Data augmentation	Accuracy(%): 53.2	60.5	Augmented CNN for subcentimeter pulmonary adenocarcinoma CLF.
Bu et al (2020) [358]	3D CGAN	LUNA16 [180]	CT	Data augmentation	Sensitivity(%): 97.81	98.57	Squeeze-and-excitation mechanism and residual learning for nodule detection.
Nishio et al (2020) [361]	3D pix2pix	LUNA16 [180]	CT	Data augmentation	Accuracy(%): 85	85	Nodule size CLF. Masked image + mask + nodule size conditioned paired translation.
Onishi et al (2020) [414]	WGAN	Private	CT	Data augmentation	Specificity(%): 66.7	77.8	AlexNet pretrained on synthetic, fine-tuned on real nodules for malign/benign CLF.
Teramoto et al (2020) [415]	PGGAN	Private	Cytopathology	Data augmentation	Accuracy(%): 81.0	85.3	Malignancy CLF: CNN pretrained on synthetic cytology images, fine-tuned on real.
Others							
Schlegl et al (2017) [349]	AnoGAN	Private	OCT	Anomaly detection	ROC AUC: 0.73	0.89	D representations trained on healthy retinal image patches to score abnormal patches.
Zhang et al (2018) [416]	DCGANs, WGAN, BEGANs	Private	OCT	Data augmentation	Accuracy(%): 95.67	98.83	CLF of thyroid/non-thyroid tissue. Comparative study for GAN data augmentation.
Chaudhan et al (2019) [417]	MG-GAN	NCBI [418]	Expression microarray data	Data augmentation	Accuracy(%): P:71.43, L:68.21 B:69.8 C:67.59	93.6, 88.1, 90.3, 91.7	Prostate, Lung, Breast, Colon. Interesting for fusion with imaging data.
Liu et al (2019) [419]	WGAN-based	Private	Serum sample staging data	Data augmentation	Accuracy(%): 64.52	70.97	Synthetic training data for CLF of stages of Hepatoocellular carcinoma.
Rubin et al (2019) [420]	TOP-GAN	Private	Holographic microscopy	Data augmentation	AUC(%): 89.2	94.7	Pretrained D adapted to CLF of optical path delay maps of cancer cells (colon, skin).

mours that correlate with specific tumour grade. The authors show that when inferring BenignGAN on malignant tumour tissue images after training it exclusively on benign ones, it generates less realistic results. This allows for quantitative measurement of the differences between the original and the generated image, whereby these differences can be interpreted as tumour grade.

Kapil et al [367] explore AC-GAN [43] on digital pathology imagery for semi-supervised quantification of the Non-Small-Cell-Lung-Cancer biomarker *programmed death ligand 1 (PD-L1)*. Their class-conditional generator receives a one-hot encoded PD-L1 label as input to generate a respective biopsy tissue image, while their discriminator receives the image and predicts both PD-L1 label and whether the image is fake or real. The AC-GAN method compares favourably to other supervised and non-generative semi-supervised approaches, and also systematically yields high agreement with visual¹⁹ tumour proportional scoring (TPS).

As for the analysis of the TME, Quiros et al [425] propose PathologyGAN, which they train on breast and colorectal cancer tissue imagery. This allows for learning the most important tissue phenotype descriptions, and provides a continuous latent representation space, enabling quantification and profiling of differences and similarities between different tumours' tissues. Quiros et al show that lesions encoded in an (adversarially trained) model's latent space enable using vector distance measures to find similar lesions that are close in the latent space within large patient cohorts. We highlight the research potential in lesion latent space representations to assess inter-tumour heterogeneity. Also, the treatment strategies and successes of patients with a similar lesion can inform the decision-making process of selecting treatments for a lesion at hand, as denoted by Figure 3(m).

Outlook on Genotypic Tumour Profiling with Phenotypic Data. A further challenge is that targeted oncological therapies require genomic and immunological tumour profiling [279] and effective linking of tumour genotype and phenotype. Biopsies only allow to analyse the biopsied portion of the tumour's genotype, while also increas-

ing patient risk due to the possibility of dislodging and seeding of neoplastic altered cells [426, 283]. Therefore, a trade-off²⁰ exists between minimising the number of biopsies and maximising the biopsy-based information about a tumour's genotype. These reasons and the fact that current methods are invasive, expensive, and time-consuming [279] make genotypic tumour profiling an important issue to be addressed by AI cancer imaging methods. In particular adversarial deep learning models are promising to generate the non-biopsied portion of a tumour's genotype after being trained on paired genotype and radiology imaging data²¹. We recommend future studies to explore this line of research, which is regarded as a key challenge for AI in cancer imaging [24, 283].

4.5.2. Treatment Planning and Response Prediction

Challenges for Cancer Treatment Predictions. A considerable number of malignancies and tumour stages have various possible treatment options and almost no head-to-head evidence to compare them to. Due to that, oncologists need to subjectively select an approved therapy based on their individual experience and exposure [67].

Furthermore, despite existing treatment response assessment frameworks in oncology, inter- and intra-observer variability regarding choice and measurement of target lesions exists among oncologists and radiologists [427]. To achieve consistency and accuracy in standardised treatment response reporting frameworks [427], AI and GAN methods can identify quantitative biomarkers²² from medical images in a reproducible manner useful for risk and treatment response predicts [106].

Apart from the treatment response assessment, treatment response prediction is also challenging, particularly for cancer treatments such as immunotherapy [24]. In cancer immunogenomics, for instance, unsolved challenges comprise the integration of multi-modal data (e.g., radiomic and genomic biomarkers [24]), immunogenic-

¹⁹A visual estimation of pathologists of the tumour cell percentage showing PD-L1 staining.

²⁰Due to this and due to the high intra-tumour heterogeneity, available biopsy data likely only describes a subset of tumour's clonal cell population.

²¹Imaging data on which the entire lesion is visible to allow learning correlations between phenotypic tumour manifestations and genotype signatures.

²²For example, characteristics and density variations of the parenchyma patterns on breast images [24]

ity prediction for neoantigens, and the longitudinal non-invasive monitoring of the therapy response [67]. In regard to the sustainability of a therapy, the inter- and intra-tumour heterogeneity (e.g., in size, shape, morphology, kinetics, texture, etiology) and potential sub-clone treatment survival complicates individual treatment prediction, selection, and response interpretation [24].

GAN Treatment Effect Estimation Examples. In line with Figure 3(n), Yoon et al [428] propose the conditional GAN framework ‘GANITE’, where individual treatment effect prediction allows for accounting for unseen, counterfactual outcomes of treatment. GANITE consists of two GANs: first, a counterfactual GAN is trained on feature and treatment vectors along with the factual outcome data. Then, the trained generator’s output is used for creating a dataset, on which the other GAN, called ITE (Individual Treatment Response) GAN, is being trained. GANITE provides confidence intervals along with the prediction, while being readily scalable for any number of treatments. However, it does not allow for taking time, dosage or other treatment parameters into account. MGANITE, proposed by Ge et al [429], extends GANITE by introducing dosage quantification, and thus enables continuous and categorical treatment effect estimations. SCIGAN [430] also extends upon GANITE and predicts outcomes of continuous rather than one-time interventions and the authors further provide theoretical justification for GANs’ success in learning counterfactual outcomes. As to the problem of individual treatment response prediction, we suggest that quantitative comparisons of GAN-generated expected post-treatment images with real post-treatment images can yield interesting insight for tumour interpretation. We encourage future work to explore generating such post-treatment tumour images given a treatment parameter and a pre-treatment tumour image as conditional inputs. With varying treatment parameters as input, it is to be investigated whether GANs can inform treatment selection by simulating various treatment scenarios prior to treatment allocation or whether GANs can help to understand and evaluate treatment effects by generating counterfactual outcome images after treatment application.

Goldsborough et al [431] presented an approach called CytoGAN, where they synthesises fluorescence microscopy cell images using DCGAN, LSGAN, or

WGAN. The discriminator’s latent representations learnt during synthesis enable grouping encoded cell images together that have similar cellular reactions to treatment by chemicals of known classes (morphological profiling)²³. Even though the authors reported that CytoGAN obtained inferior result²⁴ compared to classical, widely applied methods such as CellProfiler [432], using GANs to group tumour cells representations to inform chemical cancer treatment allocation decisions is an interesting approach in the realm of treatment selection, development [433, 434] and response prediction.

GAN Radiation Dose Planning Examples. As radiation therapy planning is labour-intensive and time-consuming, researchers have been spurred to pursue automated planning processes [435]. As outlined in the following and suggested by Figure 3(o), the challenge of automated radiation therapy planning can be approached using GANs.

By framing radiation dose planning as an image colourisation problem, Mahmood et al [436] introduced an end-to-end GAN-based solution, which predicts 3D radiation dose distributions from CT without the requirement of hand-crafted features. They trained their model on Oropharyngeal cancer data along with three traditional ML models and a standard CNN as baselines. The authors trained a pix2pix [55] GAN on 2D CT imagery, and then fed the generated dose distributions to an inverse optimisation (IO) model [437], in order to generate optimised plans. Their evaluation showed that their GAN plans outperformed the baseline methods in all clinical metrics.

Kazemifar [112] (in Table 2) proposed a cGAN with U-Net generator for paired MRI to CT translation. Using conventional dose calculation algorithms, the authors compared the dose computed for real CT and generated CT, where the latter showed high dosimetric accuracy. The study, hence, demonstrates the feasibility of synthetic CT for intensity-modulated proton therapy planning for brain tumour cases, where only MRI scans are available.

Maspero et al [438] proposed a GAN-assisted approach to quicken the process of MR-based radiation dose planning, by using a pix2pix for generating synthetic CTs

²³CytoGAN uses an approach comparable to the one shown in Figure 9(g).

²⁴i.e. mechanism-of-action classification accuracy

(sCTs) required for this task. They show that a conditional GAN trained on prostate cancer patient data can successfully generate sCTs of the entire pelvis.

A similar task has also been addressed by Peng et al [125]. Their work compares two GAN approaches: one is based on pix2pix and the other on a CycleGAN [54]. The main difference between these two approaches was that pix2pix was trained using registered MR-CT pairs of images, whereas CycleGAN was trained on unregistered pairs. Ultimately, the authors report pix2pix to achieve results (i.e. mean absolute error) superior to CycleGAN, and highlight difficulties in generating high-density bony tissues using CycleGAN.

The recently introduced attention-aware DoseGAN [439] overcomes the challenges of volumetric dose prediction in the presence of diverse patient anatomy. As illustrated in Figure 10, DoseGAN is based on a variation of the pix2pix architecture with a 3D encoder-decoder generator (L1 loss) and a patch-based patchGAN discriminator (adversarial loss). The generator was trained on concatenated CT, planning target volume (PTV) and organs at risk (OARs) data of prostate cancer patients, and the discriminator's objective was to distinguish the real dose volumes from the generated ones. Both qualitatively and quantitatively, DoseGAN was able to synthesise more realistic volumetric doses compared to current alternative state-of-the-art methods.

Murakami et al [440] published another GAN-based fully automated approach to dose distribution of Intensity-Modulated Radiation Therapy (IMRT) for prostate cancer. The novelty of their solution is that it does not require the tumour contour information, which is time-consuming to create, to successfully predict the dose based on the given CT dataset. Their approach consists of two pix2pix-based architectures, one trained on paired CT and radiation dose distribution images, and the other trained on paired structure images and radiation dose distribution images. From the generated radiation dose distribution images the dosimetric parameters for the PTV and OARs are computed. The generated dosimetric parameters differed on average only between 1-3% with respect to the original ground truth dosimetric parameters.

Koike et al [131] proposed a CycleGAN for dose estimation for head and neck CT images with metal artifact removal in CT-to-CT image translation as described in Table 2). Providing consistent dose calculation against metal

artifacts for head and neck IMRT, their approach achieves dose calculation performance similar to commercial metal artifact removal methods.

4.5.3. Disease Tracking and Monitoring

Challenges in Tracking and Modelling Tumour Progression. Tumour progression is challenging to model [441] and commonly requires rich, multi-modal longitudinal data sets. As cancerous cells acquire growth advantages through genetic mutation in a process arguably analogous to Darwinian evolution [6], it is difficult to predict which of the many sub-clones in the TME will outgrow the other clones. A tumour lesion is, hence, constantly evolving in phenotype and genotype [24] and might acquire dangerous further mutations over time, anytime. The TME's respective impact is exemplified by Dimitriou et al's [270] stage II colorectal cancer outcome classification performance gain being likely attributable to the high prognostic value of the TME information in their training data.

In addition, concurrent conditions and alterations in the organ system surrounding a tumour, but also in distant organs may not only remain undetected, but could also influence patient health and progression [24]. GANs can generate hypothetical comorbidity data²⁵ to aid awareness, testing, finding, and analysis of complex disease and comorbidity patterns. A further difficulty for tumour progression modelling is the a priori unknown effect of treatment. Treatment effects may even remain partly unknown after treatment for example in the case of radiation therapy²⁶ [444] or after surgery²⁷ [24].

GAN Tumour Progression Modelling Examples. Relating to Figure 3(p), GANs can not only diversify the training data, but can also be applied to simulate and explore disease progression scenarios [460]. For instance, Elazab et al [460] propose GP-GAN, which uses stacked 3D conditional GANs for growth prediction of glioma based on

²⁵For example from EHR [442, 443], imaging data, or a combination thereof.

²⁶Radiation therapy can result in destruction of the normal tissue (e.g., radionecrosis) surrounding the tumour. Such heterogeneous normal tissue can become difficult to characterise and distinguish from the cancerous tissue [444].

²⁷It is challenging to quantify the volume of remaining tumour residuals after surgical removal [24].

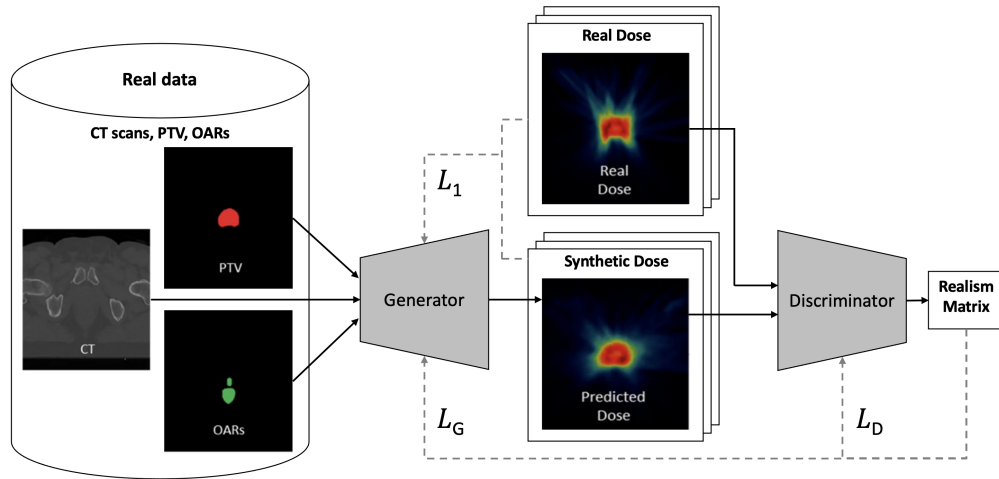


Figure 10: GAN architecture of DoseGAN adapted from Kearney et al [439] and based on pix2pix [55]. Given concatenated CT scans, planning target volume (PTV) and organs at risk (OARs), the generator of DoseGAN addresses the challenge of volumetric dose prediction for prostate cancer patients.

longitudinal MR images. The generator is based on the U-Net architecture [58] and the segmented feature maps are used in the training process. Kim et al [459] trained a CycleGAN on concatenated pre-treatment MR, CT and dose images (i.e. resulting in one 3-channel image) of patients with hepatocellular carcinoma to generate follow-up enhanced MR images. This enables tumour image progression prediction after radiation treatment, whereby CycleGAN outperformed a vanilla GAN baseline.

Li et al’s [461] proposed deep convolutional (DC) [51] - AlexNet (AL) [19] GAN (DC-AL GAN) is trained on longitudinal diffusion tensor imaging (DTI) data of pseudoprogession (PsP) and true tumour progression (TTP) in glioblastoma multiforme (GBM) patients. Both of these progression types can occur after standard treatment²⁸ and they are often difficult to differentiate due to similarities in shape and intensity. In DC-AL GAN, representations are extracted from various layers of its AlexNet discriminator that is trained on discriminating between real and generated DTI images. These representations are then used to train a support vector machine (SVM) classifier to distinguish between PsP and TTP samples achieving promising performance.

²⁸Pseudoprogession occurs in 20-30% of GBM patients [461].

We recommend further studies to extend on these first adversarial learning disease progression modelling approaches. One potential research direction are GANs that simulate environment and tumour dependent progression patterns based on conditional input data such as the tumour’s gene expression data [117] or the progressed time between original image and generated progression image (e.g., time passed between image acquisitions or since treatment exposure). To this end, unexpected changes of a tumour may be uncovered between time points or deviations from a tumour’s biopsy proven genotypic growth expectations²⁹.

5. Discussion and Future Perspectives

As presented in Figure 2(c), we have included 163 of the surveyed GAN publications in the timeframe from 2017 until March 7th 2021. We observe that the numbers of cancer imaging GANs publications has been increasing from 2017 to 2020 from 9 to 64 with a surprising slight drop between 2018 to 2019 (41 to 37). The final

²⁹For example, by comparing the original patient image after progression with the GAN-generated predicted image (or its latent representation) after progression for time spans of interest.

Table 6: Overview of adversarially-trained models applied to treatment and monitoring challenges. Publications are clustered by section and ordered by year in ascending order.

Publication	Method	Dataset	Modality	Task	Highlights
Disease Prognosis					
Kim et al (2018) [422]	GAN-based	TCGA [445], Reac-tome [446, 447]	[non-imaging] multi-omics cancer data	Data synthesis	Biomarker gene identification for pancreas, breast, kidney, brain, and stomach cancer with GANs and PageRank.
Ahmed et al (2021) [423]	omicsGAN	TCGA [448, 449]	[non-imaging] ovarian/breast gene expression	Paired translation	microRNA to mRNA translation and vice versa. Synthetic data improves cancer outcome classification.
Tumour Profiling					
Kapil et al (2018) [367]	AC-GAN	Private	Lung histopathology	Classification	AC-GAN CLF of PD-L1 levels for lung tumour tissue images obtained via needle biopsies.
Vu et al (2019) [424]	BenignGAN	Private	Colorectal histopathology	Paired translation	Edge map-to-image. As trained on only benign, malignant images quantifiable via lower realism.
Quiros et al (2021) [425]	PathologyGAN	VGH/NKI [450], PathologyGAN NCT [451]	Breast/colorectal histopathology	Representation learning	Learning tissue phenotype descriptions and latent space representations of tumour histology image patches.
Treatment Response Prediction					
Kadurin et al (2017) [433, 434]	AAE-based druGAN	Pubchem BioAssay [452]	[non-imaging] Molecular fingerprint data	Representation learning	AAE for anti-cancer agent drug discovery. AAE input/output: molecular fingerprints & log concentration vectors.
Goldsbrough et al (2017) [431]	CytoGAN	BBBC021 [453]	Cytopathology	Representation learning	Grouping cells with similar treatment response via learned cell image latent representations.
Yoon et al (2018) [428]	GANITE	USA 89-91 Twins [454]	[non-imaging] individualized treatment effects	Conditional synthesis	cGANs for individual treatment effect prediction, including unseen counterfactual outcomes and confidence intervals.
Ge et al (2018) [429]	MGANITE	AML clinical trial [455]	[non-imaging] individualized treatment effects	Conditional synthesis	GANITE extension introducing dosage quantification and continuous and categorical treatment effect estimation.
Bica et al (2020) [430]	SCIGAN	TCGA [456], News [457, 458], MIMIC III [265]	[non-imaging] individualized treatment effects	Conditional synthesis	GANITE extension introducing continuous interventions and theoretical explanation for GAN counterfactuals.
Radiation Dose Planning					
Mahmood et al (2018) [436]	pix2pix-based	Private	Oropharyngeal CT	Paired translation	Translating CT to 3D dose distributions without requiring hand-crafted features.
Maspero et al (2018) [438]	pix2pix	Private	Prostate/rectal/cervical CT/MRI	Paired translation	MR-to-CT translation for MR-based radiation dose planning without CT acquisition.
Murakami et al (2018) [440]	pix2pix	Private	Prostate CT	Paired translation	CT-to-radiation dose distribution image translation without time-consuming contour/organs at risk (OARs) data.
Peng et al (2020) [125]	pix2pix, CycleGAN	Private	Nasopharyngeal CT/MRI	Unpaired/Paired translation	Comparison of pix2pix & CycleGAN-based generation of CT from MR for radiation dose planning.
Kearney et al (2020) [439]	DoseGAN	Private	Prostate CT/PTV/OARs	Paired translation	Synthesis of volumetric dosimetry from CT+PTV+OARs even in the presence of diverse patient anatomy.
Disease Tracking & Monitoring					
Kim et al (2019) [459]	CycleGAN	Private	Liver MRI/CT/dose	Unpaired translation	Pre-treatment MR+CT+dose translation to post-treatment MRI → predicting hepatocellular carcinoma progression.
Elazab et al (2020) [460]	GP-GAN	Private, 2014 [178]	BRATS Cranial MRI	Paired translation	3D U-Net G generating progression image from longitudinal MRI to predict glioma growth between time-step.
Li et al (2020) [461]	DC-AL GAN, DCGAN	Private	Cranial MRI	Image synthesis	CLF uses D representations to distinguish pseudo- and true glioblastoma progression.

number of respective publications for 2021 is still pending. The trend towards publications that propose GANs to solve cancer imaging challenges demonstrates the considerable research attention that GANs have been receiving in this field. Following our literature review in Section 4, the need for further research in GANs seems not yet to be met. We were able to highlight various lines of research for GANs in oncology, radiology, and pathology that have received limited research attention or are untapped research potentials. These potentials indicate a continuation of the trend towards more GAN applications and standardised integration of GAN generated synthetic data into medical image analysis pipelines and software solutions.

In regard to imaging modalities, we analyse in Figure 2(b) how much research attention each modality has

received in terms of the number of corresponding publications. By far, MRI and CT are the most dominant modalities with 57, and 54 publications, respectively, followed by MMG (13), dermoscopy (12) and PET (6). The wide spread between MRI and CT and less investigated domains such as endoscopy (3), ultrasound (3), and tomosynthesis (0) is to be critically examined. Due to variations in the imaging data between these modalities (e.g., spatial resolutions, pixel dimensions, domain shifts), it cannot be readily assumed that a GAN application with desirable results in one modality will produce equally desirable results in another. Due to that and with awareness of the clinical importance of MRI and CT, we suggest a more balanced application of GANs across modalities including experiments on rare modalities to demonstrate the clinical versatility and applicability of GAN-based solu-

tions.

In comparison, the GAN-based solutions per anatomy are more evenly spread, but still show a clear trend towards brain, head, neck (47), lung, chest, thorax (33) and breast (25). We suspect these spreads are due to the availability of few well-known widely-used curated benchmark datasets [178, 144, 313, 33] resulting in underexposure of organs and modalities with less publicly available data resources. Where possible, we recommend evaluating GANs on a range of different tasks and organs. This can avoid iterating towards non-transferable solutions tuned for specific datasets with limited generalisation capabilities. Said generalisation capabilities are critical for beneficial usage in clinical environments where dynamic data processing requirements and dataset shifts (e.g., multi-vendor, multi-scanner, multi-modal, multi-organ, multi-centre) commonly exist.

Figure 2(a) displays the distribution of GAN publications across cancer imaging challenge categories that correspond to the subsections of Section 4. While the sections 4.4 detection and diagnosis (54) and 4.4 data annotation and segmentation (44), and 4.1 data scarcity and usability (35) have received much research attention, the sections 4.5 treatment and monitoring (18) and 4.2 data access and privacy (12) contain substantially less GAN-related publications. This spread can be anticipated considering that classification and segmentation are popular computer vision problems and common objectives in publicly available medical imaging benchmark datasets. Early detected cancerous cells likely have had less time to acquire malignant genetic mutations [6, 462] than their latter detected counterparts, which, by then, might have acquired more treatment-resistant alterations and subclone cell populations. Hence, automated early detection, location and diagnosis can provide high clinical impact via improved cancer treatment prospects, which likely influences the trend towards detection and segmentation related GAN publications.

Nonetheless, we also promote future work on the less researched open challenges in Section 4.2, where we describe the promising research potential of GANs in patient data privacy and security. We note that secure patient data is required for legal and ethical patient data sharing and usage, which, on the other hand, is required for successful training of state-of-the-art detection and segmentation models. As diagnosis is an intermediate step in the

clinical workflow, we further encourage more research on GAN solutions extending to subsequent clinical workflow steps such as oncological treatment planning and disease monitoring as elaborated in Section 4.5.

6. Conclusion

In closing, we emphasise the versatility and the resulting modality-independent wide applicability of the unsupervised adversarial learning scheme of GANs. In this survey, we strive to consider and communicate this versatility by describing the wide variety of problems in the cancer imaging domain that can be approached with GANs. For example, we highlight GAN solutions that range from domain adaptation to patient privacy preserving distributed data synthesis, to adversarial segmentation mask discrimination, to multi-modal radiation dose estimation, amongst others.

Before reviewing and describing GAN solutions, we surveyed the literature to understand the current challenges in the field of cancer imaging with a focus on radiology, but without excluding non-radiology modalities common to cancer imaging. After screening and understanding the cancer imaging challenges, we grouped them into the challenge categories Data Scarcity and Usability, Data Access and Privacy, Data Annotation and Segmentation, Detection and Diagnosis, and Treatment and Monitoring. After categorisation, we surveyed the literature for GANs applied to the field of cancer imaging and assigned each relevant GAN publication to its respective cancer imaging challenge category. Finally, we provide a comprehensive analysis for each challenge and its assigned GAN publications to determine to what extent it has and can be solved using GANs. To this end, we also highlight research potential for challenges where we were able to propose a GAN solution that has not yet been covered by the literature.

With this work, we strive to uncover and motivate promising lines of research in adversarial learning that we imagine to ultimately benefit the field of cancer imaging in clinical practice.

Acknowledgments

This project has received funding from the European Union’s Horizon 2020 research and innovation pro-

gramme under grant agreement No 952103.

References

- [1] C. Messiou, J. Hillengass, S. Delorme, F. E. Lecouvet, L. A. Mouloupoulos, D. J. Collins, M. D. Blackledge, N. Abildgaard, B. Østergaard, H.-P. Schlemmer, et al., Guidelines for acquisition, interpretation, and reporting of whole-body mri in myeloma: myeloma response assessment and diagnosis system (my-rads), *Radiology* 291 (1) (2019) 5–13.
- [2] M. Arnold, M. J. Rutherford, A. Bardot, J. Ferlay, T. M. Andersson, T. Å. Myklebust, H. Tervonen, V. Thursfield, D. Ransom, L. Shack, et al., Progress in cancer survival, mortality, and incidence in seven high-income countries 1995–2014 (icbp survmark-2): a population-based study, *The Lancet Oncology* 20 (11) (2019) 1493–1505.
- [3] J. Ferlay, I. Soerjomataram, R. Dikshit, S. Eser, C. Mathers, M. Rebelo, D. M. Parkin, D. Forman, F. Bray, Cancer incidence and mortality worldwide: sources, methods and major patterns in globocan 2012, *International journal of cancer* 136 (5) (2015) E359–E386.
- [4] W. H. Organization, *Cancer* (2018). URL <https://www.who.int/news-room/fact-sheets/detail/cancer>
- [5] A. Jemal, F. Bray, M. M. Center, J. Ferlay, E. Ward, D. Forman, Global cancer statistics, *CA: a cancer journal for clinicians* 61 (2) (2011) 69–90.
- [6] D. Hanahan, R. A. Weinberg, The hallmarks of cancer, *cell* 100 (1) (2000) 57–70.
- [7] L. Norton, R. Simon, H. D. Brereton, A. E. Bogen, Predicting the course of gompertzian growth, *Nature* 264 (5586) (1976) 542–545.
- [8] J. V. Frangioni, New technologies for human cancer imaging, *Journal of clinical oncology* 26 (24) (2008) 4012.
- [9] B. M. Fischer, M. W. Olsen, C. D. Ley, T. L. Klausen, J. Mortensen, L. Højgaard, P. E. Kristjansen, How few cancer cells can be detected by positron emission tomography? a frequent question addressed by an in vitro study, *European journal of nuclear medicine and molecular imaging* 33 (6) (2006) 697–702.
- [10] J. N. Itri, R. R. Tappouni, R. O. McEachern, A. J. Pesch, S. H. Patel, Fundamentals of diagnostic error in imaging, *Radiographics* 38 (6) (2018) 1845–1865.
- [11] G. McCreadie, T. Oliver, Eight ct lessons that we learned the hard way: an analysis of current patterns of radiological error and discrepancy with particular emphasis on ct, *Clinical radiology* 64 (5) (2009) 491–499.
- [12] A. Swiecicki, N. Konz, M. Buda, M. A. Mazurowski, A generative adversarial network-based abnormality detection using only normal images for model training with application to digital breast tomosynthesis, *Scientific reports* 11 (1) (2021) 1–13.
- [13] R. J. McDonald, K. M. Schwartz, L. J. Eckel, F. E. Diehn, C. H. Hunt, B. J. Bartholmai, B. J. Erickson, D. F. Kallmes, The effects of changes in utilization and technological advancements of cross-sectional imaging on radiologist workload, *Academic radiology* 22 (9) (2015) 1191–1198.
- [14] J. G. Elmore, C. K. Wells, C. H. Lee, D. H. Howard, A. R. Feinstein, Variability in radiologists’ interpretations of mammograms, *New England Journal of Medicine* 331 (22) (1994) 1493–1499.
- [15] M. Woo, S. C. Lowe, A. M. Devane, R. W. Gimbel, Intervention to reduce interobserver variability in computed tomographic measurement of cancer lesions among experienced radiologists, *Current problems in diagnostic radiology*.
- [16] K. Fukushima, Neocognitron: A self-organizing neural network model for a mechanism of pattern recognition unaffected by shift in position, *Biological Cybernetics* 36 (4) (1980) 193–202. doi: [10.1007/BF00344251](https://doi.org/10.1007/BF00344251).

- [17] Y. LeCun, B. Boser, J. S. Denker, D. Henderson, R. E. Howard, W. Hubbard, L. D. Jackel, Back-propagation applied to handwritten zip code recognition, *Neural computation* 1 (4) (1989) 541–551.
- [18] D. Cireşan, U. Meier, J. Masci, J. Schmidhuber, Multi-column deep neural network for traffic sign classification, *Neural networks* 32 (2012) 333–338.
- [19] A. Krizhevsky, I. Sutskever, G. E. Hinton, ImageNet classification with deep convolutional neural networks, *Advances in neural information processing systems* 25 (2012) 1097–1105.
- [20] D. C. Cireşan, A. Giusti, L. M. Gambardella, J. Schmidhuber, Mitosis detection in breast cancer histology images with deep neural networks, in: *International conference on medical image computing and computer-assisted intervention*, Springer, 2013, pp. 411–418.
- [21] D. Shen, G. Wu, H.-I. Suk, Deep learning in medical image analysis, *Annual review of biomedical engineering* 19 (2017) 221–248.
- [22] S. K. Zhou, H. Greenspan, C. Davatzikos, J. S. Duncan, B. van Ginneken, A. Madabhushi, J. L. Prince, D. Rueckert, R. M. Summers, A review of deep learning in medical imaging: Imaging traits, technology trends, case studies with progress highlights, and future promises, *Proceedings of the IEEE* (2021) 1–19.
- [23] G. Litjens, T. Kooi, B. E. Bejnordi, A. A. A. Setio, F. Ciompi, M. Ghafoorian, J. A. Van Der Laak, B. Van Ginneken, C. I. Sánchez, A survey on deep learning in medical image analysis, *Medical image analysis* 42 (2017) 60–88.
- [24] W. L. Bi, A. Hosny, M. B. Schabath, M. L. Giger, N. J. Birkbak, A. Mehrtash, T. Allison, O. Arnaout, C. Abbosh, I. F. Dunn, et al., Artificial intelligence in cancer imaging: clinical challenges and applications, *CA: a cancer journal for clinicians* 69 (2) (2019) 127–157.
- [25] I. Goodfellow, J. Pouget-Abadie, M. Mirza, B. Xu, D. Warde-Farley, S. Ozair, A. Courville, Y. Bengio, Generative adversarial nets, in: *Advances in neural information processing systems*, 2014, pp. 2672–2680.
- [26] X. Yi, E. Walia, P. Babyn, Generative adversarial network in medical imaging: A review, *Medical image analysis* 58 (2019) 101552.
- [27] S. Kazemina, C. Baur, A. Kuijper, B. van Ginneken, N. Navab, S. Albarqouni, A. Mukhopadhyay, Gans for medical image analysis, *Artificial Intelligence in Medicine* (2020) 101938.
- [28] M. E. Tschuchnig, G. J. Oostingh, M. Gadermayr, Generative adversarial networks in digital pathology: a survey on trends and future potential, *Patterns* 1 (6) (2020) 100089.
- [29] V. Sorin, Y. Barash, E. Konen, E. Klang, Creating artificial images for radiology applications using generative adversarial networks (gans)—a systematic review, *Academic radiology*.
- [30] L. Lan, L. You, Z. Zhang, Z. Fan, W. Zhao, N. Zeng, Y. Chen, X. Zhou, Generative adversarial networks and its applications in biomedical informatics, *Frontiers in Public Health* 8 (2020) 164.
- [31] N. K. Singh, K. Raza, Medical image generation using generative adversarial networks, *arXiv preprint arXiv:2005.10687*.
- [32] I. Goodfellow, Y. Bengio, A. Courville, *Deep Learning*, Vol. 1, MIT Press, 2016, <http://www.deeplearningbook.org>.
- [33] I. C. Moreira, I. Amaral, I. Domingues, A. Cardoso, M. J. Cardoso, J. S. Cardoso, Inbreast: toward a full-field digital mammographic database, *Academic radiology* 19 (2) (2012) 236–248.
- [34] M. Mirza, S. Osindero, Conditional generative adversarial nets, *arXiv preprint arXiv:1411.1784*.
- [35] F. Farnia, A. Ozdaglar, Gans may have no nash equilibria, *arXiv preprint arXiv:2002.09124*.
- [36] J. F. Nash, et al., Equilibrium points in n-person games, *Proceedings of the national academy of sciences* 36 (1) (1950) 48–49.

- [37] N. Kodali, J. Abernethy, J. Hays, Z. Kira, On convergence and stability of gans, arXiv preprint arXiv:1705.07215.
- [38] L. Mescheder, A. Geiger, S. Nowozin, Which training methods for gans do actually converge?, in: International conference on machine learning, PMLR, 2018, pp. 3481–3490.
- [39] T. Karras, T. Aila, S. Laine, J. Lehtinen, Progressive growing of gans for improved quality, stability, and variation, arXiv preprint arXiv:1710.10196.
- [40] T. Karras, S. Laine, T. Aila, A style-based generator architecture for generative adversarial networks, in: Proceedings of the IEEE/CVF Conference on Computer Vision and Pattern Recognition, 2019, pp. 4401–4410.
- [41] T. Karras, S. Laine, M. Aittala, J. Hellsten, J. Lehtinen, T. Aila, Analyzing and improving the image quality of stylegan, in: Proceedings of the IEEE/CVF Conference on Computer Vision and Pattern Recognition, 2020, pp. 8110–8119.
- [42] E. R. Chan, M. Monteiro, P. Kellnhofer, J. Wu, G. Wetzstein, pi-gan: Periodic implicit generative adversarial networks for 3d-aware image synthesis, arXiv preprint arXiv:2012.00926.
- [43] A. Odena, C. Olah, J. Shlens, Conditional image synthesis with auxiliary classifier gans, in: International conference on machine learning, PMLR, 2017, pp. 2642–2651.
- [44] H. Park, Y. Yoo, N. Kwak, Mc-gan: Multi-conditional generative adversarial network for image synthesis, arXiv preprint arXiv:1805.01123.
- [45] R. D. Hjelm, A. P. Jacob, T. Che, A. Trischler, K. Cho, Y. Bengio, Boundary-seeking generative adversarial networks, arXiv preprint arXiv:1702.08431.
- [46] Z. Wang, Q. She, T. E. Ward, Generative adversarial networks in computer vision: A survey and taxonomy, arXiv preprint arXiv:1906.01529.
- [47] X. Mao, Q. Li, H. Xie, R. Y. K. Lau, Z. Wang, S. P. Smolley, Least squares generative adversarial networks (2017). [arXiv:1611.04076](https://arxiv.org/abs/1611.04076).
- [48] M. Arjovsky, S. Chintala, L. Bottou, Wasserstein gan (2017). [arXiv:1701.07875](https://arxiv.org/abs/1701.07875).
- [49] I. Gulrajani, F. Ahmed, M. Arjovsky, V. Dumoulin, A. C. Courville, [Improved training of wasserstein gans](https://arxiv.org/abs/1705.09217), in: I. Guyon, U. V. Luxburg, S. Bengio, H. Wallach, R. Fergus, S. Vishwanathan, R. Garnett (Eds.), Advances in Neural Information Processing Systems, Vol. 30, Curran Associates, Inc., 2017.
URL <https://proceedings.neurips.cc/paper/2017/file/892c3b1c6dccb52936e27cbd0ff683d6-Paper.pdf>
- [50] S. Ioffe, C. Szegedy, Batch normalization: Accelerating deep network training by reducing internal covariate shift, in: International conference on machine learning, PMLR, 2015, pp. 448–456.
- [51] A. Radford, L. Metz, S. Chintala, Unsupervised representation learning with deep convolutional generative adversarial networks, arXiv preprint arXiv:1511.06434.
- [52] K. Simonyan, A. Zisserman, Very deep convolutional networks for large-scale image recognition, arXiv preprint arXiv:1409.1556.
- [53] C. Ledig, L. Theis, F. Huszár, J. Caballero, A. Cunningham, A. Acosta, A. Aitken, A. Tejani, J. Totz, Z. Wang, et al., Photo-realistic single image super-resolution using a generative adversarial network, in: Proceedings of the IEEE conference on computer vision and pattern recognition, 2017, pp. 4681–4690.
- [54] J.-Y. Zhu, T. Park, P. Isola, A. A. Efros, Unpaired image-to-image translation using cycle-consistent adversarial networks, in: Proceedings of the IEEE international conference on computer vision, 2017, pp. 2223–2232.

- [55] P. Isola, J.-Y. Zhu, T. Zhou, A. A. Efros, Image-to-image translation with conditional adversarial networks, in: *Proceedings of the IEEE conference on computer vision and pattern recognition*, 2017, pp. 1125–1134.
- [56] T. Park, M.-Y. Liu, T.-C. Wang, J.-Y. Zhu, Semantic image synthesis with spatially-adaptive normalization, in: *Proceedings of the IEEE/CVF Conference on Computer Vision and Pattern Recognition*, 2019, pp. 2337–2346.
- [57] T.-C. Wang, M.-Y. Liu, J.-Y. Zhu, A. Tao, J. Kautz, B. Catanzaro, High-resolution image synthesis and semantic manipulation with conditional gans, in: *Proceedings of the IEEE conference on computer vision and pattern recognition*, 2018, pp. 8798–8807.
- [58] O. Ronneberger, P. Fischer, T. Brox, U-net: Convolutional networks for biomedical image segmentation, in: *International Conference on Medical image computing and computer-assisted intervention*, Springer, 2015, pp. 234–241.
- [59] Y. Jiang, S. Chang, Z. Wang, Transgan: Two transformers can make one strong gan (2021). [arXiv: 2102.07074](https://arxiv.org/abs/2102.07074).
- [60] A. Vaswani, N. Shazeer, N. Parmar, J. Uszkoreit, L. Jones, A. N. Gomez, L. Kaiser, I. Polosukhin, Attention is all you need, *arXiv preprint arXiv:1706.03762*.
- [61] Y. Ganin, V. Lempitsky, Unsupervised domain adaptation by backpropagation, in: *International conference on machine learning*, PMLR, 2015, pp. 1180–1189.
- [62] K. Kamnitsas, C. Baumgartner, C. Ledig, V. Newcombe, J. Simpson, A. Kane, D. Menon, A. Nori, A. Criminisi, D. Rueckert, et al., Unsupervised domain adaptation in brain lesion segmentation with adversarial networks, in: *International conference on information processing in medical imaging*, Springer, 2017, pp. 597–609.
- [63] K. Clark, B. Vendt, K. Smith, J. Freymann, J. Kirby, P. Koppel, S. Moore, S. Phillips, D. Maffitt, M. Pringle, et al., The Cancer Imaging Archive (TCIA): maintaining and operating a public information repository, *Journal of digital imaging* 26 (6) (2013) 1045–1057.
- [64] C. Han, H. Hayashi, L. Rundo, R. Araki, W. Shimoda, S. Muramatsu, Y. Furukawa, G. Mauri, H. Nakayama, Gan-based synthetic brain mr image generation, in: *2018 IEEE 15th International Symposium on Biomedical Imaging (ISBI 2018)*, IEEE, 2018, pp. 734–738.
- [65] J. Quionero-Candela, M. Sugiyama, A. Schwaighofer, N. D. Lawrence, *Dataset shift in machine learning*, The MIT Press, 2009.
- [66] H. Shimodaira, Improving predictive inference under covariate shift by weighting the log-likelihood function, *Journal of statistical planning and inference* 90 (2) (2000) 227–244.
- [67] O. Troyanskaya, Z. Trajanoski, A. Carpenter, S. Thrun, N. Razavian, N. Oliver, Artificial intelligence and cancer, *Nature Cancer* 1 (2) (2020) 149–152.
- [68] D. C. Castro, I. Walker, B. Glocker, Causality matters in medical imaging, *Nature Communications* 11 (1) (2020) 1–10.
- [69] S. Santurkar, L. Schmidt, A. Madry, A classification-based study of covariate shift in gan distributions, in: *International Conference on Machine Learning*, PMLR, 2018, pp. 4480–4489.
- [70] S. Arora, A. Risteski, Y. Zhang, Do gans learn the distribution? some theory and empirics, in: *International Conference on Learning Representations*, 2018.
- [71] O. Diaz, K. Kushibar, R. Osuala, A. Linardos, L. Garrucho, L. Igual, P. Radeva, F. Prior, P. Gkontra, K. Lekadir, Data preparation for artificial intelligence in medical imaging: A comprehensive guide to open-access platforms and tools, *Physica Medica* 83 (2021) 25–37. [doi:10.1016/j.ejmp.2021.02.007](https://doi.org/10.1016/j.ejmp.2021.02.007).

- [72] K. Zhou, Z. Liu, Y. Qiao, T. Xiang, C. C. Loy, Domain generalization: A survey, arXiv preprint arXiv:2103.02503.
- [73] M. M. Rahman, C. Fookes, M. Baktashmotlagh, S. Sridharan, Multi-component image translation for deep domain generalization, in: 2019 IEEE Winter Conference on Applications of Computer Vision (WACV), IEEE, 2019, pp. 579–588.
- [74] H. Li, S. J. Pan, S. Wang, A. C. Kot, Domain generalization with adversarial feature learning, in: Proceedings of the IEEE Conference on Computer Vision and Pattern Recognition, 2018, pp. 5400–5409.
- [75] R. Volpi, H. Namkoong, O. Sener, J. Duchi, V. Murino, S. Savarese, Generalizing to unseen domains via adversarial data augmentation, arXiv preprint arXiv:1805.12018.
- [76] M. W. Lafarge, J. P. Pluim, K. A. Eppenhof, M. Veta, Learning domain-invariant representations of histological images, *Frontiers in medicine* 6 (2019) 162.
- [77] X. Chen, Y. Li, L. Yao, E. Adeli, Y. Zhang, Generative adversarial u-net for domain-free medical image augmentation, arXiv preprint arXiv:2101.04793.
- [78] J. Gohagan, P. Marcus, R. Fagerstrom, P. Pinsky, B. Kramer, P. Prorok, L. S. S. R. Group, et al., Baseline findings of a randomized feasibility trial of lung cancer screening with spiral ct scan vs chest radiograph: the lung screening study of the national cancer institute, *Chest* 126 (1) (2004) 114–121.
- [79] J. K. Gohagan, P. M. Marcus, R. M. Fagerstrom, P. F. Pinsky, B. S. Kramer, P. C. Prorok, S. Ascher, W. Bailey, B. Brewer, T. Church, et al., Final results of the lung screening study, a randomized feasibility study of spiral ct versus chest x-ray screening for lung cancer, *Lung cancer* 47 (1) (2005) 9–15.
- [80] N. L. S. T. R. Team, The national lung screening trial: overview and study design, *Radiology* 258 (1) (2011) 243–253.
- [81] H. Yu, S. Hong, X. Yang, J. Ni, Y. Dan, B. Qin, Recognition of multiple imbalanced cancer types based on dna microarray data using ensemble classifiers, *BioMed research international* 2013.
- [82] A. S. Adamson, A. Smith, Machine learning and health care disparities in dermatology, *JAMA dermatology* 154 (11) (2018) 1247–1248.
- [83] A. J. Larrazabal, N. Nieto, V. Peterson, D. H. Milone, E. Ferrante, Gender imbalance in medical imaging datasets produces biased classifiers for computer-aided diagnosis, *Proceedings of the National Academy of Sciences* 117 (23) (2020) 12592–12594.
- [84] X. Li, Z. Cui, Y. Wu, L. Gu, T. Harada, Estimating and improving fairness with adversarial learning, arXiv preprint arXiv:2103.04243.
- [85] V. Sampath, I. Mautua, J. J. A. Martín, A. Gutierrez, A survey on generative adversarial networks for imbalance problems in computer vision tasks, *Journal of big Data* 8 (1) (2021) 1–59.
- [86] S. S. Mullick, S. Datta, S. Das, Generative adversarial minority oversampling, in: Proceedings of the IEEE/CVF International Conference on Computer Vision, 2019, pp. 1695–1704.
- [87] L. Liberman, J. H. Menell, Breast imaging reporting and data system (bi-rads), *Radiologic Clinics* 40 (3) (2002) 409–430.
- [88] K. Kazuhiro, R. A. Werner, F. Toriumi, M. S. Javadi, M. G. Pomper, L. B. Solnes, F. Verde, T. Higuchi, S. P. Rowe, Generative adversarial networks for the creation of realistic artificial brain magnetic resonance images, *Tomography* 4 (4) (2018) 159.
- [89] X. Hu, A. G. Chung, P. Fieguth, F. Khalvati, M. A. Haider, A. Wong, Prostategan: Mitigating data bias via prostate diffusion imaging synthesis with generative adversarial networks, arXiv preprint arXiv:1811.05817.

- [90] S. Addepalli, G. K. Nayak, A. Chakraborty, V. B. Radhakrishnan, Degan: Data-enriching gan for retrieving representative samples from a trained classifier, in: *Proceedings of the AAAI Conference on Artificial Intelligence*, Vol. 34, 2020, pp. 3130–3137.
- [91] P. Sattigeri, S. C. Hoffman, V. Chenthamarakshan, K. R. Varshney, Fairness gan, arXiv preprint arXiv:1805.09910.
- [92] T. Wang, J. Zhao, M. Yatskar, K.-W. Chang, V. Ordonez, Balanced datasets are not enough: Estimating and mitigating gender bias in deep image representations, in: *Proceedings of the IEEE/CVF International Conference on Computer Vision*, 2019, pp. 5310–5319.
- [93] B. H. Zhang, B. Lemoine, M. Mitchell, Mitigating unwanted biases with adversarial learning, in: *Proceedings of the 2018 AAAI/ACM Conference on AI, Ethics, and Society*, 2018, pp. 335–340.
- [94] D. Xu, S. Yuan, L. Zhang, X. Wu, Fairgan: Fairness-aware generative adversarial networks, in: *2018 IEEE International Conference on Big Data (Big Data)*, IEEE, 2018, pp. 570–575.
- [95] A. Beutel, J. Chen, Z. Zhao, E. H. Chi, Data decisions and theoretical implications when adversarially learning fair representations, arXiv preprint arXiv:1707.00075.
- [96] A. Ghorbani, V. Natarajan, D. Coz, Y. Liu, Dermgan: synthetic generation of clinical skin images with pathology, in: *Machine Learning for Health Workshop*, PMLR, 2020, pp. 155–170.
- [97] R. Kim, C.-Y. Ock, B. Keam, T. M. Kim, J. H. Kim, J. C. Paeng, S. K. Kwon, J. H. Hah, T.-K. Kwon, D.-W. Kim, et al., Predictive and prognostic value of pet/ct imaging post-chemoradiotherapy and clinical decision-making consequences in locally advanced head & neck squamous cell carcinoma: a retrospective study, *BMC cancer* 16 (1) (2016) 1–9.
- [98] L. Chen, Q. Yang, J. Bao, D. Liu, X. Huang, J. Wang, Direct comparison of pet/ct and mri to predict the pathological response to neoadjuvant chemotherapy in breast cancer: a meta-analysis, *Scientific reports* 7 (1) (2017) 1–10.
- [99] B. Barbaro, L. Leccisotti, F. M. Vecchio, M. Di Matteo, T. Serra, M. Salsano, A. Poscia, C. Coco, R. Persiani, S. Alfieri, et al., The potential predictive value of mri and pet-ct in mucinous and nonmucinous rectal cancer to identify patients at high risk of metastatic disease, *The British journal of radiology* 90 (1069) (2017) 20150836.
- [100] Q. Chang, Z. Yan, L. Baskaran, H. Qu, Y. Zhang, T. Zhang, S. Zhang, D. N. Metaxas, Multi-modal asyndgan: Learn from distributed medical image data without sharing private information, arXiv preprint arXiv:2012.08604.
- [101] Q. Chang, H. Qu, Y. Zhang, M. Sabuncu, C. Chen, T. Zhang, D. N. Metaxas, Synthetic learning: Learn from distributed asynchronized discriminator gan without sharing medical image data, in: *Proceedings of the IEEE/CVF Conference on Computer Vision and Pattern Recognition*, 2020, pp. 13856–13866.
- [102] J. Haubold, R. Hosch, L. Umutlu, A. Wetter, P. Haubold, A. Radbruch, M. Forsting, F. Nensa, S. Koitka, Contrast agent dose reduction in computed tomography with deep learning using a conditional generative adversarial network, *European Radiology* (2021) 1–9.
- [103] J. Zhao, D. Li, Z. Kassam, J. Howey, J. Chong, B. Chen, S. Li, Tripartite-gan: synthesizing liver contrast-enhanced mri to improve tumor detection, *Medical image analysis* 63 (2020) 101667.
- [104] Y. Wang, L. Zhou, B. Yu, L. Wang, C. Zu, D. S. Lalush, W. Lin, X. Wu, J. Zhou, D. Shen, 3d auto-context-based locality adaptive multi-modality gans for pet synthesis, *IEEE transactions on medical imaging* 38 (6) (2018) 1328–1339.
- [105] K. Zhao, L. Zhou, S. Gao, X. Wang, Y. Wang, X. Zhao, H. Wang, K. Liu, Y. Zhu, H. Ye, Study of low-dose pet image recovery using supervised learning with cyclegan, *PloS one* 15 (9) (2020) e0238455.

- [106] A. Hosny, C. Parmar, J. Quackenbush, L. H. Schwartz, H. J. Aerts, Artificial intelligence in radiology, *Nature Reviews Cancer* 18 (8) (2018) 500–510.
- [107] J. M. Wolterink, A. M. Dinkla, M. H. Savenije, P. R. Seevinck, C. A. van den Berg, I. Išgum, Deep mr to ct synthesis using unpaired data, in: International workshop on simulation and synthesis in medical imaging, Springer, 2017, pp. 14–23.
- [108] V. Kearney, B. P. Ziemer, A. Perry, T. Wang, J. W. Chan, L. Ma, O. Morin, S. S. Yom, T. D. Solberg, Attention-aware discrimination for mr-to-ct image translation using cycle-consistent generative adversarial networks, *Radiology: Artificial Intelligence* 2 (2) (2020) e190027.
- [109] C. Tanner, F. Ozdemir, R. Profanter, V. Vishnevsky, E. Konukoglu, O. Goksel, Generative adversarial networks for mr-ct deformable image registration, *arXiv preprint arXiv:1807.07349*.
- [110] B. Kaiser, S. Albarqouni, Mri to ct translation with gans, *arXiv preprint arXiv:1901.05259*.
- [111] D. Nie, R. Trullo, J. Lian, C. Petitjean, S. Ruan, Q. Wang, D. Shen, Medical image synthesis with context-aware generative adversarial networks, in: International conference on medical image computing and computer-assisted intervention, Springer, 2017, pp. 417–425.
- [112] S. Kazemifar, A. M. Barragán Montero, K. Souris, S. T. Rivas, R. Timmerman, Y. K. Park, S. Jiang, X. Geets, E. Sterpin, A. Owrangi, Dosimetric evaluation of synthetic ct generated with gans for mri-only proton therapy treatment planning of brain tumors, *Journal of applied clinical medical physics* 21 (5) (2020) 76–86.
- [113] D. Prokopenko, J. V. Stadelmann, H. Schulz, S. Renisch, D. V. Dylov, Unpaired synthetic image generation in radiology using gans, in: Workshop on Artificial Intelligence in Radiation Therapy, Springer, 2019, pp. 94–101.
- [114] A. Ben-Cohen, E. Klang, S. P. Raskin, M. M. Amitai, H. Greenspan, Virtual pet images from ct data using deep convolutional networks: initial results, in: International workshop on simulation and synthesis in medical imaging, Springer, 2017, pp. 49–57.
- [115] L. Bi, J. Kim, A. Kumar, D. Feng, M. Fulham, Synthesis of positron emission tomography (pet) images via multi-channel generative adversarial networks (gans), in: molecular imaging, reconstruction and analysis of moving body organs, and stroke imaging and treatment, Springer, 2017, pp. 43–51.
- [116] K. Armanious, C. Jiang, M. Fischer, T. Küstner, T. Hepp, K. Nikolaou, S. Gatidis, B. Yang, Medgan: Medical image translation using gans, *Computerized medical imaging and graphics* 79 (2020) 101684.
- [117] Z. Xu, X. Wang, H.-C. Shin, D. Yang, H. Roth, F. Milletari, L. Zhang, D. Xu, Correlation via synthesis: End-to-end image generation and radiogenomic learning based on generative adversarial network, in: *Medical Imaging with Deep Learning*, PMLR, 2020, pp. 857–866.
- [118] J. P. Cohen, M. Luck, S. Honari, Distribution matching losses can hallucinate features in medical image translation, in: International conference on medical image computing and computer-assisted intervention, Springer, 2018, pp. 529–536.
- [119] J. P. Cohen, M. Luck, S. Honari, How to cure cancer (in images) with unpaired image translation, in: International Conference on Medical Imaging with Deep Learning (MIDL 2018)—Abstract track, 2018.
- [120] J. M. Wolterink, K. Kamnitsas, C. Ledig, I. Išgum, Generative adversarial networks and adversarial methods in biomedical image analysis, *arXiv preprint arXiv:1810.10352*.
- [121] G. Modanwal, A. Vellal, M. A. Mazurowski, Normalization of breast mris using cycle-consistent generative adversarial networks, *arXiv preprint arXiv:1912.08061*.

- [122] S. Fossen-Romsaas, A. Storm-Johannessen, A. S. Lundervold, Synthesizing skin lesion images using cyclegans—a case study.
- [123] C. Hognon, F. Tixier, O. Gallinato, T. Colin, D. Visvikis, V. Jaouen, Standardization of multi-centric image datasets with generative adversarial networks, in: IEEE Nuclear Science Symposium and Medical Imaging Conference 2019, 2019.
- [124] S. Mathew, S. Nadeem, S. Kumari, A. Kaufman, Augmenting colonoscopy using extended and directional cyclegan for lossy image translation, in: Proceedings of the IEEE/CVF Conference on Computer Vision and Pattern Recognition, 2020, pp. 4696–4705.
- [125] Y. Peng, S. Chen, A. Qin, M. Chen, X. Gao, Y. Liu, J. Miao, H. Gu, C. Zhao, X. Deng, et al., Magnetic resonance-based synthetic computed tomography images generated using generative adversarial networks for nasopharyngeal carcinoma radiotherapy treatment planning, *Radiotherapy and Oncology* 150 (2020) 217–224.
- [126] J. Jiang, Y.-C. Hu, N. Tyagi, P. Zhang, A. Rimmer, G. S. Mageras, J. O. Deasy, H. Veeraraghavan, Tumor-aware, adversarial domain adaptation from ct to mri for lung cancer segmentation, in: International Conference on Medical Image Computing and Computer-Assisted Intervention, Springer, 2018, pp. 777–785.
- [127] V. Sandfort, K. Yan, P. J. Pickhardt, R. M. Summers, Data augmentation using generative adversarial networks (cyclegan) to improve generalizability in ct segmentation tasks, *Scientific reports* 9 (1) (2019) 1–9.
- [128] E. Pusey, R. B. Lufkin, R. Brown, M. A. Solomon, D. D. Stark, R. Tarr, W. Hanafee, Magnetic resonance imaging artifacts: mechanism and clinical significance., *Radiographics* 6 (5) (1986) 891–911.
- [129] S. Nehmeh, Y. Erdi, C. Ling, K. Rosenzweig, O. Squire, L. Braban, E. Ford, K. Sidhu, G. Mageras, S. Larson, et al., Effect of respiratory gating on reducing lung motion artifacts in pet imaging of lung cancer, *Medical physics* 29 (3) (2002) 366–371.
- [130] T. Vu, M. Li, H. Humayun, Y. Zhou, J. Yao, A generative adversarial network for artifact removal in photoacoustic computed tomography with a linear-array transducer, *Experimental Biology and Medicine* 245 (7) (2020) 597–605.
- [131] Y. Koike, Y. Anetai, H. Takegawa, S. Ohira, S. Nakamura, N. Tanigawa, Deep learning-based metal artifact reduction using cycle-consistent adversarial network for intensity-modulated head and neck radiation therapy treatment planning, *Physica Medica* 78 (2020) 8–14.
- [132] M. Mardani, E. Gong, J. Y. Cheng, S. Vasanawala, G. Zaharchuk, M. Alley, N. Thakur, S. Han, W. Dally, J. M. Pauly, et al., Deep generative adversarial networks for compressed sensing automates mri, arXiv preprint arXiv:1706.00051.
- [133] G. Yang, S. Yu, H. Dong, G. Slabaugh, P. L. Dragotti, X. Ye, F. Liu, S. Arridge, J. Keegan, Y. Guo, D. Firmin, Dagan: Deep de-aliasing generative adversarial networks for fast compressed sensing mri reconstruction, *IEEE Transactions on Medical Imaging* 37 (6) (2018) 1310–1321. doi: [10.1109/TMI.2017.2785879](https://doi.org/10.1109/TMI.2017.2785879).
- [134] K. H. Kim, W.-J. Do, S.-H. Park, Improving resolution of mr images with an adversarial network incorporating images with different contrast, *Medical physics* 45 (7) (2018) 3120–3131.
- [135] Y. Gu, Z. Zeng, H. Chen, J. Wei, Y. Zhang, B. Chen, Y. Li, Y. Qin, Q. Xie, Z. Jiang, et al., MedsrGAN: medical images super-resolution using generative adversarial networks, *Multimedia Tools and Applications* 79 (2020) 21815–21840.
- [136] C. You, G. Li, Y. Zhang, X. Zhang, H. Shan, M. Li, S. Ju, Z. Zhao, Z. Zhang, W. Cong, et al., Ct super-resolution gan constrained by the identical, residual, and cycle learning ensemble (gan-circle), *IEEE transactions on medical imaging* 39 (1) (2019) 188–203.

- [137] F. Shahidi, Breast cancer histopathology image super-resolution using wide-attention gan with improved wasserstein gradient penalty and perceptual loss, *IEEE Access* 9 (2021) 32795–32809.
- [138] Y. Li, G. Han, X. Wu, Z. H. Li, K. Zhao, Z. Zhang, Z. Liu, C. Liang, Normalization of multicenter ct radiomics by a generative adversarial network method, *Physics in Medicine & Biology* 66 (5) (2021) 055030.
- [139] L. Wei, Y. Lin, W. Hsu, Using a generative adversarial network for ct normalization and its impact on radiomic features, in: 2020 IEEE 17th International Symposium on Biomedical Imaging (ISBI), IEEE, 2020, pp. 844–848.
- [140] A. Borji, Pros and cons of gan evaluation measures: New developments, *arXiv preprint arXiv:2103.09396*.
- [141] D. Korkinof, H. Harvey, A. Heindl, E. Karpati, G. Williams, T. Rijken, P. Kecskemethy, B. Glocker, Perceived realism of high resolution generative adversarial network derived synthetic mammograms, *Radiology: Artificial Intelligence* (2020) e190181.
- [142] M. J. Chuquicusma, S. Hussein, J. Burt, U. Bagci, How to fool radiologists with generative adversarial networks? a visual turing test for lung cancer diagnosis, in: 2018 IEEE 15th international symposium on biomedical imaging (ISBI 2018), IEEE, 2018, pp. 240–244.
- [143] A. B. Levine, J. Peng, D. Farnell, M. Nurse, Y. Wang, J. R. Naso, H. Ren, H. Farahani, C. Chen, D. Chiu, et al., Synthesis of diagnostic quality cancer pathology images by generative adversarial networks, *The Journal of pathology* 252 (2) (2020) 178–188.
- [144] S. G. Armato III, G. McLennan, L. Bidaut, M. F. McNitt-Gray, C. R. Meyer, A. P. Reeves, B. Zhao, D. R. Aberle, C. I. Henschke, E. A. Hoffman, et al., The lung image database consortium (LIDC) and image database resource initiative (IDRI): a completed reference database of lung nodules on CT scans, *Medical physics* 38 (2) (2011) 915–931.
- [145] P. Brennan, A. Silman, Statistical methods for assessing observer variability in clinical measures., *BMJ: British Medical Journal* 304 (6840) (1992) 1491.
- [146] V. Mahajan, V. Venugopal, Audit of artificial intelligence algorithms and its impact in relieving shortage of specialist doctors, *Artificial Intelligence: Applications in Healthcare Delivery* (2020) 207.
- [147] A. Rimmer, Radiologist shortage leaves patient care at risk, warns royal college, *BMJ: British Medical Journal (Online)* 359.
- [148] Z. Wang, A. C. Bovik, H. R. Sheikh, E. P. Simoncelli, Image quality assessment: from error visibility to structural similarity, *IEEE transactions on image processing* 13 (4) (2004) 600–612.
- [149] B. Yu, L. Zhou, L. Wang, Y. Shi, J. Fripp, P. Bourgeat, Ea-gans: edge-aware generative adversarial networks for cross-modality mr image synthesis, *IEEE transactions on medical imaging* 38 (7) (2019) 1750–1762.
- [150] R. Zhang, P. Isola, A. A. Efros, E. Shechtman, O. Wang, The unreasonable effectiveness of deep features as a perceptual metric, in: *Proceedings of the IEEE conference on computer vision and pattern recognition*, 2018, pp. 586–595.
- [151] T. Salimans, I. Goodfellow, W. Zaremba, V. Cheung, A. Radford, X. Chen, Improved techniques for training gans, *arXiv preprint arXiv:1606.03498*.
- [152] M. Heusel, H. Ramsauer, T. Unterthiner, B. Nessler, S. Hochreiter, Gans trained by a two time-scale update rule converge to a local nash equilibrium, *arXiv preprint arXiv:1706.08500*.
- [153] M. J. Chong, D. Forsyth, Effectively unbiased fid and inception score and where to find them, in: *Proceedings of the IEEE/CVF Conference on Computer Vision and Pattern Recognition*, 2020, pp. 6070–6079.
- [154] T. DeVries, A. Romero, L. Pineda, G. W. Taylor, M. Drozdal, On the evaluation of conditional gans, *arXiv preprint arXiv:1907.08175*.

- [155] A. Borji, Pros and cons of gan evaluation measures, *Computer Vision and Image Understanding* 179 (2019) 41–65.
- [156] J. Korpiahkola, T. Sipola, S. Puuska, T. Kokkonen, One-pixel attack deceives automatic detection of breast cancer, *arXiv preprint arXiv:2012.00517*.
- [157] Z. W. Lim, M. L. Lee, W. Hsu, T. Y. Wong, Building trust in deep learning system towards automated disease detection, in: *Proceedings of the AAAI Conference on Artificial Intelligence*, Vol. 33, 2019, pp. 9516–9521.
- [158] X. Hu, R. Guo, J. Chen, H. Li, D. Waldmannstetter, Y. Zhao, B. Li, K. Shi, B. Menze, Coarse-to-fine adversarial networks and zone-based uncertainty analysis for NK/T-cell lymphoma segmentation in CT/PET images, *IEEE journal of biomedical and health informatics* 24 (9) (2020) 2599–2608.
- [159] R. Alshehhi, A. Alshehhi, Quantification of uncertainty in brain tumor segmentation using generative network and bayesian active learning., in: *VISI-GRAPP (4: VISAPP)*, 2021, pp. 701–709.
- [160] M. Abdar, F. Pourpanah, S. Hussain, D. Rezazadegan, L. Liu, M. Ghavamzadeh, P. Fieguth, X. Cao, A. Khosravi, U. R. Acharya, et al., A review of uncertainty quantification in deep learning: Techniques, applications and challenges, *arXiv preprint arXiv:2011.06225*.
- [161] V. Edupuganti, M. Mardani, J. Cheng, S. Vasanaawala, J. Pauly, Uncertainty analysis of vae-gans for compressive medical imaging, *arXiv preprint arXiv:1901.11228*.
- [162] D. P. Kingma, M. Welling, Auto-encoding variational bayes, *arXiv preprint arXiv:1312.6114*.
- [163] C. M. Stein, Estimation of the mean of a multivariate normal distribution, *The annals of Statistics* (1981) 1135–1151.
- [164] R. Tanno, D. E. Worrall, E. Kaden, A. Ghosh, F. Grussu, A. Bizzi, S. N. Sotiropoulos, A. Criminisi, D. C. Alexander, Uncertainty modelling in deep learning for safer neuroimage enhancement: Demonstration in diffusion mri, *NeuroImage* 225 (2021) 117366.
- [165] Y. Gal, Z. Ghahramani, Dropout as a bayesian approximation: Representing model uncertainty in deep learning, in: *international conference on machine learning*, PMLR, 2016, pp. 1050–1059.
- [166] B. Lakshminarayanan, A. Pritzel, C. Blundell, Simple and scalable predictive uncertainty estimation using deep ensembles, *arXiv preprint arXiv:1612.01474*.
- [167] C. J. Kelly, A. Karthikesalingam, M. Suleyman, G. Corrado, D. King, Key challenges for delivering clinical impact with artificial intelligence, *BMC medicine* 17 (1) (2019) 1–9.
- [168] J. M. Durán, K. R. Jongsma, Who is afraid of black box algorithms? on the epistemological and ethical basis of trust in medical ai, *Journal of Medical Ethics* 47 (5) (2021) 329–335.
- [169] N. C. Codella, D. Gutman, M. E. Celebi, B. Helba, M. A. Marchetti, S. W. Dusza, A. Kalloo, K. Liopyris, N. Mishra, H. Kittler, et al., Skin lesion analysis toward melanoma detection: A challenge at the 2017 international symposium on biomedical imaging (isbi), hosted by the international skin imaging collaboration (isic), in: *2018 IEEE 15th International Symposium on Biomedical Imaging (ISBI 2018)*, IEEE, 2018, pp. 168–172.
- [170] B. T. Wyman, D. J. Harvey, K. Crawford, M. A. Bernstein, O. Carmichael, P. E. Cole, P. K. Crane, C. DeCarli, N. C. Fox, J. L. Gunter, et al., Standardization of analysis sets for reporting results from adni mri data, *Alzheimer’s & Dementia* 9 (3) (2013) 332–337.
- [171] M. W. Weiner, D. P. Veitch, P. S. Aisen, L. A. Beckett, N. J. Cairns, R. C. Green, D. Harvey, C. R. Jack Jr, W. Jagust, J. C. Morris, et al., The alzheimer’s disease neuroimaging initiative 3: Continued innovation for clinical trial improvement, *Alzheimer’s & Dementia* 13 (5) (2017) 561–571.

- [172] [Brainweb: Simulated brain database.](#)
URL <https://brainweb.bic.mni.mcgill.ca/brainweb/>
- [173] O. Jimenez-del Toro, H. Müller, M. Krenn, K. Grunberg, A. A. Taha, M. Winterstein, I. Eggel, A. Foncubierta-Rodríguez, O. Goksel, A. Jakab, et al., Cloud-based evaluation of anatomical structure segmentation and landmark detection algorithms: Visceral anatomy benchmarks, *IEEE transactions on medical imaging* 35 (11) (2016) 2459–2475.
- [174] J. M. Fitzpatrick, [Rire - retrospective image registration evaluation](#) (1998).
URL <https://www.insight-journal.org/rire/>
- [175] N. C. I. C. P. T. A. Consortium, et al., Radiology data from the clinical proteomic tumor analysis consortium glioblastoma multiforme [cptac-gbm] collection [data set], *Cancer Imaging Archive*.
- [176] M. Vallières, E. Kayrivest, L. Perrin, et al., Data from head-neck-pet-ct. the cancer imaging archive (2017).
- [177] M. Zhou, A. Leung, S. Echegaray, A. Gentles, J. B. Shrager, K. C. Jensen, G. J. Berry, S. K. Plevritis, D. L. Rubin, S. Napel, et al., Non-small cell lung cancer radiogenomics map identifies relationships between molecular and imaging phenotypes with prognostic implications, *Radiology* 286 (1) (2018) 307–315.
- [178] B. H. Menze, A. Jakab, S. Bauer, J. Kalpathy-Cramer, K. Farahani, J. Kirby, Y. Burren, N. Porz, J. Slotboom, R. Wiest, et al., The multimodal brain tumor image segmentation benchmark (brats), *IEEE transactions on medical imaging* 34 (10) (2014) 1993–2024.
- [179] AAPM, [2016 nih-aapm-mayo clinic low dose ct grand challenge.](#)
URL <https://www.aapm.org/grandchallenge/lowdosect/>
- [180] A. A. A. Setio, A. Traverso, T. De Bel, M. S. Berens, C. van den Bogaard, P. Cerello, H. Chen, Q. Dou, M. E. Fantacci, B. Geurts, et al., Validation, comparison, and combination of algorithms for automatic detection of pulmonary nodules in computed tomography images: the luna16 challenge, *Medical image analysis* 42 (2017) 1–13.
- [181] B. E. Treeby, B. T. Cox, k-wave: Matlab toolbox for the simulation and reconstruction of photoacoustic wave fields, *Journal of biomedical optics* 15 (2) (2010) 021314.
- [182] Y. Benhammou, B. Achchab, F. Herrera, S. Tabik, Breakhis based breast cancer automatic diagnosis using deep learning: Taxonomy, survey and insights, *Neurocomputing* 375 (2020) 9–24.
- [183] G. Litjens, P. Bandi, B. Ehteshami Bejnordi, O. Geessink, M. Balkenhol, P. Bult, A. Halilovic, M. Hermsen, R. van de Loo, R. Vogels, et al., 1399 h&e-stained sentinel lymph node sections of breast cancer patients: the camelyon dataset, *GigaScience* 7 (6) (2018) giy065.
- [184] X. Yu, X. Cai, Z. Ying, T. Li, G. Li, Singlegan: Image-to-image translation by a single-generator network using multiple generative adversarial learning, in: *Asian Conference on Computer Vision*, Springer, 2018, pp. 341–356.
- [185] [Ixi dataset.](#)
URL <http://brain-development.org/ixi-dataset/>
- [186] R. L. Grossman, A. P. Heath, V. Ferretti, H. E. Varmus, D. R. Lowy, W. A. Kibbe, L. M. Staudt, Toward a shared vision for cancer genomic data, *New England Journal of Medicine* 375 (12) (2016) 1109–1112.
- [187] A. Esteva, A. Robicquet, B. Ramsundar, V. Kuleshov, M. DePristo, K. Chou, C. Cui, G. Corrado, S. Thrun, J. Dean, A guide to deep learning in healthcare, *Nature medicine* 25 (1) (2019) 24–29.
- [188] The Health Insurance Portability and Accountability Act (HIPAA), <http://purl.fdlp.gov/GPO/gpo10291>, [Online; accessed 26-November-2020] (2004).

- [189] European Parliament and Council of European Union (2016) Regulation (EU) 2016/679, <https://eur-lex.europa.eu/legal-content/EN/TXT/HTML/?uri=CELEX:32016R0679>, [Online; accessed 26-November-2020] (2016).
- [190] B. McMahan, E. Moore, D. Ramage, S. Hampson, B. A. y Arcas, Communication-efficient learning of deep networks from decentralized data, in: *Artificial Intelligence and Statistics*, PMLR, 2017, pp. 1273–1282.
- [191] G. A. Kaissis, M. R. Makowski, D. Rückert, R. F. Braren, Secure, privacy-preserving and federated machine learning in medical imaging, *Nature Machine Intelligence* 2 (6) (2020) 305–311.
- [192] M. J. Sheller, B. Edwards, G. A. Reina, J. Martin, S. Pati, A. Kotrotsou, M. Milchenko, W. Xu, D. Marcus, R. R. Colen, et al., Federated learning in medicine: facilitating multi-institutional collaborations without sharing patient data, *Scientific reports* 10 (1) (2020) 1–12.
- [193] B. Hitaj, G. Ateniese, F. Perez-Cruz, Deep models under the gan: information leakage from collaborative deep learning, in: *Proceedings of the 2017 ACM SIGSAC Conference on Computer and Communications Security*, 2017, pp. 603–618.
- [194] R. Shokri, V. Shmatikov, Privacy-preserving deep learning, in: *Proceedings of the 22nd ACM SIGSAC conference on computer and communications security*, 2015, pp. 1310–1321.
- [195] M. Lyu, D. Su, N. Li, Understanding the sparse vector technique for differential privacy, *arXiv preprint arXiv:1603.01699*.
- [196] C. Dwork, Differential privacy, in: M. Bugliesi, B. Preneel, V. Sassone, I. Wegener (Eds.), *Automata, Languages and Programming*, Springer Berlin Heidelberg, Berlin, Heidelberg, 2006, pp. 1–12.
- [197] W. Li, F. Milletari, D. Xu, N. Rieke, J. Hancox, W. Zhu, M. Baust, Y. Cheng, S. Ourselin, M. J. Cardoso, et al., Privacy-preserving federated brain tumour segmentation, in: *International Workshop on Machine Learning in Medical Imaging*, Springer, 2019, pp. 133–141.
- [198] C. Hardy, E. Le Merrer, B. Sericola, M-dgan: Multi-discriminator generative adversarial networks for distributed datasets, in: *2019 IEEE international parallel and distributed processing symposium (IPDPS)*, IEEE, 2019, pp. 866–877.
- [199] B. Xin, W. Yang, Y. Geng, S. Chen, S. Wang, L. Huang, Private fl-gan: Differential privacy synthetic data generation based on federated learning, in: *ICASSP 2020-2020 IEEE International Conference on Acoustics, Speech and Signal Processing (ICASSP)*, IEEE, 2020, pp. 2927–2931.
- [200] R. Guerraoui, A. Guirguis, A.-M. Kermarrec, E. L. Merrer, Fegan: Scaling distributed gans, in: *Proceedings of the 21st International Middleware Conference*, 2020, pp. 193–206.
- [201] M. Rasouli, T. Sun, R. Rajagopal, Fedgan: Federated generative adversarial networks for distributed data, *arXiv preprint arXiv:2006.07228*.
- [202] Y. Zhang, H. Qu, Q. Chang, H. Liu, D. Metaxas, C. Chen, Training federated gans with theoretical guarantees: A universal aggregation approach, *arXiv preprint arXiv:2102.04655*.
- [203] H.-C. Shin, N. A. Tenenholtz, J. K. Rogers, C. G. Schwarz, M. L. Senjem, J. L. Gunter, K. P. Andriole, M. Michalski, Medical image synthesis for data augmentation and anonymization using generative adversarial networks, in: *International workshop on simulation and synthesis in medical imaging*, Springer, 2018, pp. 1–11.
- [204] N. Papernot, M. Abadi, U. Erlingsson, I. Goodfellow, K. Talwar, Semi-supervised knowledge transfer for deep learning from private training data, *arXiv preprint arXiv:1610.05755*.
- [205] S. Chen, R. Jia, G.-J. Qi, Improved techniques for model inversion attack, *arXiv preprint arXiv:2010.04092*.

- [206] L. Xie, K. Lin, S. Wang, F. Wang, J. Zhou, Differentially private generative adversarial network, arXiv preprint arXiv:1802.06739.
- [207] A. Torfi, E. A. Fox, C. K. Reddy, Differentially private synthetic medical data generation using convolutional gans, arXiv preprint arXiv:2012.11774.
- [208] J. Jordon, J. Yoon, M. Van Der Schaar, Pate-gan: Generating synthetic data with differential privacy guarantees, in: International Conference on Learning Representations, 2018.
- [209] N. Papernot, S. Song, I. Mironov, A. Raghunathan, K. Talwar, Ú. Erlingsson, Scalable private learning with pate, arXiv preprint arXiv:1802.08908.
- [210] K. Fernandes, J. S. Cardoso, J. Fernandes, [Transfer learning with partial observability applied to cervical cancer screening](#), in: Iberian conference on pattern recognition and image analysis, Springer, 2017, pp. 243–250.
URL <https://archive.ics.uci.edu/ml/datasets/Cervical%2Bcancer%2B%2528Risk%2BFactors%2529>
- [211] B. K. Beaulieu-Jones, Z. S. Wu, C. Williams, R. Lee, S. P. Bhavnani, J. B. Byrd, C. S. Greene, Privacy-preserving generative deep neural networks support clinical data sharing, *Circulation: Cardiovascular Quality and Outcomes* 12 (7) (2019) e005122.
- [212] H. Bae, D. Jung, S. Yoon, Anomigan: Generative adversarial networks for anonymizing private medical data, in: Pacific Symposium on Biocomputing. Pacific Symposium on Biocomputing, Vol. 25, World Scientific, 2020, pp. 563–574.
- [213] T. Stadler, B. Oprisanu, C. Troncoso, Synthetic data – anonymisation groundhog day (2021). [arXiv:2011.07018](#).
- [214] J. Yoon, L. N. Drumright, M. Van Der Schaar, Anonymization through data synthesis using generative adversarial networks (ads-gan), *IEEE journal of biomedical and health informatics* 24 (8) (2020) 2378–2388.
- [215] C. G. Schwarz, W. K. Kremers, T. M. Therneau, R. R. Sharp, J. L. Gunter, P. Vemuri, A. Arani, A. J. Spsychalla, K. Kantarci, D. S. Knopman, et al., Identification of anonymous mri research participants with face-recognition software, *New England Journal of Medicine* 381 (17) (2019) 1684–1686.
- [216] Y. Wu, F. Yang, H. Ling, Privacy-protective-gan for face de-identification, arXiv preprint arXiv:1806.08906.
- [217] H. Hukkelås, R. Mester, F. Lindseth, Deepprivacy: A generative adversarial network for face anonymization, in: International Symposium on Visual Computing, Springer, 2019, pp. 565–578.
- [218] T. Li, L. Lin, Anonymousnet: Natural face de-identification with measurable privacy, in: Proceedings of the IEEE/CVF Conference on Computer Vision and Pattern Recognition Workshops, 2019, pp. 0–0.
- [219] M. Maximov, I. Elezi, L. Leal-Taixé, Ciagan: Conditional identity anonymization generative adversarial networks, in: Proceedings of the IEEE/CVF Conference on Computer Vision and Pattern Recognition, 2020, pp. 5447–5456.
- [220] F. Ségonne, A. M. Dale, E. Busa, M. Glessner, D. Salat, H. K. Hahn, B. Fischl, A hybrid approach to the skull stripping problem in mri, *Neuroimage* 22 (3) (2004) 1060–1075.
- [221] A. Bischoff-Grethe, I. B. Ozyurt, E. Busa, B. T. Quinn, C. Fennema-Notestine, C. P. Clark, S. Morris, M. W. Bondi, T. L. Jernigan, A. M. Dale, et al., A technique for the deidentification of structural brain MR images, *Human brain mapping* 28 (9) (2007) 892–903.
- [222] N. Schimke, M. Kuehler, J. Hale, Preserving privacy in structural neuroimages, in: IFIP Annual Conference on Data and Applications Security and Privacy, Springer, 2011, pp. 301–308.
- [223] M. Milchenko, D. Marcus, Obscuring surface anatomy in volumetric imaging data, *Neuroinformatics* 11 (1) (2013) 65–75.

- [224] D. Abramian, A. Eklund, Refacing: reconstructing anonymized facial features using gans, in: 2019 IEEE 16th International Symposium on Biomedical Imaging (ISBI 2019), IEEE, 2019, pp. 1104–1108.
- [225] L. A. V. der Goten, T. Hepp, Z. Akata, K. Smith, *Adversarial privacy preservation in {mri} scans of the brain* (2021).
URL <https://openreview.net/forum?id=2NH1-ETnHxk>
- [226] E. Wu, K. Wu, D. Cox, W. Lotter, Conditional infilling gans for data augmentation in mammogram classification, in: *Image analysis for moving organ, breast, and thoracic images*, Springer, 2018, pp. 98–106.
- [227] A. S. Becker, L. Jendele, O. Skopek, N. Berger, S. Ghafoor, M. Marcon, E. Konukoglu, Injecting and removing suspicious in breast imaging with cyclegan: A pilot study of automated adversarial attacks using neural networks on small images, *European journal of radiology* 120 (2019) 108649.
- [228] Y. Mirsky, T. Mahler, I. Shelef, Y. Elovici, Ct-gan: Malicious tampering of 3d medical imagery using deep learning, in: 28th {USENIX} Security Symposium ({USENIX} Security 19), 2019, pp. 461–478.
- [229] B. N. Kim, J. Dolz, P.-M. Jodoin, C. Desrosiers, Privacy-net: An adversarial approach for identity-obfuscated segmentation of medical images, *arXiv preprint arXiv:1909.04087*.
- [230] A. Makhzani, J. Shlens, N. Jaitly, I. Goodfellow, B. Frey, Adversarial autoencoders, *arXiv preprint arXiv:1511.05644*.
- [231] A. Creswell, A. Pouplin, A. A. Bharath, Denoising adversarial autoencoders: classifying skin lesions using limited labelled training data, *IET Computer Vision* 12 (8) (2018) 1105–1111.
- [232] N. Raval, A. Machanavajjhala, L. P. Cox, Protecting visual secrets using adversarial nets, in: 2017 IEEE Conference on Computer Vision and Pattern Recognition Workshops (CVPRW), IEEE, 2017, pp. 1329–1332.
- [233] Z. Wu, Z. Wang, Z. Wang, H. Jin, Towards privacy-preserving visual recognition via adversarial training: A pilot study, in: *Proceedings of the European Conference on Computer Vision (ECCV)*, 2018, pp. 606–624.
- [234] T.-Y. Yang, C. Brinton, P. Mittal, M. Chiang, A. Lan, Learning informative and private representations via generative adversarial networks, in: 2018 IEEE International Conference on Big Data (Big Data), IEEE, 2018, pp. 1534–1543.
- [235] F. Pittaluga, S. Koppal, A. Chakrabarti, Learning privacy preserving encodings through adversarial training, in: 2019 IEEE Winter Conference on Applications of Computer Vision (WACV), IEEE, 2019, pp. 791–799.
- [236] P. Vincent, H. Larochelle, Y. Bengio, P.-A. Manzagol, Extracting and composing robust features with denoising autoencoders, in: *Proceedings of the 25th international conference on Machine learning*, 2008, pp. 1096–1103.
- [237] J. Chen, J. Konrad, P. Ishwar, Vgan-based image representation learning for privacy-preserving facial expression recognition, in: *Proceedings of the IEEE Conference on Computer Vision and Pattern Recognition Workshops*, 2018, pp. 1570–1579.
- [238] W. Oleszkiewicz, P. Kairouz, K. Piczak, R. Rajagopal, T. Trzciński, Siamese generative adversarial privatizer for biometric data, in: *Asian Conference on Computer Vision*, Springer, 2018, pp. 482–497.
- [239] J. Bromley, I. Guyon, Y. LeCun, Signature verification using a ‘siamese’ time delay neural network.
- [240] C. H. Sudre, W. Li, T. Vercauteren, S. Ourselin, M. J. Cardoso, Generalised dice overlap as a deep learning loss function for highly unbalanced segmentations, in: *Deep learning in medical image analysis and multimodal learning for clinical decision support*, Springer, 2017, pp. 240–248.

- [241] I. J. Goodfellow, J. Shlens, C. Szegedy, Explaining and harnessing adversarial examples, arXiv preprint arXiv:1412.6572.
- [242] A. Kurakin, I. Goodfellow, S. Bengio, Y. Dong, F. Liao, M. Liang, T. Pang, J. Zhu, X. Hu, C. Xie, et al., Adversarial attacks and defences competition, in: *The NIPS'17 Competition: Building Intelligent Systems*, Springer, 2018, pp. 195–231.
- [243] X. Ma, Y. Niu, L. Gu, Y. Wang, Y. Zhao, J. Bailey, F. Lu, Understanding adversarial attacks on deep learning based medical image analysis systems, *Pattern Recognition* 110 (2021) 107332.
- [244] L. Chen, P. Bentley, K. Mori, K. Misawa, M. Fujiwara, D. Rueckert, Intelligent image synthesis to attack a segmentation cnn using adversarial learning, in: *International Workshop on Simulation and Synthesis in Medical Imaging*, Springer, 2019, pp. 90–99.
- [245] S. G. Finlayson, J. D. Bowers, J. Ito, J. L. Zittrain, A. L. Beam, I. S. Kohane, Adversarial attacks on medical machine learning, *Science* 363 (6433) (2019) 1287–1289.
- [246] M. Paschali, S. Conjeti, F. Navarro, N. Navab, Generalizability vs. robustness: investigating medical imaging networks using adversarial examples, in: *International Conference on Medical Image Computing and Computer-Assisted Intervention*, Springer, 2018, pp. 493–501.
- [247] Y. Li, H. Zhang, C. Bermudez, Y. Chen, B. A. Landman, Y. Vorobeychik, Anatomical context protects deep learning from adversarial perturbations in medical imaging, *Neurocomputing* 379 (2020) 370–378.
- [248] M. Z. Joel, S. Umrao, E. Chang, R. Choi, D. X. Yang, J. Duncan, A. Omuro, R. Herbst, H. Krumholz, S. Aneja, Adversarial attack vulnerability of deep learning models for oncologic images, medRxivdoi:10.1101/2021.01.17.21249704.
- [249] A. Vatian, N. Gusarova, N. Dobrenko, S. Dudorov, N. Nigmatullin, A. Shalyto, A. Lobantsev, Impact of adversarial examples on the efficiency of interpretation and use of information from high-tech medical images, in: *2019 24th Conference of Open Innovations Association (FRUCT)*, IEEE, 2019, pp. 472–478.
- [250] P. Lambin, E. Rios-Velazquez, R. Leijenaar, S. Carvalho, R. G. Van Stiphout, P. Granton, C. M. Zegers, R. Gillies, R. Boellard, A. Dekker, et al., Radiomics: extracting more information from medical images using advanced feature analysis, *European journal of cancer* 48 (4) (2012) 441–446.
- [251] A. Barucci, E. Neri, Adversarial radiomics: the rising of potential risks in medical imaging from adversarial learning (2020).
- [252] M. Lopez, N. Posada, D. C. Moura, R. R. Pollán, J. M. F. Valiente, C. S. Ortega, M. Solar, G. Diaz-Herrero, I. Ramos, J. Loureiro, et al., Bcdr: a breast cancer digital repository, in: *15th International conference on experimental mechanics*, Vol. 1215, 2012.
- [253] A. Madry, A. Makelov, L. Schmidt, D. Tsipras, A. Vladu, Towards deep learning models resistant to adversarial attacks, arXiv preprint arXiv:1706.06083.
- [254] X. He, S. Yang, G. Li, H. Li, H. Chang, Y. Yu, Non-local context encoder: Robust biomedical image segmentation against adversarial attacks, in: *Proceedings of the AAAI Conference on Artificial Intelligence*, Vol. 33, 2019, pp. 8417–8424.
- [255] H. Park, A. Bayat, M. Sabokrou, J. S. Kirschke, B. H. Menze, Robustification of segmentation models against adversarial perturbations in medical imaging, in: *International Workshop on Predictive Intelligence In MEDicine*, Springer, 2020, pp. 46–57.
- [256] S. Liu, A. A. A. Setio, F. C. Ghesu, E. Gibson, S. Grbic, B. Georgescu, D. Comaniciu, No surprises: Training robust lung nodule detection for

- low-dose ct scans by augmenting with adversarial attacks, *IEEE Transactions on Medical Imaging* 40 (1) (2020) 335–345.
- [257] R. Paul, M. Schabath, R. Gillies, L. Hall, D. Goldgof, Mitigating adversarial attacks on medical image understanding systems, in: *2020 IEEE 17th International Symposium on Biomedical Imaging (ISBI)*, IEEE, 2020, pp. 1517–1521.
- [258] A. Huq, M. T. Pervin, Analysis of adversarial attacks on skin cancer recognition, in: *2020 International Conference on Data Science and Its Applications (ICoDSA)*, IEEE, 2020, pp. 1–4.
- [259] H. Hirano, A. Minagi, K. Takemoto, Universal adversarial attacks on deep neural networks for medical image classification, *BMC medical imaging* 21 (1) (2021) 1–13.
- [260] S. C. Wetstein, C. González-Gonzalo, G. Bortsova, B. Liefers, F. Dubost, I. Katramados, L. Hogeweg, B. van Ginneken, J. P. Pluim, M. de Bruijne, et al., Adversarial attack vulnerability of medical image analysis systems: Unexplored factors, *arXiv preprint arXiv:2006.06356*.
- [261] P. Samangouei, M. Kabkab, R. Chellappa, Defense-gan: Protecting classifiers against adversarial attacks using generative models, *arXiv preprint arXiv:1805.06605*.
- [262] S. Bakas, M. Reyes, A. Jakab, S. Bauer, M. Rempfler, A. Crimi, R. T. Shinohara, C. Berger, S. M. Ha, M. Rozycki, et al., Identifying the best machine learning algorithms for brain tumor segmentation, progression assessment, and overall survival prediction in the brats challenge, *arXiv preprint arXiv:1811.02629*.
- [263] N. Kumar, R. Verma, S. Sharma, S. Bhargava, A. Vahadane, A. Sethi, A dataset and a technique for generalized nuclear segmentation for computational pathology, *IEEE transactions on medical imaging* 36 (7) (2017) 1550–1560.
- [264] Y. LeCun, L. Bottou, Y. Bengio, P. Haffner, Gradient-based learning applied to document recognition, *Proceedings of the IEEE* 86 (11) (1998) 2278–2324.
- [265] A. E. Johnson, T. J. Pollard, L. Shen, H. L. Li-Wei, M. Feng, M. Ghassemi, B. Moody, P. Szolovits, L. A. Celi, R. G. Mark, Mimic-iii, a freely accessible critical care database, *Scientific data* 3 (1) (2016) 1–9.
- [266] C. Blake, Uci repository of machine learning databases, <http://www.ics.uci.edu/~mllearn/MLRepository.html>.
- [267] K. Marek, D. Jennings, S. Lasch, A. Siderowf, C. Tanner, T. Simuni, C. Coffey, K. Kieburzt, E. Flagg, S. Chowdhury, et al., The parkinson progression marker initiative (ppmi), *Progress in neurobiology* 95 (4) (2011) 629–635.
- [268] P. J. LaMontagne, T. L. Benzinger, J. C. Morris, S. Keefe, R. Hornbeck, C. Xiong, E. Grant, J. Hasenstab, K. Moulder, A. Vlassenko, et al., Oasis-3: longitudinal neuroimaging, clinical, and cognitive dataset for normal aging and alzheimer disease, *MedRxiv* [doi:10.1101/2019.12.13.19014902](https://doi.org/10.1101/2019.12.13.19014902).
- [269] F. H. Gilles, C. J. Tavaré, E. B. Laurence, P. C. Burger, A. J. Yates, I. F. Pollack, J. L. Finlay, Pathologist interobserver variability of histologic features in childhood brain tumors: results from the ccg-945 study, *Pediatric and Developmental Pathology* 11 (2) (2008) 108–117.
- [270] N. Dimitriou, O. Arandjelović, D. J. Harrison, P. D. Caie, A principled machine learning framework improves accuracy of stage ii colorectal cancer prognosis, *NPJ digital medicine* 1 (1) (2018) 1–9.
- [271] B. Martin, E. Schäfer, E. Jakubowicz, P. Mayr, R. Ihringer, M. Anthuber, G. Schenkirsch, T. Schaller, B. Märkl, Interobserver variability in the h&e-based assessment of tumor budding in pt3/4 colon cancer: does it affect the prognostic relevance?, *Virchows Archiv* 473 (2) (2018) 189–197.
- [272] C. E. Klaver, N. Bulkman, P. Drillenburgh, H. I. Grabsch, N. C. van Grieken, A. Karrenbeld,

- L. Koens, I. van Lijnschoten, J. Meijer, I. D. Nagtegaal, et al., Interobserver, intraobserver, and interlaboratory variability in reporting pt4a colon cancer, *Virchows Archiv* 476 (2) (2020) 219–230.
- [273] K. D. Hopper, C. Kasales, M. A. Van Slyke, T. A. Schwartz, T. R. TenHave, J. A. Jozefiak, Analysis of interobserver and intraobserver variability in ct tumor measurements., *AJR. American journal of roentgenology* 167 (4) (1996) 851–854.
- [274] L. Hadjiiski, H.-c. Cho, H.-P. Chan, B. Sahiner, M. A. Helvie, C. Paramagul, A. V. Nees, Inter-and intra-observer variability of radiologists evaluating cbir systems, in: *International Workshop on Digital Mammography*, Springer, 2012, pp. 482–489.
- [275] S. Teh, S. Ranguis, P. Fagan, Inter-observer variability between radiologists reporting on cerebellopontine angle tumours on magnetic resonance imaging, *The Journal of laryngology and otology* 131 (S1) (2017) S47–S49.
- [276] M. K. Wilson, T. Chawla, L. Wang, M. Friedlander, A. M. Oza, S. Lheureux, Inter and intra-observer variability with the assessment of recist in ovarian cancer. (2018).
- [277] A. P. Brady, Error and discrepancy in radiology: inevitable or avoidable?, *Insights into imaging* 8 (1) (2017) 171–182.
- [278] E. Huynh, A. Hosny, C. Guthier, D. S. Bitterman, S. F. Petit, D. A. Haas-Kogan, B. Kann, H. J. Aerts, R. H. Mak, Artificial intelligence in radiation oncology, *Nature Reviews Clinical Oncology* 17 (12) (2020) 771–781.
- [279] R. Cuocolo, M. Caruso, T. Perillo, L. Ugga, M. Petretta, Machine learning in oncology: A clinical appraisal, *Cancer letters* 481 (2020) 55–62.
- [280] T. Drew, M. L.-H. Võ, J. M. Wolfe, The invisible gorilla strikes again: Sustained inattention blindness in expert observers, *Psychological science* 24 (9) (2013) 1848–1853.
- [281] N. Sharma, L. M. Aggarwal, Automated medical image segmentation techniques, *Journal of medical physics/Association of Medical Physicists of India* 35 (1) (2010) 3.
- [282] D. Kang, J. E. Park, Y.-H. Kim, J. H. Kim, J. Y. Oh, J. Kim, Y. Kim, S. T. Kim, H. S. Kim, Diffusion radiomics as a diagnostic model for atypical manifestation of primary central nervous system lymphoma: development and multicenter external validation, *Neuro-oncology* 20 (9) (2018) 1251–1261.
- [283] C. Parmar, P. Grossmann, J. Bussink, P. Lambin, H. J. Aerts, Machine learning methods for quantitative radiomic biomarkers, *Scientific reports* 5 (1) (2015) 1–11.
- [284] Y. Balagurunathan, V. Kumar, Y. Gu, J. Kim, H. Wang, Y. Liu, D. B. Goldgof, L. O. Hall, R. Korn, B. Zhao, et al., Test–retest reproducibility analysis of lung ct image features, *Journal of digital imaging* 27 (6) (2014) 805–823.
- [285] B. Zhao, Y. Tan, W.-Y. Tsai, J. Qi, C. Xie, L. Lu, L. H. Schwartz, Reproducibility of radiomics for deciphering tumor phenotype with imaging, *Scientific reports* 6 (1) (2016) 1–7.
- [286] X. Xiao, J. Zhao, Y. Qiang, J. Chong, X. Yang, N. G.-F. Kazihise, B. Chen, S. Li, Radiomics-guided gan for segmentation of liver tumor without contrast agents, in: *International Conference on Medical Image Computing and Computer-Assisted Intervention*, Springer, 2019, pp. 237–245.
- [287] M. Foroozandeh, A. Eklund, Synthesizing brain tumor images and annotations by combining progressive growing GAN and SPADE, *arXiv preprint arXiv:2009.05946*.
- [288] T. Wang, Y. Lei, W. J. Curran, T. Liu, X. Yang, Contrast-enhanced MRI synthesis from non-contrast MRI using attention CycleGAN, in: *Medical Imaging 2021: Biomedical Applications in Molecular, Structural, and Functional Imaging*, Vol. 11600, International Society for Optics and Photonics, 2021, p. 116001L.
- [289] Y. Huo, Z. Xu, S. Bao, C. Bermudez, H. Moon, P. Parvathaneni, T. K. Moyo, M. R. Savona, A. As-sad, R. G. Abramson, et al., Splenomegaly seg-

- mentation on multi-modal MRI using deep convolutional networks, *IEEE transactions on medical imaging* 38 (5) (2018) 1185–1196.
- [290] H. Lee, J. Jo, H. Lim, Study on Optimal Generative Network for Synthesizing Brain Tumor-Segmented MR Images, *Mathematical Problems in Engineering* 2020.
- [291] K. Abhishek, G. Hamarneh, Mask2lesion: Mask-constrained adversarial skin lesion image synthesis, in: *International Workshop on Simulation and Synthesis in Medical Imaging*, Springer, 2019, pp. 71–80.
- [292] D. A. B. Oliveira, Implanting synthetic lesions for improving liver lesion segmentation in CT exams, *arXiv preprint arXiv:2008.04690*.
- [293] D. A. B. Oliveira, Controllable Skin Lesion Synthesis Using Texture Patches, Bézier Curves and Conditional GANs, in: *2020 IEEE 17th International Symposium on Biomedical Imaging (ISBI)*, IEEE, 2020, pp. 1798–1802.
- [294] S. Kim, B. Kim, H. Park, Synthesis of Brain Tumor MR Images for Learning Data Augmentation, *arXiv preprint arXiv:2003.07526*.
- [295] A. B. Qasim, I. Ezhov, S. Shit, O. Schoppe, J. C. Paetzold, A. Sekuboyina, F. Kofler, J. Lipkova, H. Li, B. Menze, Red-GAN: Attacking class imbalance via conditioned generation. Yet another medical imaging perspective., in: *Medical Imaging with Deep Learning*, PMLR, 2020, pp. 655–668.
- [296] P. Luc, C. Couprie, S. Chintala, J. Verbeek, Semantic segmentation using adversarial networks, *arXiv preprint arXiv:1611.08408*.
- [297] M. D. Cirillo, D. Abramian, A. Eklund, Vox2Vox: 3D-GAN for brain tumour segmentation, *arXiv preprint arXiv:2003.13653*.
- [298] W. C. Hung, Y. H. Tsai, Y. T. Liou, Y.-Y. Lin, M. H. Yang, Adversarial learning for semi-supervised semantic segmentation, in: *29th British Machine Vision Conference, BMVC 2018*, 2019.
- [299] Z. Shi, Q. Hu, Y. Yue, Z. Wang, O. M. S. AL-Othmani, H. Li, Automatic Nodule Segmentation Method for CT Images Using Aggregation-U-Net Generative Adversarial Networks, *Sensing and Imaging* 21 (1) (2020) 1–16.
- [300] D. Nie, D. Shen, Adversarial confidence learning for medical image segmentation and synthesis, *International Journal of Computer Vision* (2020) 1–20.
- [301] S. Kohl, D. Bonekamp, H.-P. Schlemmer, K. Yaqubi, M. Hohenfellner, B. Hadaschik, J.-P. Radtke, K. Maier-Hein, Adversarial networks for the detection of aggressive prostate cancer, *arXiv preprint arXiv:1702.08014*.
- [302] B. Billot, E. Robinson, A. V. Dalca, J. E. Iglesias, Partial Volume Segmentation of Brain MRI Scans of Any Resolution and Contrast, in: *International Conference on Medical Image Computing and Computer-Assisted Intervention*, Springer, 2020, pp. 177–187.
- [303] M. Rezaei, K. Harmuth, W. Gierke, T. Kellermeier, M. Fischer, H. Yang, C. Meinel, A conditional adversarial network for semantic segmentation of brain tumor, in: *International MICCAI Brainlesion Workshop*, Springer, 2017, pp. 241–252.
- [304] C. Li, M. Wand, Precomputed real-time texture synthesis with markovian generative adversarial networks, in: *European conference on computer vision*, Springer, 2016, pp. 702–716.
- [305] S. Bakas, H. Akbari, A. Sotiras, M. Bilello, M. Rozycki, J. S. Kirby, J. B. Freymann, K. Farahani, C. Davatzikos, Advancing the cancer genome atlas glioma mri collections with expert segmentation labels and radiomic features, *Scientific data* 4 (1) (2017) 1–13.
- [306] T. C. Mok, A. C. Chung, Learning data augmentation for brain tumor segmentation with coarse-to-fine generative adversarial networks, in: *International MICCAI Brainlesion Workshop*, Springer, 2018, pp. 70–80.

- [307] B. Yu, L. Zhou, L. Wang, J. Fripp, P. Bourgeat, 3D cGAN based cross-modality MR image synthesis for brain tumor segmentation, in: 2018 IEEE 15th International Symposium on Biomedical Imaging (ISBI 2018), IEEE, 2018, pp. 626–630.
- [308] N. Codella, V. Rotemberg, P. Tschandl, M. E. Celebi, S. Dusza, D. Gutman, B. Helba, A. Kalloo, K. Liopyris, M. Marchetti, et al., Skin lesion analysis toward melanoma detection 2018: A challenge hosted by the international skin imaging collaboration (ISIC), arXiv preprint arXiv:1902.03368.
- [309] X. Han, L. Qi, Q. Yu, Z. Zhou, Y. Zheng, Y. Shi, Y. Gao, Deep symmetric adaptation network for cross-modality medical image segmentation, arXiv preprint arXiv:2101.06853.
- [310] Y. Xue, T. Xu, H. Zhang, L. R. Long, X. Huang, Segan: Adversarial network with multi-scale l1 loss for medical image segmentation, *Neuroinformatics* 16 (3) (2018) 383–392.
- [311] E. Giacomello, D. Loiacono, L. Mainardi, Brain mri tumor segmentation with adversarial networks, in: 2020 International Joint Conference on Neural Networks (IJCNN), IEEE, 2020, pp. 1–8.
- [312] V. K. Singh, S. Romani, H. A. Rashwan, F. Akram, N. Pandey, M. M. K. Sarker, S. Abdulwahab, J. Torrents-Barrena, A. Saleh, M. Arquez, et al., Conditional generative adversarial and convolutional networks for X-ray breast mass segmentation and shape classification, in: International Conference on Medical Image Computing and Computer-Assisted Intervention, Springer, 2018, pp. 833–840.
- [313] M. Heath, K. Bowyer, D. Kopans, R. Moore, P. Kegelmeyer, The digital database for screening mammography, iwdm-2000, in: Fifth International Workshop on Digital Mammography., Medical Physics Publishing, 2001, pp. 212–218, ISBN: 1-930524-00-5.
- [314] M. Caballo, D. R. Pangallo, R. M. Mann, I. Sechopoulos, Deep learning-based segmentation of breast masses in dedicated breast CT imaging: radiomic feature stability between radiologists and artificial intelligence, *Computers in biology and medicine* 118 (2020) 103629.
- [315] A. Negi, A. N. J. Raj, R. Nersisson, Z. Zhuang, M. Murugappan, RDA-UNET-WGAN: An Accurate Breast Ultrasound Lesion Segmentation Using Wasserstein Generative Adversarial Networks, *Arabian Journal for Science and Engineering* 45 (8) (2020) 6399–6410.
- [316] L. Chen, H. Song, C. Wang, Y. Cui, J. Yang, X. Hu, L. Zhang, Liver tumor segmentation in CT volumes using an adversarial densely connected network, *BMC bioinformatics* 20 (16) (2019) 1–13.
- [317] P. Bilic, P. F. Christ, E. Vorontsov, G. Chlebus, H. Chen, Q. Dou, C.-W. Fu, X. Han, P.-A. Heng, J. Hesser, et al., The liver tumor segmentation benchmark (lits), arXiv preprint arXiv:1901.04056.
- [318] F. Prior, K. Smith, A. Sharma, J. Kirby, L. Tarbox, K. Clark, W. Bennett, T. Nolan, J. Freymann, The public cancer radiology imaging collections of the cancer imaging archive, *Scientific data* 4 (1) (2017) 1–7.
- [319] A. L. Simpson, M. Antonelli, S. Bakas, M. Bilello, K. Farahani, B. Van Ginneken, A. Kopp-Schneider, B. A. Landman, G. Litjens, B. Menze, et al., A large annotated medical image dataset for the development and evaluation of segmentation algorithms, arXiv preprint arXiv:1902.09063.
- [320] K. Yan, X. Wang, L. Lu, R. M. Summers, Deeplesion: automated mining of large-scale lesion annotations and universal lesion detection with deep learning, *Journal of medical imaging* 5 (3) (2018) 036501.
- [321] D. Jin, Z. Xu, Y. Tang, A. P. Harrison, D. J. Mollura, CT-realistic lung nodule simulation from 3D conditional generative adversarial networks for robust lung segmentation, in: International Conference on Medical Image Computing and Computer-Assisted Intervention, Springer, 2018, pp. 732–740.

- [322] X. Dong, Y. Lei, T. Wang, M. Thomas, L. Tang, W. J. Curran, T. Liu, X. Yang, Automatic multiorgan segmentation in thorax CT images using U-net-GAN, *Medical physics* 46 (5) (2019) 2157–2168.
- [323] J. Yang, H. Veeraraghavan, S. G. Armato III, K. Farahani, J. S. Kirby, J. Kalpathy-Kramer, W. van Elmpt, A. Dekker, X. Han, X. Feng, et al., Autosegmentation for thoracic radiation treatment planning: a grand challenge at AAPM 2017, *Medical physics* 45 (10) (2018) 4568–4581.
- [324] Y.-B. Tang, Y.-X. Tang, J. Xiao, R. M. Summers, XLSor: A robust and accurate lung segmentor on chest X-Rays using criss-cross attention and customized radiorealistic abnormalities generation, in: *International Conference on Medical Imaging with Deep Learning*, PMLR, 2019, pp. 457–467.
- [325] X. Huang, M.-Y. Liu, S. Belongie, J. Kautz, Multimodal unsupervised image-to-image translation, in: *Proceedings of the European conference on computer vision (ECCV)*, 2018, pp. 172–189.
- [326] J. Shiraishi, S. Katsuragawa, J. Ikezoe, T. Matsumoto, T. Kobayashi, K.-i. Komatsu, M. Matsui, H. Fujita, Y. Kodera, K. Doi, Development of a digital image database for chest radiographs with and without a lung nodule: receiver operating characteristic analysis of radiologists’ detection of pulmonary nodules, *American Journal of Roentgenology* 174 (1) (2000) 71–74.
- [327] S. Jaeger, A. Karargyris, S. Candemir, L. Folio, J. Siegelman, F. Callaghan, Z. Xue, K. Palaniappan, R. K. Singh, S. Antani, et al., Automatic tuberculosis screening using chest radiographs, *IEEE transactions on medical imaging* 33 (2) (2013) 233–245.
- [328] F. Munawar, S. Azmat, T. Iqbal, C. Grönlund, H. Ali, Segmentation of lungs in chest X-ray image using generative adversarial networks, *IEEE Access* 8 (2020) 153535–153545.
- [329] A. Grall, A. Hamidinekoo, P. Malcolm, R. Zwigelaar, Using a conditional generative adversarial network (cGAN) for prostate segmentation, in: *Annual Conference on Medical Image Understanding and Analysis*, Springer, 2019, pp. 15–25.
- [330] G. Litjens, R. Toth, W. van de Ven, C. Hoeks, S. Kerkstra, B. van Ginneken, G. Vincent, G. Guillard, N. Birbeck, J. Zhang, et al., Evaluation of prostate segmentation algorithms for MRI: the PROMISE12 challenge, *Medical image analysis* 18 (2) (2014) 359–373.
- [331] Z. Zhang, T. Zhao, H. Gay, B. Sun, W. Zhang, Semi-supervised Semantic Segmentation of Organs at Risk on 3D Pelvic CT Images, *arXiv preprint arXiv:2009.09571*.
- [332] U. Cem Birbiri, A. Hamidinekoo, A. Grall, P. Malcolm, R. Zwigelaar, Investigating the performance of generative adversarial networks for prostate tissue detection and segmentation, *Journal of Imaging* 6 (9) (2020) 83.
- [333] X. Liu, S. Guo, H. Zhang, K. He, S. Mu, Y. Guo, X. Li, Accurate colorectal tumor segmentation for CT scans based on the label assignment generative adversarial network, *Medical physics* 46 (8) (2019) 3532–3542.
- [334] J. Poorneshwaran, S. S. Kumar, K. Ram, J. Joseph, M. Sivaprakasam, Polyp segmentation using generative adversarial network, in: *2019 41st Annual International Conference of the IEEE Engineering in Medicine and Biology Society (EMBC)*, IEEE, 2019, pp. 7201–7204.
- [335] D. Vázquez, J. Bernal, F. J. Sánchez, G. Fernández-Esparrach, A. M. López, A. Romero, M. Drozdal, A. Courville, A benchmark for endoluminal scene segmentation of colonoscopy images, *Journal of healthcare engineering* 2017.
- [336] X. Xie, J. Chen, Y. Li, L. Shen, K. Ma, Y. Zheng, MI2GAN: Generative Adversarial Network for Medical Image Domain Adaptation Using Mutual Information Constraint, in: *International Conference on Medical Image Computing and Computer-Assisted Intervention*, Springer, 2020, pp. 516–525.

- [337] J. Silva, A. Histace, O. Romain, X. Dray, B. Granado, Toward embedded detection of polyps in wce images for early diagnosis of colorectal cancer, *International journal of computer assisted radiology and surgery* 9 (2) (2014) 283–293.
- [338] A. C. Quiros, R. Murray-Smith, K. Yuan, PathologyGAN: Learning deep representations of cancer tissue, *arXiv preprint arXiv:1907.02644*.
- [339] A. Brock, J. Donahue, K. Simonyan, Large scale GAN training for high fidelity natural image synthesis, *arXiv preprint arXiv:1809.11096*.
- [340] A. Jolicoeur-Martineau, The relativistic discriminator: a key element missing from standard GAN, *arXiv preprint arXiv:1807.00734*.
- [341] S. Pandey, P. R. Singh, J. Tian, An image augmentation approach using two-stage generative adversarial network for nuclei image segmentation, *Biomedical Signal Processing and Control* 57 (2020) 101782.
- [342] V. Ljosa, K. L. Sokolnicki, A. E. Carpenter, Annotated high-throughput microscopy image sets for validation., *Nature methods* 9 (7) (2012) 637–637.
- [343] Y. Chi, L. Bi, J. Kim, D. Feng, A. Kumar, Controlled synthesis of dermoscopic images via a new color labeled generative style transfer network to enhance melanoma segmentation, in: 2018 40th Annual International Conference of the IEEE Engineering in Medicine and Biology Society (EMBC), IEEE, 2018, pp. 2591–2594.
- [344] M. Sarker, M. Kamal, H. A. Rashwan, M. Abdel-Nasser, V. K. Singh, S. F. Banu, F. Akram, F. U. Chowdhury, K. A. Choudhury, S. Chambon, et al., MobileGAN: Skin lesion segmentation using a lightweight generative adversarial network, *arXiv preprint arXiv:1907.00856*.
- [345] A. Zaman, S. H. Park, H. Bang, C.-w. Park, I. Park, S. Joung, Generative approach for data augmentation for deep learning-based bone surface segmentation from ultrasound images, *International journal of computer assisted radiology and surgery* 15 (2020) 931–941.
- [346] K. Chaitanya, N. Karani, C. F. Baumgartner, E. Erdil, A. Becker, O. Donati, E. Konukoglu, Semi-supervised task-driven data augmentation for medical image segmentation, *Medical Image Analysis* 68 (2021) 101934.
- [347] O. Bernard, A. Lalonde, C. Zotti, F. Cervenansky, X. Yang, P.-A. Heng, I. Cetin, K. Lekadir, O. Camara, M. A. G. Ballester, et al., Deep learning techniques for automatic MRI cardiac multi-structures segmentation and diagnosis: is the problem solved?, *IEEE transactions on medical imaging* 37 (11) (2018) 2514–2525.
- [348] D. E. Newman-Toker, Z. Wang, Y. Zhu, N. Nassery, A. S. S. Tehrani, A. C. Schaffer, C. W. Yu-Moe, G. D. Clemens, M. Fanai, D. Siegal, Rate of diagnostic errors and serious misdiagnosis-related harms for major vascular events, infections, and cancers: toward a national incidence estimate using the “big three”, *Diagnosis* 8 (1) (2021) 67–84.
- [349] T. Schlegl, P. Seeböck, S. M. Waldstein, U. Schmidt-Erfurth, G. Langs, Unsupervised anomaly detection with generative adversarial networks to guide marker discovery, in: *International conference on information processing in medical imaging*, Springer, 2017, pp. 146–157.
- [350] X. Chen, N. Pawlowski, M. Rajchl, B. Glocker, E. Konukoglu, Deep generative models in the real-world: An open challenge from medical imaging, *arXiv preprint:1806.05452*.
- [351] Y. Kuang, T. Lan, X. Peng, G. E. Selasi, Q. Liu, J. Zhang, Unsupervised multi-discriminator generative adversarial network for lung nodule malignancy classification, *IEEE Access* 8 (2020) 77725–77734.
- [352] T. Schlegl, P. Seeböck, S. M. Waldstein, G. Langs, U. Schmidt-Erfurth, f-anogan: Fast unsupervised anomaly detection with generative adversarial networks, *Medical image analysis* 54 (2019) 30–44.
- [353] S. Benson, R. Beets-Tan, Gan-based anomaly detection in multi-modal mri images, *bioRxiv* [doi: 10.1101/2020.07.10.197087](https://doi.org/10.1101/2020.07.10.197087).

- [354] S. Guan, M. Loew, Breast cancer detection using synthetic mammograms from generative adversarial networks in convolutional neural networks, *Journal of Medical Imaging* 6 (3) (2019) 031411.
- [355] L. Jendele, O. Skopek, A. S. Becker, E. Konukoglu, Adversarial augmentation for enhancing classification of mammography images, *arXiv preprint arXiv:1902.07762*.
- [356] J. Lee, R. M. Nishikawa, Simulating breast mammogram using conditional generative adversarial network: application towards finding mammographically-occult cancer, in: *Medical Imaging 2020: Computer-Aided Diagnosis*, Vol. 11314, International Society for Optics and Photonics, 2020, p. 1131418.
- [357] C. Han, Y. Kitamura, A. Kudo, A. Ichinose, L. Rundo, Y. Furukawa, K. Umamoto, Y. Li, H. Nakayama, Synthesizing Diverse Lung Nodules Wherever Massively: 3D Multi-Conditional GAN-based CT Image Augmentation for Object Detection (2019). [arXiv:1906.04962](https://arxiv.org/abs/1906.04962).
- [358] T. Bu, Z. Yang, S. Jiang, G. Zhang, H. Zhang, L. Wei, 3d conditional generative adversarial network-based synthetic medical image augmentation for lung nodule detection, *International Journal of Imaging Systems and Technology*.
- [359] J. Hu, L. Shen, G. Sun, Squeeze-and-excitation networks, in: *Proceedings of the IEEE conference on computer vision and pattern recognition*, 2018, pp. 7132–7141.
- [360] K. He, X. Zhang, S. Ren, J. Sun, Deep residual learning for image recognition, in: *Proceedings of the IEEE conference on computer vision and pattern recognition*, 2016, pp. 770–778.
- [361] M. Nishio, C. Muramatsu, S. Noguchi, H. Nakai, K. Fujimoto, R. Sakamoto, H. Fujita, Attribute-guided image generation of three-dimensional computed tomography images of lung nodules using a generative adversarial network, *Computers in Biology and Medicine* 126 (2020) 104032.
- [362] G. Van Tulder, M. de Bruijne, Why does synthesized data improve multi-sequence classification?, in: *International Conference on Medical Image Computing and Computer-Assisted Intervention*, Springer, 2015, pp. 531–538.
- [363] A. Rau, P. E. Edwards, O. F. Ahmad, P. Riordan, M. Janatka, L. B. Lovat, D. Stoyanov, Implicit domain adaptation with conditional generative adversarial networks for depth prediction in endoscopy, *International journal of computer assisted radiology and surgery* 14 (7) (2019) 1167–1176.
- [364] C. Muramatsu, M. Nishio, T. Goto, M. Oiwa, T. Morita, M. Yakami, T. Kubo, K. Togashi, H. Fujita, Improving breast mass classification by shared data with domain transformation using a generative adversarial network, *Computers in biology and medicine* 119 (2020) 103698.
- [365] S. Loeb, M. A. Bjurlin, J. Nicholson, T. L. Tammela, D. F. Penson, H. B. Carter, P. Carroll, R. Etzioni, Overdiagnosis and overtreatment of prostate cancer, *European urology* 65 (6) (2014) 1046–1055.
- [366] H. Li, M. L. Giger, B. Q. Huynh, N. O. Antropova, Deep learning in breast cancer risk assessment: evaluation of convolutional neural networks on a clinical dataset of full-field digital mammograms, *Journal of medical imaging* 4 (4) (2017) 041304.
- [367] A. Kapil, A. Meier, A. Zuraw, K. E. Steele, M. C. Rebelatto, G. Schmidt, N. Brieu, Deep semi supervised generative learning for automated tumor proportion scoring on nslc tissue needle biopsies, *Scientific reports* 8 (1) (2018) 1–10.
- [368] M. A. Shafto, L. K. Tyler, M. Dixon, J. R. Taylor, J. B. Rowe, R. Cusack, A. J. Calder, W. D. Marslen-Wilson, J. Duncan, T. Dalgleish, et al., The cambridge centre for ageing and neuroscience (cam-can) study protocol: a cross-sectional, lifespan, multidisciplinary examination of healthy cognitive ageing, *BMC neurology* 14 (1) (2014) 1–25.
- [369] S.-L. Liew, J. M. Anglin, N. W. Banks, M. Sondag, K. L. Ito, H. Kim, J. Chan, J. Ito, C. Jung,

- N. Khoshab, et al., A large, open source dataset of stroke anatomical brain images and manual lesion segmentations, *Scientific data* 5 (1) (2018) 1–11.
- [370] C. Han, L. Rundo, R. Araki, Y. Furukawa, G. Mauri, H. Nakayama, H. Hayashi, Infinite brain mr images: Pggan-based data augmentation for tumor detection, in: *Neural approaches to dynamics of signal exchanges*, Springer, 2020, pp. 291–303.
- [371] C. Han, L. Rundo, R. Araki, Y. Nagano, Y. Furukawa, G. Mauri, H. Nakayama, H. Hayashi, Combining noise-to-image and image-to-image gans: Brain mr image augmentation for tumor detection, *IEEE Access* 7 (2019) 156966–156977.
- [372] K. Schmainda, M. Prah, Data from brain-tumor-progression, *The Cancer Imaging Archive*.
- [373] C. Han, K. Murao, S. Satoh, Learning More with Less: GAN-based Medical Image Augmentation, [arXiv:1904.00838](https://arxiv.org/abs/1904.00838).
- [374] L. Sun, J. Wang, Y. Huang, X. Ding, H. Greenspan, J. Paisley, An adversarial learning approach to medical image synthesis for lesion detection, *IEEE journal of biomedical and health informatics* 24 (8) (2020) 2303–2314.
- [375] M. M. R. Siddiquee, Z. Zhou, N. Tajbakhsh, R. Feng, M. B. Gotway, Y. Bengio, J. Liang, Learning fixed points in generative adversarial networks: From image-to-image translation to disease detection and localization, in: *Proceedings of the IEEE/CVF International Conference on Computer Vision*, 2019, pp. 191–200.
- [376] R. S. Lee, F. Gimenez, A. Hoogi, D. Rubin, Curated breast imaging subset of ddsd, *The cancer imaging archive* 8 (2016) 2016.
- [377] E. Wu, K. Wu, W. Lotter, Synthesizing lesions using contextual gans improves breast cancer classification on mammograms, [arXiv preprint arXiv:2006.00086](https://arxiv.org/abs/2006.00086).
- [378] M. D. Halling-Brown, L. M. Warren, D. Ward, E. Lewis, A. Mackenzie, M. G. Wallis, L. S. Wilkinson, R. M. Given-Wilson, R. McAviney, K. C. Young, Optimam mammography image database: A large-scale resource of mammography images and clinical data, *Radiology: Artificial Intelligence* (2020) e200103.
- [379] B. Alyafi, O. Diaz, R. Martí, Dcgans for realistic breast mass augmentation in x-ray mammography, in: *Medical Imaging 2020: Computer-Aided Diagnosis*, Vol. 11314, International Society for Optics and Photonics, 2020, p. 1131420.
- [380] S. D. Desai, S. Giraddi, N. Verma, P. Gupta, S. Ramya, Breast cancer detection using gan for limited labeled dataset, in: *2020 12th International Conference on Computational Intelligence and Communication Networks (CICN)*, IEEE, 2020, pp. 34–39.
- [381] B. Swiderski, L. Gielata, P. Olszewski, S. Osowski, M. Kołodziej, Deep neural system for supporting tumor recognition of mammograms using modified gan, *Expert Systems with Applications* 164 (2021) 113968.
- [382] S. Kansal, S. Goel, J. Bhattacharya, V. Srivastava, Generative adversarial network–convolution neural network based breast cancer classification using optical coherence tomographic images, *Laser Physics* 30 (11) (2020) 115601.
- [383] T. Shen, K. Hao, C. Gou, F.-Y. Wang, Mass image synthesis in mammogram with contextual information based on gans, *Computer Methods and Programs in Biomedicine* 202 (2021) 106019.
- [384] T. Pang, J. H. D. Wong, W. L. Ng, C. S. Chan, Semi-supervised gan-based radiomics model for data augmentation in breast ultrasound mass classification, *Computer Methods and Programs in Biomedicine* 203 (2021) 106018.
- [385] M. Frid-Adar, I. Diamant, E. Klang, M. Amitai, J. Goldberger, H. Greenspan, Gan-based synthetic medical image augmentation for increased cnn performance in liver lesion classification, *Neurocomputing* 321 (2018) 321–331.
- [386] K. Doman, T. Konishi, Y. Mekada, Lesion image synthesis using dcgans for metastatic liver cancer

- detection, *Deep Learning in Medical Image Analysis* (2020) 95–106.
- [387] T. Kitasaka, *Jamit cad contest*.
URL <http://www.jamit.jp/english/index.html>
- [388] *3dircadb*.
URL <https://www.ircad.fr/research/3dircadb/>
- [389] T. Kanayama, Y. Kurose, K. Tanaka, K. Aida, S. Satoh, M. Kitsuregawa, T. Harada, Gastric cancer detection from endoscopic images using synthesis by gan, in: *International Conference on Medical Image Computing and Computer-Assisted Intervention*, Springer, 2019, pp. 530–538.
- [390] Y. Shin, H. A. Qadir, I. Balasingham, Abnormal colon polyp image synthesis using conditional adversarial networks for improved detection performance, *IEEE Access* 6 (2018) 56007–56017.
- [391] J. Bernal, F. J. Sánchez, G. Fernández-Esparrach, D. Gil, C. Rodríguez, F. Vilariño, Wm-dova maps for accurate polyp highlighting in colonoscopy: Validation vs. saliency maps from physicians, *Computerized Medical Imaging and Graphics* 43 (2015) 99–111.
- [392] Q. Angermann, J. Bernal, C. Sánchez-Montes, M. Hammami, G. Fernández-Esparrach, X. Dray, O. Romain, F. J. Sánchez, A. Histace, Towards real-time polyp detection in colonoscopy videos: Adapting still frame-based methodologies for video sequences analysis, in: *Computer Assisted and Robotic Endoscopy and Clinical Image-Based Procedures*, Springer, 2017, pp. 29–41.
- [393] H. Yu, X. Zhang, Synthesis of prostate mr images for classification using capsule network-based gan model, *Sensors* 20 (20) (2020) 5736.
- [394] P. Choyke, B. Turkbey, P. Pinto, M. Merino, B. Wood, Data from prostate-mri, The Cancer Imaging Archive. Available online: <http://doi.org/10.7937/K9>.
- [395] J. Krause, H. I. Grabsch, M. Kloor, M. Jendrusch, A. Echle, R. D. Buelow, P. Boor, T. Luedde, T. J. Brinker, C. Trautwein, et al., Deep learning detects genetic alterations in cancer histology generated by adversarial networks, *The Journal of Pathology* 254 (1) (2021) 70–79.
- [396] P. A. van den Brandt, R. A. Goldbohm, P. V. Veer, A. Volovics, R. J. Hermus, F. Sturmans, A large-scale prospective cohort study on diet and cancer in the netherlands, *Journal of clinical epidemiology* 43 (3) (1990) 285–295.
- [397] A. Bissoto, F. Perez, E. Valle, S. Avila, Skin lesion synthesis with generative adversarial networks, in: *OR 2.0 context-aware operating theaters, computer assisted robotic endoscopy, clinical image-based procedures, and skin image analysis*, Springer, 2018, pp. 294–302.
- [398] L. Ballerini, R. B. Fisher, B. Aldridge, J. Rees, A color and texture based hierarchical k-nn approach to the classification of non-melanoma skin lesions, in: *Color Medical Image Analysis*, Springer, 2013, pp. 63–86.
- [399] G. Argenziano, H. Soyer, V. De Giorgi, D. Piccolo, P. Carli, M. Delfino, et al., *Dermoscopy: a tutorial*, EDRA, Medical Publishing & New Media 16.
- [400] C. Baur, S. Albarqouni, N. Navab, Melanogans: high resolution skin lesion synthesis with gans, arXiv preprint arXiv:1804.04338.
- [401] H. Rashid, M. A. Tanveer, H. A. Khan, Skin lesion classification using gan based data augmentation, in: *2019 41st Annual International Conference of the IEEE Engineering in Medicine and Biology Society (EMBC)*, IEEE, 2019, pp. 916–919.
- [402] P. Tschandl, C. Rosendahl, H. Kittler, The HAM10000 dataset, a large collection of multi-source dermatoscopic images of common pigmented skin lesions, *Scientific data* 5 (1) (2018) 1–9.
- [403] M. Combalia, N. C. Codella, V. Rotemberg, B. Helba, V. Vilaplana, O. Reiter, C. Carrera, A. Barreiro, A. C. Halpern, S. Puig, et al.,

- BCN20000: Dermoscopic lesions in the wild, arXiv preprint arXiv:1908.02288.
- [404] Z. Qin, Z. Liu, P. Zhu, Y. Xue, A gan-based image synthesis method for skin lesion classification, *Computer Methods and Programs in Biomedicine* 195 (2020) 105568.
- [405] H. Salehinejad, S. Valaee, T. Dowdell, E. Colak, J. Barfett, Generalization of deep neural networks for chest pathology classification in x-rays using generative adversarial networks, in: *2018 IEEE International Conference on Acoustics, Speech and Signal Processing (ICASSP)*, IEEE, 2018, pp. 990–994.
- [406] D. Zhao, D. Zhu, J. Lu, Y. Luo, G. Zhang, Synthetic medical images using f&bgan for improved lung nodules classification by multi-scale vgg16, *symmetry* 10 (10) (2018) 519.
- [407] Y. Onishi, A. Teramoto, M. Tsujimoto, T. Tsukamoto, K. Saito, H. Toyama, K. Imaizumi, H. Fujita, Automated pulmonary nodule classification in computed tomography images using a deep convolutional neural network trained by generative adversarial networks, *BioMed research international* 2019.
- [408] C. Gao, S. Clark, J. Furst, D. Raicu, Augmenting lidc dataset using 3d generative adversarial networks to improve lung nodule detection, in: *Medical Imaging 2019: Computer-Aided Diagnosis*, Vol. 10950, International Society for Optics and Photonics, 2019, p. 109501K.
- [409] J. Yang, S. Liu, S. Grbic, A. A. A. Setio, Z. Xu, E. Gibson, G. Chabin, B. Georgescu, A. F. Laine, D. Comaniciu, Class-aware adversarial lung nodule synthesis in ct images, in: *2019 IEEE 16th International Symposium on Biomedical Imaging (ISBI 2019)*, IEEE, 2019, pp. 1348–1352.
- [410] Q. Wang, X. Zhang, W. Chen, K. Wang, X. Zhang, Class-aware multi-window adversarial lung nodule synthesis conditioned on semantic features, in: *International Conference on Medical Image Computing and Computer-Assisted Intervention*, Springer, 2020, pp. 589–598.
- [411] S. S. Ghosal, I. Sarkar, I. El Hallaoui, Lung nodule classification using convolutional autoencoder and clustering augmented learning method (calm)., in: *HSDM@ WSDM*, 2020, pp. 19–26.
- [412] B. Sun, F. Liu, Y. Zhou, S. Jin, Q. Li, X. Jin, Classification of lung nodules based on gan and 3d cnn, in: *Proceedings of the 4th International Conference on Computer Science and Application Engineering*, 2020, pp. 1–5.
- [413] Y. Wang, L. Zhou, M. Wang, C. Shao, L. Shi, S. Yang, Z. Zhang, M. Feng, F. Shan, L. Liu, Combination of generative adversarial network and convolutional neural network for automatic sub-centimeter pulmonary adenocarcinoma classification, *Quantitative imaging in medicine and surgery* 10 (6) (2020) 1249.
- [414] Y. Onishi, A. Teramoto, M. Tsujimoto, T. Tsukamoto, K. Saito, H. Toyama, K. Imaizumi, H. Fujita, Multiplanar analysis for pulmonary nodule classification in ct images using deep convolutional neural network and generative adversarial networks, *International journal of computer assisted radiology and surgery* 15 (1) (2020) 173–178.
- [415] A. Teramoto, T. Tsukamoto, A. Yamada, Y. Kiriya, K. Imaizumi, K. Saito, H. Fujita, Deep learning approach to classification of lung cytological images: Two-step training using actual and synthesized images by progressive growing of generative adversarial networks, *PLoS one* 15 (3) (2020) e0229951.
- [416] Q. Zhang, H. Wang, H. Lu, D. Won, S. W. Yoon, Medical image synthesis with generative adversarial networks for tissue recognition, in: *2018 IEEE International Conference on Healthcare Informatics (ICHI)*, IEEE, 2018, pp. 199–207.
- [417] P. Chaudhari, H. Agrawal, K. Kotecha, Data augmentation using mg-gan for improved cancer classification on gene expression data, *Soft Computing* (2019) 1–11.

- [418] R. Edgar, M. Domrachev, A. E. Lash, Gene expression omnibus: Ncbi gene expression and hybridization array data repository, *Nucleic acids research* 30 (1) (2002) 207–210.
- [419] Y. Liu, Y. Zhou, X. Liu, F. Dong, C. Wang, Z. Wang, Wasserstein gan-based small-sample augmentation for new-generation artificial intelligence: a case study of cancer-staging data in biology, *Engineering* 5 (1) (2019) 156–163.
- [420] M. Rubin, O. Stein, N. A. Turko, Y. Nygate, D. Roitshtain, L. Karako, I. Barnea, R. Giryas, N. T. Shaked, Top-gan: Stain-free cancer cell classification using deep learning with a small training set, *Medical image analysis* 57 (2019) 176–185.
- [421] I. P. Nearchou, D. A. Soutar, H. Ueno, D. J. Harrison, O. Arandelovic, P. D. Caie, A comparison of methods for studying the tumor microenvironment’s spatial heterogeneity in digital pathology specimens, *Journal of Pathology Informatics*.
- [422] M. Kim, I. Oh, J. Ahn, An improved method for prediction of cancer prognosis by network learning, *Genes* 9 (2018) 478. doi:10.3390/genes9100478.
- [423] K. T. Ahmed, J. Sun, J. Yong, W. Zhang, Multi-omics data integration by generative adversarial network, bioRxiv doi:10.1101/2021.03.13.435251.
- [424] Q. D. Vu, K. Kim, J. T. Kwak, Unsupervised tumor characterization via conditional generative adversarial networks, *IEEE journal of biomedical and health informatics*.
- [425] A. C. Quiros, R. Murray-Smith, K. Yuan, Pathologygan: Learning deep representations of cancer tissue (2021). arXiv:1907.02644.
- [426] K. Shyamala, H. Girish, S. Murgod, Risk of tumor cell seeding through biopsy and aspiration cytology, *Journal of International Society of Preventive & Community Dentistry* 4 (1) (2014) 5.
- [427] M. A. Levy, D. L. Rubin, Tool support to enable evaluation of the clinical response to treatment, in: *AMIA Annual Symposium Proceedings*, Vol. 2008, American Medical Informatics Association, 2008, p. 399.
- [428] J. Yoon, J. Jordon, M. Schaar, Ganite: Estimation of individualized treatment effects using generative adversarial nets, in: *ICLR*, 2018.
- [429] Q. Ge, X. Huang, S. Fang, S. Guo, Y. Liu, W. Lin, M. Xiong, Conditional generative adversarial networks for individualized treatment effect estimation and treatment selection, *Frontiers in Genetics* 11 (2020) 1578. doi:10.3389/fgene.2020.585804.
- [430] I. Bica, J. Jordon, M. van der Schaar, Estimating the effects of continuous-valued interventions using generative adversarial networks, arXiv preprint arXiv:2002.12326.
- [431] P. Goldsborough, N. Pawlowski, J. Caicedo, S. Singh, A. Carpenter, CytoGAN: Generative Modeling of Cell Images doi:10.1101/227645.
- [432] S. Singh, M. A. Bray, T. R. Jones, A. E. Carpenter, Pipeline for illumination correction of images for high-throughput microscopy, *J Microsc* 256 (3) (2014) 231–236.
- [433] A. Kadurin, A. Aliper, A. Kazennov, P. Mamoshina, Q. Vanhaelen, K. Khrabrov, A. Zhavoronkov, The cornucopia of meaningful leads: Applying deep adversarial autoencoders for new molecule development in oncology, *Oncotarget* 8 (7) (2017) 10883–10890.
- [434] A. Kadurin, S. Nikolenko, K. Khrabrov, A. Aliper, A. Zhavoronkov, drugan: an advanced generative adversarial autoencoder model for de novo generation of new molecules with desired molecular properties in silico, *Molecular pharmaceuticals* 14 (9) (2017) 3098–3104.
- [435] M. B. Sharpe, K. L. Moore, C. G. Orton, Within the next ten years treatment planning will become fully automated without the need for human intervention, *Medical Physics* 41 (12) (2014) 120601. doi:10.1118/1.4894496.

- [436] R. Mahmood, A. Babier, A. McNiven, A. Diamant, T. C. Chan, Automated treatment planning in radiation therapy using generative adversarial networks, in: *Machine Learning for Healthcare Conference*, PMLR, 2018, pp. 484–499.
- [437] A. Babier, J. J. Boutilier, M. B. Sharpe, A. L. McNiven, T. C. Chan, Inverse optimization of objective function weights for treatment planning using clinical dose-volume histograms, *Physics in Medicine & Biology* 63 (10) (2018) 105004.
- [438] M. Maspero, M. H. Savenije, A. M. Dinkla, P. R. Seevinck, M. P. Intven, I. M. Jurgenliemk-Schulz, L. G. Kerkmeijer, C. A. van den Berg, Dose evaluation of fast synthetic-ct generation using a generative adversarial network for general pelvis mr-only radiotherapy, *Physics in Medicine & Biology* 63 (18) (2018) 185001.
- [439] V. Kearney, J. W. Chan, T. Wang, A. Perry, M. Descovich, O. Morin, S. S. Yom, T. D. Solberg, Dosegan: a generative adversarial network for synthetic dose prediction using attention-gated discrimination and generation, *Scientific reports* 10 (1) (2020) 1–8.
- [440] Y. Murakami, T. Magome, K. Matsumoto, T. Sato, Y. Yoshioka, M. Oguchi, Fully automated dose prediction using generative adversarial networks in prostate cancer patients, *PLoS One* 15 (5) (2020) e0232697.
- [441] S. Huang, J. Yang, S. Fong, Q. Zhao, Artificial intelligence in cancer diagnosis and prognosis: Opportunities and challenges, *Cancer letters* 471 (2020) 61–71.
- [442] U. Hwang, S. Choi, H.-B. Lee, S. Yoon, Adversarial training for disease prediction from electronic health records with missing data, *arXiv preprint arXiv:1711.04126*.
- [443] M. Dashtban, W. Li, Predicting risk of hospital readmission for comorbidity patients through a novel deep learning framework, in: *Proceedings of the 53rd Hawaii International Conference on System Sciences*, 2020.
- [444] N. Verma, M. C. Cowperthwaite, M. G. Burnett, M. K. Markey, Differentiating tumor recurrence from treatment necrosis: a review of neuro-oncologic imaging strategies, *Neuro-oncology* 15 (5) (2013) 515–534.
- [445] K. Tomczak, P. Czerwińska, M. Wiznerowicz, The Cancer Genome Atlas (TCGA): an immeasurable source of knowledge, *Contemp Oncol (Pozn)* 19 (1A) (2015) 68–77.
- [446] D. Croft, A. F. Mundo, R. Haw, M. Milacic, J. Weiser, G. Wu, M. Caudy, P. Garapati, M. Gillespie, M. R. Kamdar, B. Jassal, S. Jupe, L. Matthews, B. May, S. Palatnik, K. Rothfels, V. Shamovsky, H. Song, M. Williams, E. Birney, H. Hermjakob, L. Stein, P. D’Eustachio, The Reactome pathway knowledgebase, *Nucleic Acids Res* 42 (Database issue) (2014) D472–477.
- [447] A. Fabregat, K. Sidiropoulos, G. Viteri, O. Forner, P. Marin-Garcia, V. Arnau, P. D’Eustachio, L. Stein, H. Hermjakob, Reactome pathway analysis: a high-performance in-memory approach, *BMC Bioinformatics* 18 (1) (2017) 142.
- [448] C. G. A. R. Network, et al., Integrated genomic analyses of ovarian carcinoma, *Nature* 474 (7353) (2011) 609–615.
- [449] G. Ciriello, M. L. Gatza, A. H. Beck, M. D. Wilkerson, S. K. Rhie, A. Pastore, H. Zhang, M. McLellan, C. Yau, C. Kandoth, et al., Comprehensive molecular portraits of invasive lobular breast cancer, *Cell* 163 (2) (2015) 506–519.
- [450] A. H. Beck, A. R. Sangoi, S. Leung, R. J. Marinelli, T. O. Nielsen, M. J. van de Vijver, R. B. West, M. van de Rijn, D. Koller, Systematic analysis of breast cancer morphology uncovers stromal features associated with survival, *Sci Transl Med* 3 (108) (2011) 108ra113.
- [451] J. N. Kather, N. Halama, A. Marx, [100,000 histological images of human colorectal cancer and healthy tissue](https://doi.org/10.5281/zenodo.1214456) (Apr. 2018). doi:10.5281/zenodo.1214456. URL <https://doi.org/10.5281/zenodo.1214456>

- [452] Y. Wang, T. Suzek, J. Zhang, J. Wang, S. He, T. Cheng, B. A. Shoemaker, A. Gindulyte, S. H. Bryant, PubChem BioAssay: 2014 update, *Nucleic Acids Res* 42 (Database issue) (2014) D1075–1082.
- [453] V. Ljosa, K. L. Sokolnicki, A. E. Carpenter, Annotated high-throughput microscopy image sets for validation, *Nat Methods* 9 (7) (2012) 637.
- [454] D. Almond, K. Y. Chay, D. S. Lee, The costs of low birth weight, Working Paper 10552, National Bureau of Economic Research (June 2004). doi: [10.3386/w10552](https://doi.org/10.3386/w10552).
- [455] S. M. Kornblau, R. Tibes, Y. H. Qiu, W. Chen, H. M. Kantarjian, M. Andreeff, K. R. Coombes, G. B. Mills, Functional proteomic profiling of AML predicts response and survival, *Blood* 113 (1) (2009) 154–164.
- [456] J. N. Weinstein, E. A. Collisson, G. B. Mills, K. R. M. Shaw, B. A. Ozenberger, K. Ellrott, I. Shmulevich, C. Sander, J. M. Stuart, The cancer genome atlas pan-cancer analysis project, *Nature genetics* 45 (10) (2013) 1113–1120.
- [457] P. Schwab, L. Linhardt, S. Bauer, J. M. Buhmann, W. Karlen, Learning counterfactual representations for estimating individual dose-response curves, in: *Proceedings of the AAAI Conference on Artificial Intelligence*, Vol. 34, 2020, pp. 5612–5619.
- [458] F. Johansson, U. Shalit, D. Sontag, Learning representations for counterfactual inference, in: *International conference on machine learning*, PMLR, 2016, pp. 3020–3029.
- [459] H. S. Kim, J. Jung, C. Jeong, J. Kwak, E. Choi, S. Lee, S. Yoon, B. Cho, Prediction of hepatic parenchymal change in gd-eob-dtpa mr images after stereotactic body radiation therapy by cycle gan deep neural network, *International Journal of Radiation Oncology*Biophysics* 105 (2019) E135. doi: [10.1016/j.ijrobp.2019.06.2171](https://doi.org/10.1016/j.ijrobp.2019.06.2171).
- [460] A. Elazab, C. Wang, S. J. S. Gardezi, H. Bai, Q. Hu, T. Wang, C. Chang, B. Lei, Gp-gan: Brain tumor growth prediction using stacked 3d generative adversarial networks from longitudinal mr images, *Neural Networks* 132 (2020) 321–332. doi: [10.1016/j.neunet.2020.09.004](https://doi.org/10.1016/j.neunet.2020.09.004).
- [461] M. Li, H. Tang, M. D. Chan, X. Zhou, X. Qian, Dc-gan: pseudoprogression and true tumor progression of glioblastoma multiform image classification based on dcgan and alexnet, *Medical physics* 47 (3) (2020) 1139–1150.
- [462] D. Hanahan, R. A. Weinberg, Hallmarks of cancer: the next generation, *Cell* 144 (5) (2011) 646–674.